Quantum Chemical Prediction of ^{19}F NMR Shifts for Perfluorinated Arenes and Magnetic Exchange Coupling Constants for Diradicals

Dissertation

zur Erlangung des Doktorgrades

der Naturwissenschaften

vorgelegt beim

Fachbereich Biochemie, Chemie und Pharmazie der

Johann Wolfgang Goethe Universität

zu Frankfurt am Main

von

Ram Niwas

aus
Muzaffarnagar (Indien)

Frankfurt 2016

D30

vom Fachbereich Biochemie, Chemie und Pharmazie der
Johann Wolfgang Goethe-Universität als Dissertation angenommen.

DEKAN: Prof. Dr. Michael Karas

1. GUTACHTER: Prof. Dr. Max Holthausen
2. GUTACHTER: Prof. Dr. Andreas Terfort

DATUM DER DISPUTATION:

Table of Contents

1. Introduction

1.1 Essentials of Quantum Chemical Calculations

Nowadays, computational methods are used extensively to investigate the electronic structure and properties of molecules and materials. The rapid progress in computer science and technology has made highly efficient computational implementation of ever new theoretical methods possible. Hence computational chemistry has become an important field of research that offers easily accessible tools to predict properties accurately for applications in chemistry and material sciences.

Nuclear magnetic resonance (NMR) is one of the most powerful and widely used spectroscopic techniques for the determination of the structure and dynamics of novel compounds [1-3].Other techniques used for structure determination are X-ray crystallography, Mossbauer spectroscopy, Raman spectroscopy, mass spectrometry, optical rotary dispersion, circular dichroism, optical spectroscopy and electron microscopy. The recent advances in NMR instrumentation and methodology provide new possibilities for the NMR applications [4, 5].

The NMR indirect spin-spin coupling constant is determined by the molecular structure and thus influenced by internal flexibility and intermolecular interactions. The NMR chemical shifts as well as spin-spin coupling constants measured in the laboratory represent averages over the values belonging to all geometrical arrangements arising during the course of the NMR experiment. Spin-spin coupling constants are more sensitive to changes in the molecular geometry than chemical shift values. Therefore, to obtain structural information for complicated structures, most experimentalists employ coupling constants or the nuclear Overhauser effect; that is the transfer of nuclear spin polarization from one nuclear spin population to another via cross-relaxation, this effect can be used to determine intra and inter molecular distances.
.

Furthermore well-developed two and three dimensional NMR techniques yield a lot of structural information. In spite of their great success, there is always scope for a wrong structural assignment because extracting structural information out of experimental NMR spectra that is not always simple. Therefore, experimentalists have to be careful with structural assignments based on observed spectra [6] and even very often it is necessary to take help from theoretical NMR calculation. NMR

chemical shift values and spin-spin coupling constants can be commutated by quantum mechanical calculations, which can help in interpreting the experimental NMR data. Therefore, reliable computational methods for predicting NMR chemical shifts are needed.

Over the years significant efforts have been made develop methodologies to predict accurate experimental NMR parameters [7-9]. However, to employ such methodologies on a regular basis, the error in computed values need to be within a few ppm for the ^{19}F and ^{13}C chemical shifts and even smaller for the ^{1}H shift [10-12]. The problem is further complicated by the fact that novel chemical species are often large molecules with functionalities that produce chemical shifts within narrow spectral regions [13, 14]. Thus, accurate calculations need to be achieved at a modest computational cost and yet they should be able to account for the observed structural and environmental differences [14, 15].

1.2 Why is ^{19}F NMR Interesting?

In the recent past, fluoro-compounds have made a large impact in organic and pharmaceutical research because fluorine shows unusual and fascinating properties [16-18], attracting the interest of the academic, medical and industrial communities. The wide spectrum of possible applications of fluorinated molecules has stimulated the discovery of new fluorinating reagents and fluorination processes. Because of its steric and polar characteristics, even a single fluorine substituent, placed at a favorable position within a molecule can have a remarkable effect on the physical and chemical properties of that molecule. Fluorine NMR spectroscopy is a valuable tool to identify synthesized molecules. Fluorine NMR has some advantages over proton NMR as it covers a wide range of chemical shift values. The fluorine atom has lone pairs of electrons that make it highly sensitive to its chemical environment [19].

It contains more distinct signals and is easier to interpret than proton NMR [21-23]. Hence ^{19}F NMR spectra can provide valuable information about protein-drug complexes and thereby facilitate the characterization of potential lead compounds at reduced cost. Because of the positive effects of fluorine labeling and the additional value of the fluorine atom as a critical component of several highly effective drug compounds currently in the market [20] NMR monitoring the ^{19}F nuclei of fluorine containing ligands as selective markers has gained popularity [21-24].

1.3   Objective of ^{19}F NMR Chemical Shift Calculations

Organic semiconductors are an active area of research driven by potential applications that include light-emitting diodes [25] photovoltaics [26] and field-effect transistors (OFETs) [27] solar cells [3-5]. Discussions on the impact of fluorine on physical and chemical properties of compounds have appeared in numerous reviews and textbooks [18, 20]. There are also a number of recent reviews on the subject of fluorine in medicinal chemistry[20]. The fluoro-chemistry research and fluorochemical industry had an increasingly dominant role from last few years. The main reason for this is the extraordinary stability of these fluorine substituted molecules. perfluorinated arenes are found to be resistant against the influence of water, oxygen, and light. Fluorinated and non-fluorinated arenes have nearly the same shape, which often results in very similar packing and also very similar charge transport properties [28]. Furthermore, the density of states is comparable. However, perfluorination leads to a collective lowering of all valence orbital energies. As a result, the charge carriers differ: whereas most organic semi-conductors are p-conductors, and the charge carriers in the perfluorinated molecules are electrons. This change in the charge transport mechanism carries tremendous potential, e.g. in the development of new organic light-emitting devices (OLEDs) or bipolar amplifiers. Extended perfluoroacenes are potential candidates for electron-transport materials. They have inherently low electron affinities and improved electron-transport (n-type) materials are generally needed to develop more efficient devices. Electron-deficient heterocyclic compounds have been investigated as n-type materials [29]. Fluorine substitution lowers the orbital energy levels and increases the stability of devices operating under ambient conditions [28]. The typical reaction for the synthesis of perfluorinated molecules is the so-called HALEX (halogen exchange) reaction, during which chlorine atoms at the molecular backbone are substituted by fluorine atoms. This reaction is limited to a certain size of molecules, so new synthetic strategies need to be established.

A promising method for the production of larger, fluorine-carrying molecules seems to be the electron-induced annelation of smaller molecules. In fact halogen-substituted molecules are much more prone to C-C bond formation than the respective non-halogenated molecules. This opens up a route for manufacturing extended π-systems.

Synthesis of fluoroanthracene based extended pie system is possible via nucleophilic substitution on fluoroanthracene, but   identifying   resulted product from such

nucleophilic substitution reaction is not always easy because there are three different possibilities in case of fluoroanthracene where substitution might take place and chemical environment of these three sites are also not very much different. So An interpretation of such resulted products NMR spectra is not always a simple exercise and that makes life difficult to extract structural information from the experimental data, though theoretical interpretation of such spectra might be helpful.

The importance of accurate NMR chemical shift calculations to facilitate the assignment of complex NMR signals has been recognized widely [24, 30-32]. However, to use the available computational methods on a regular basis, the error in the predicted shifts should be minimal at a modest computational cost [12, 33, 34].

Our aim in this thesis is to find a DFT based approach that allows the prediction of ^{19}F NMR chemical shifts accurately to within 2-4 ppm of the true value, accuracy within this range will be helpful in resolving substitution products. This target accuracy is needed to discriminate, e.g., substitution patterns in fluoroaromatic systems. The computation of accurate ^{19}F chemical shift values is useful to identify the substituted products at each stage of the nulceophilic aromatic exchange of halogens (Halex reaction). A number of quantum chemical methods have been developed to predict accurate ^{19}F NMR chemical shifts and several methods analyze to assign the observed ^{19}F NMR spectra, a variety of methods have been developed. Various schemes to calculate ^{19}F NMR chemical shifts, including methods for the correction of the calculated values with the help of empirical parameters have been evaluated in this thesis. Computational chemists have managed to achieve a combination of accuracy and efficiency which allows for the treatment of molecules containing several hundred atoms. To date, it has been shown in the literature that many of the existing density functionals, when combined with very large basis sets, are capable of predicting accurate NMR chemical shifts [35]. In chapters 4 and 5 a comprehensive evaluation of various DFT schemes to compute accurate NMR shifts is presented. It is shown how DFT calculations can help to understand NMR properties in more detail and aid in the interpretation of NMR spectra, thus enabling the extraction of the information encoded in the NMR spectra.

As discussed above in ^{19}F shift calculation our aim is to find a quantum chemical method based methods that can predict ^{19}F shifts for fluoro-aromatics within 2-4 ppm.

In the next part of this thesis we aimed at find computation approach that can be used to predict accurate magnetic couplings (2J) in organic diradicals. Such methods will be helpful in designing novel magnetic materials.

The development of novel magnetic materials has relied for centuries on solid-state synthesis protocols requiring harsh conditions. Recently, however, an alternative approach has received increasing attention, i.e. the rational design of magnetic materials. A "molecules-to-materials" approach is envisaged aiming at a detailed control of material properties at the molecular level [36]. To this end, a toolbox of molecular building blocks (i.e. spin-carriers and bridging elements) with smoothly varying properties (spin, magnetic moments, redox potentials, exchange coupling) is to be developed. For the de-novo design of such building blocks and a detailed understanding of the resulting spin-spin interactions, accurate predictions by quantum chemical calculations is very much important. In recent past different methods have been developed to compute accurate magnetic exchange couplings and tested on varieties of magnetic systems such as hypothetically designed H-He-H, The multiplet structure arises from the distribution of four electrons in three orbitals and on synthesized molecules such as bisnitronyl nitroxide[37-40]. The procedure outline in literature that the full configuration interaction (FCI) method can estimate the most accurate J couplings but it cannot be used for any practically usable systems. An alternate method that predict reliable magnetic couplings are DDCI or full CASPT2 and though this methods cannot be applied for most of the interesting systems and for such methods selection of an active space also play major role in J estimation. On other hand computationally viable DFT models have been found to correctly reproduce the sign of the exchange-coupling constants in all cases, but they are not reliable for a quantitative estimation of the absolute values.

This project is a part of a collaborative project between theoretical and experimental chemist and physicists and here we aimed at complement or to guide the preparative work on the development of molecular building blocks used to form extended coordination polymers and we intended to understanding and control of the magnetic properties of the resulting materials. Two schemes given below shows that magnetic material can be designed using nitronyl nitroxide as diradical and coupled via pie spacer (1) or it can be designed using metal diradical and pi spacer (2) .in each case i

is very important to predict accurate magnetic coupling for basic building blocks, nitronyl nitroxide and coupled systems
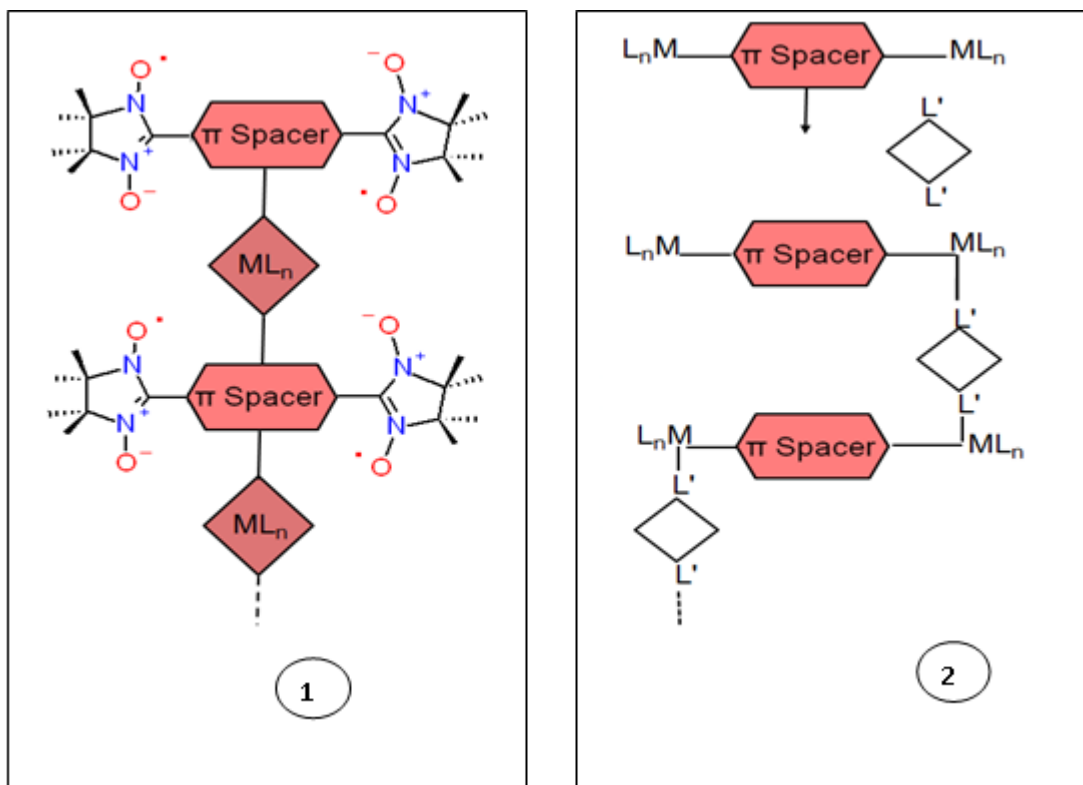
Figure 1. 1: Magnetically coupled via ditopic ligands (1) transition metal complex fragments (2)

We intended to do here density functional calculations on the molecular building blocks and the extended coordination polymers at all stages of the materials development process. The aim was to understand and control the magnetic properties of the resulting materials at a molecular level and help preparative work of magnetic material designed.

1.4 Objective of Magnetic Coupling Constant Calculations

The calculation of J for these molecules is highly geometry-sensitive. This is the reason why theoretical investigations on radical-radical spin systems reported in the literature generally use geometry parameters from X-ray data for known compounds [41]. A large number of calculations on crystallographic geometries have shown that an application of the broken symmetry approach within the DFT scheme is a suitable tactic to determine the sign and magnitude of the magnetic

exchange couplings in spin dimers[39, 40].The main objective of this study is to find a computational approach (a combination of density functionals and basis sets) to estimate magnetic exchange coupling accurately and to the extent accurate that model based predicted magnetic coupling could help in synthesizing required coupling strength magnetically coupled dimers . The quality of a required approach will be judged based on its accuracy, reliability and computational cost. Such an approach should be computationally easy to apply to large chemical systems. To assess the accuracy that can be expected from DFT for the description of the magnetic coupling constant J, we have performed extensive calibration calculations.

2. Theoretical Foundations of Quantum Chemical Methods

2.1 Introduction

In this chapter, a brief introduction to the quantum mechanical methods used in the calculations is presented. We have referred the conceptual part to theoretical chemistry books [42-45]. In quantum mechanics the state of a system is described by the wave function Ψ and it depends on the coordinates of the particles and the time t [46]. The solution of the time-independent Schrödinger equation can be written as

$$H\Psi = E\Psi \tag{2.1}$$

In the equation 2.1, H denotes the Hamiltonian operator and E, the eigenvalue of a stationary state wave function Ψ. The probability density of a particle is given by $|\Psi|^2$.
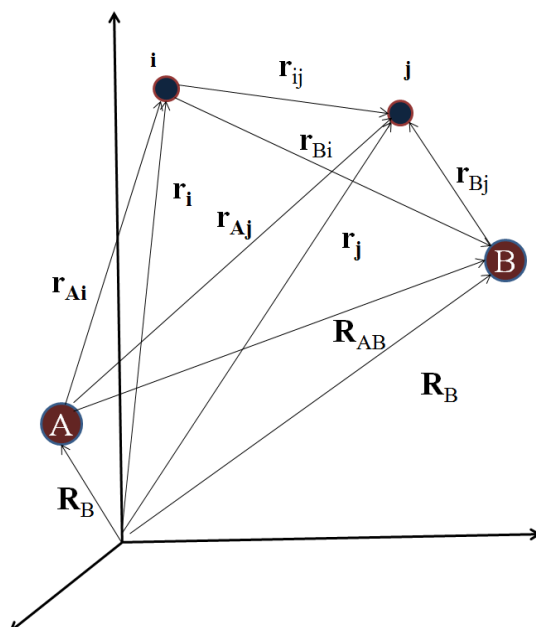
Figure 2. 1: The molecular coordinate system for AB, a diatomic molecule.

$$H = -\sum_{i=1}^{N}\frac{1}{2}\nabla_i^2 - \sum_{A=1}^{M}\frac{1}{2M_A}\nabla_A^2 - \sum_{i=1}^{N}\sum_{A=1}^{M}\frac{Z_A}{r_{iA}} + \sum_{i=1}^{N-1}\sum_{j>i}^{N}\frac{1}{r_{ij}} + \sum_{A=1}^{M-1}\sum_{B>A}^{M}\frac{Z_A Z_B}{R_{AB}}$$
$$\underbrace{\phantom{-\sum_{i=1}^{N}\frac{1}{2}\nabla_i^2}}_{T_e}\quad\underbrace{\phantom{\sum_{A=1}^{M}\frac{1}{2M_A}\nabla_A^2}}_{T_N}\quad\underbrace{\phantom{\sum_{i=1}^{N}\sum_{A=1}^{M}\frac{Z_A}{r_{iA}}}}_{V_{eN}}\quad\underbrace{\phantom{\sum_{i=1}^{N-1}\sum_{j>i}^{N}\frac{1}{r_{ij}}}}_{V_{ee}}\quad\underbrace{\phantom{\sum_{A=1}^{M-1}\sum_{B>A}^{M}\frac{Z_A Z_B}{R_{AB}}}}_{V_{NN}}$$

$$\tag{2.2}$$

In equation (2.2) M_A denotes the mass and Z_A, the charge on the nucleus A. T_e is an operator for the kinetic energy of the electrons, T_N is an operator for the kinetic energy of the nuclei, V_{eN} is an operator for columbic attraction between electrons

and the nuclei, V_{ee} is an operator for repulsion between the electrons and V_{NN} is an operator for repulsion between the nuclei. A simplification of this Hamiltonian operator is necessary to apply it to practical systems.

In the case of interacting particles, the time-independent Schrödinger equation for hydrogen atom can be solved at great extent but for most of the chemically relevant systems, only an approximate solution of the Schrödinger equation is possible. Because of the term V_{eN} in equation (2.2) it is not possible to write a wave function as the product of an electron and a nuclear wave function. Thus, further approximations depending only on the electronic wave function are used. According to the Born-Oppenheimer approximation (BO), the movement of electron and nuclei may be separated, which leads to an approximation where electrons move in the field of fixed nuclei.

The electronic Schrödinger equation for a system within the BO approximation is given by

$$H_e \Psi_e = E_e \Psi_e \qquad \text{where} \quad H_e = T_e + V_{ee} + V_{eN} \tag{2.3}$$

In equation (2.3) E_e is the electronic energy of the molecule (i.e. the potential and kinetic energy of the electrons).

The total energy of the system (E_{tot}) is

$$E_{tot} = E_e + V_{NN} \tag{2.4}$$

where V_{NN} is the internuclear repulsion and it depends on the nuclear coordinates R only in parametric form.

2.2 The Hartree-Fock Approximation

To solve the Schrödinger equation for more than two particles, further approximations are made. The Hartree-Fock (HF) method is a variational approach to approximate the ground state energy of a system and usually serves as a starting point for more accurate calculations. The HF method approximates the real N-electron wave function by a Slater determinant (Φ_{SD}), which is an antisymmetrized product of N one-electron wave functions χ_i Written as

$$\Psi_0 = \Phi_{SD}(1,2,3.....N) = \frac{1}{\sqrt{N!}} \begin{vmatrix} \chi_1(1) & \chi_2(1) & ....\chi_N(1) \\ \chi_1(2) & \chi_2(2) & ....\chi_N(2) \\ & .... & \\ & .... & \\ \chi_1(N) & \chi_2(N) & \chi_N(N) \end{vmatrix}$$

(2.5)

The formulation of the wave functions as a Slater determinant fulfills the Pauli condition of the antisymmetrized. The one-electron function χ_i is called a spin orbital consisting of a spatial part $\phi_i(\vec{r_i})$ and one of the two spin functions, $\alpha(s)$ or $\beta(s)$. This simplest form of an antisymmetric wave function is used in the Hartree-Fock method as an approximation to the exact ground state function and the variational principle is used to determine the energy of the system.

According to the variational principle, the energy associated to any guess wave function $\tilde{\Psi}$ must be higher than or equal to the exact Energy E_0.

$$\tilde{E}_0 = \left\langle \tilde{\Psi} \left| H \right| \tilde{\Psi} \right\rangle \geq E_0$$

(2.6)

The optimum wave functions will yield the lowest E_0 and the orbitals χ_i are thus varied until E_0 is minimized.

2.3 Linear Combination of Atomic Orbitals (LCAO) Approximation

The solutions to the Hartree–Fock model ϕ_i are known as the molecular orbitals (MOs). These orbitals generally span the entire molecule, just as the atomic orbitals (AOs) span the space about an atom. In chemistry the atomic properties is consider as the property of atom (or collection of atoms as functional groups) to still remains to some extent when embedded within a molecule, it seems reasonable to construct the MOs as an expansion of the AOs and   so the linear combination of atomic orbitals (LCAO) can be written as

$$\phi_i = \sum_{\mu}^{k} C_{i\mu} \chi_{\mu}$$

(2.7)

where the index μ spans over all of the atomic orbitals χ of every atom in the molecule (a total of k atomic orbitals), $C_{\mu i}$ is the expansion coefficient of AO χ_μ in MO ϕ_i.

2.4 Basis Sets

According to the Hartree-Fock-Roothaan approach, usually atom-centered atomic orbitals are specified to obtain the energy of a wave function [47]. If the set of atomic orbitals is infinite, then the variational principle tells us that we will obtain the lowest possible energy within the HF-SCF method and this is called the Hartree-Fock limit. This lowest energy is not the actual energy of the molecule; It should be consider that the HF method neglects immediate electron–electron interactions. Another hand infinite set of atomic orbitals is unattainable, and a choice must be made on how to truncate the expansion of basis set. Such a choice of atomic orbitals defines the basis set.

In general, a basis set is used in two different forms: Slater type or Gaussian type. Slater type orbitals (STOs) and Gaussian type orbitals.

$$\phi^{STO} = N r^{n-1} e^{-\zeta r} Y_{lm}\left(\vartheta, \varphi\right) \tag{2.8}$$

Here, N corresponds to the principal quantum number, the orbital exponent is termed ζ and Y_{lm} are the usual spherical harmonics that describe the angular part of the function. In fact as a rule of thumb one usually needs about three times as many GTO as STO functions to achieve similar accuracy. GTO is defined according to equation 2.9

$$\phi^{GTO}_{cartesian} = N x^i y^j z^k e^{-\alpha r^2}, \quad i+j+k = l. \tag{2.9}$$

N is a normalization factor which ensures that $\langle \eta\mu | \eta\mu \rangle = 1$ (but note that the $\eta\mu$ are not orthogonal, i. e.,($\left\langle \phi_\mu \middle| \phi_\nu \right\rangle \neq 0$ for $\mu \neq \nu$). α represents the orbital exponent which determines how compact (large α) or diffuse (small α) the resulting function is. $L = l + m + n$ is used to classify the GTO as s-functions ($L = 0$), p-functions ($L = 1$), d-functions ($L = 2$), etc.

The Gaussian type orbitals (GTO) are easy to evaluate and are widely used due to their convenient mathematical properties. On the other hand, from a physical point

of view, *Slater-type-orbitals* (STO) seem to be the natural choice for basis functions. They are simple exponentials that mimic the exact eigen functions of the hydrogen atom. Unlike the GTO functions, Slater-type-orbitals exhibit the correct cusp behavior at $r \rightarrow 0$ with a discontinuous derivative (while a GTO has a slope of zero at $r \rightarrow 0$) and the desired exponential decay in the tail regions as $r \rightarrow \infty$ (GTO fall off too rapidly). It was found that the shortcomings of GTOs are overcome by using linear combinations of GTOs to yield contracted Gaussian functions (CGF) and it represented as

$$\phi_{\tau}^{CGF} = \sum_{a}^{A} d_{a\tau} \phi_{a}^{GTO}, \qquad (2.10)$$

The original motivation for contracting was that the contraction coefficients $d_{a\tau}$ can be chosen in a way that the CGF resembles as much as possible a single STO function. The simplest and least accurate expansion of the molecular orbitals utilizes only one basis function (or one contracted function in the case of CGF sets) for each atomic orbital up to and including the valence orbitals. These basis sets are for obvious reasons called *minimal* sets. A typical representative is the STO-3G basis set, in which three primitive GTO functions are combined into one CGF. A typical representative is the STO- 3G basis set, in which three primitive GTO functions are combined into one CGF. For carbon, this basis set consists of five functions, one each describing the 1s and 2s atomic orbitals and three functions for the 2p shell (px, py, and pz). One should expect no more than only qualitative results from minimal sets and nowadays they are hardly used anymore. The next level of basis set is called double-zeta basis set. Here, the set of functions is doubled, i. e., there are two functions for each orbital (the generic name 'double-zeta' for such basis sets still points to the beginnings of computational quantum chemistry, when STO functions were in use, where the orbital exponent is called ζ). Typical examples are the 3-21G or 6-31G Gaussian basis sets developed by Pople and coworkers. In most applications, such basis sets are augmented by polarization functions, i. e., functions of higher angular momentum than those occupied in the atom, e. g., p-functions for hydrogen or d-functions for the first-row elements.

In thesis we have tested various Pople-type basis sets, 6-31G (d, p), 6-31+G(d,p), 6-311G(d,p), 6-311+G(d,p), 6-311+G(2d,p) and 6-311++g(d,p).

In the chapter we have tested "Dunning's Correlation-Consistent Basis Sets", it is pointed out that basis sets optimized at the Hartree-Fock level might and not be ideal for correlated computations, The "correlation consistent" basis sets are

optimized using correlated (CISD) wave functions cc-pVXZ means a Dunning correlation-consistent, polarized valence, X-zeta basis; X=D,T,Q,5,6,7 Functions are added in shells. cc-pVDZ for C atom consists of 3s2p1d. cc-pVTZ would be 4s3p2d1f. cc-pVQZ would be 5s4p3d2f1g.

2.5   Electron Correlation Energy

The Hartree–Fock method generates approximate solutions to the Schrödinger equation, where the real electron–electron interaction is replaced by an average interaction. At the complete basis set limit, the HF wave function extracts ~ 99% of the total energy of a system but the remaining ~1% is very important to describe the chemistry of a system. The difference between the HF energy at the complete basis set limit and the exact energy of a system, is called the electron correlation energy (E_{corr}), where[48]

$$E_{corr} = E_{exact} - E_{HF} \tag{2.11}$$

2.6   Density Functional Theory

The main quantity of DFT is the *electron density* $\rho(r)$ that obtained as the square of the wave function for an N-electron system integrated over N-1 spatial electron coordinates an N spin coordinated. Thus, the electron density is a non-negative function of only three spatial coordinates.

$$\rho(r) = N \int \cdots \int \left| \Psi\left(x_{1,}, \ldots, x_N\right) \right|^2 dx_1 dx_2 \ldots dxN \tag{2.12}$$

And it vanishes at infinity and yields the total number N of electrons in the system when integrated

$$\int \rho(r_1) dr_1 = N \tag{2.13}$$

$$\rho(r \to \infty) = 0 \tag{2.14}$$

At the position of atoms $\rho(r)$ possesses maxima. In contrast to the many-electron Wave function, the electron density is not solely a complicated mathematical structure but a physical observable and that can be experimentally determined (e.g by X-ray diffraction methods.

A theoretical foundation of DFT was given by the two Hohenberg Kohn theorems, proved that the ground-state electronic energy is determined completely by the electron density $\rho(r)$ and that there is a variational principle analogous to that in wave mechanics when using the electron density as a parameter. Thus a one-to-one relation between $\rho(r)$ of a system and energy exists, and according to density functional theory, energy is a unique functional of an electron density, $E|\rho(r)|$.

In spite of proven that the ground-state electron density and the ground-state energy are connected with each other, DFT has problem to define an exact functional to prove it.

According to wave mechanics approach, the energy funcational can be divided into three parts: kinetic energy, $T[\rho]$, an attraction between the nuclei and electrons, $E_{Ne}[\rho]$, and electron-electron repulsion, $E_{ee}[\rho]$. The nuclear-nuclear repulsion is a constant in the Born Oppenheimer approximation and a comparison of electron-electron repulsion with Hartree-Fock theory suggests that the, $E_{ee}[\rho]$ term should be spilt into a Coulomb and exchange parts, $J[\rho]$ and $K[\rho]$ including electron correlation in all terms. In the classical expression, mathematical form are known for the $E_{Ne}[\rho]$ and $J[\rho]$

$$E_{Ne}[\rho] = \int \rho(r) V_{Ne} dr = \sum_A^M \int \frac{Z_A \rho(r_1)}{r_{1A}} dr \tag{2.15}$$

$$J[\rho] = \frac{1}{2} \int\int \frac{\rho(r_1)\rho(r_2)}{r_{12}} dr_1 dr_2 \tag{2.16}$$

The prefactor ½ allows the integration to run over all space for both variables.

A non-interacting uniform electron gas model was used, in attempts at finding functionals for the kinetic and exchange energies and for such a system it can be shown that $T[\rho]$ and $K[\rho]$ are given by

$$T_{Ne}[\rho] = \frac{3}{10}\left(3\pi^2\right)^{\frac{2}{3}} \int \rho^{\frac{5}{3}}(r)\, dr \tag{2.17}$$

And

$$T_D[\rho] = -\frac{3}{4}\left(\frac{3}{\pi}\right)^{\frac{1}{3}} \int \rho^{\frac{4}{3}}(r)\, dr \tag{2.18}$$

Energy functional $E_{TF}[\rho] = T_{TF}[\rho] + E_{NE}[\rho] + J[\rho]$ is known as Thomas-Fermi theory and if the $K_D[\rho]$ part is included, then it calls Thomas-Fermi Dirac model. For atomic or a molecular systems, assumption as a non-interacting uniform electron gas is not a good approximation. These models predict total energy with 15-50% error and worst part is that these theory not able to predict bonding.

The introduction of orbitals by Kohn and Sham is a major breakthrough in computational chemistry. They had realized that the main problem in TF models is that the kinetic energy is represented poorly but the HF method performs better in this respect. Kohn and Sham then introduced the concept of a non-interacting reference system built from a set of one-electron orbitals ϕ_i in a way that the major part of the kinetic energy can be computed exactly and the remaining small part of the total energy is determined by an approximate functional.

According to Kohn Sham (KS) theory, to calculate part of the kinetic energy exactly one can assume a Hamiltonian operator as

$$\hat{H} = \hat{T}_e + \hat{V}_{ext}(\lambda) + \lambda \hat{V}_{ee} \tag{2.19}$$

With $0 \le \lambda \le 1$. The $\hat{V}_{ext}$ operator is equal to $\hat{V}_{Ne}$ for $\lambda = 1$, and for intermediate λ

Values, $\hat{V}_{ext}(\lambda)$ is adjusted as such that same density is obtained for both $\lambda = 1$ (real system) and for $\lambda = 0$ (non-interacting system). For $\lambda = 0$ the exact solution to the Schrodinger equation is given as a Slater determinant composed of molecular orbitals ϕ_i for which the exact kinetic energy functional is given as

$$T_S = \sum_{i=1}^{N} \left\langle \phi_i \left| -\frac{1}{2}\nabla_i^2 \right| \phi_i \right\rangle \tag{2.20}$$

Where the subscript S indicates, kinetics energy of a Slater determinant, $\lambda = 1$

is for interacting electrons, and is an approximation to the real kinetic energy and that is an improvement over the TF model. Kohn Sham theory calculate kinetic energy using equation 2...with assumption of non-interacting electrons, similar to HF theory though in actual electrons are interacting, means this approach does not provide total   kinetic energy of the real system.   But other hand the difference between calculated kinetic energy with above assumption and real kinetic energy is very small. In this theory the remaining kinetic energy is included as an exchange-correlation term and now the DFT energy expression is

$$E_{DFT}\left[\rho\right]=T_S\left[\rho\right]+E_{Ne}\left[\rho\right]+J\left[\rho\right]+E_{XC}\left[\rho\right]\tag{2.21}$$

$$=T_S\left[\rho\right]+\int V_{Ne\rho}\left(r\right)dr+\frac{1}{2}\int\int\frac{\rho\left(r_1\right)\rho\left(r_2\right)}{r_{12}}dr_1dr_2+E_{XC}\left[\rho\right]\tag{2.22}$$

$$=-\frac{1}{2}\sum_{i}^{N}\left\langle\phi_i\left|\nabla_i^2\right|\phi_i\right\rangle-\sum_{i}^{N}\sum_{A}^{M}\int\frac{Z_A}{r_{1A}}\left|\phi_i\left(r_1\right)\right|^2dr_1$$
$$+\frac{1}{2}\sum_{i}^{N}\sum_{j}^{N}\int\int\left|\phi_i\left(r_1\right)\right|^2\frac{1}{r_{12}}\left|\phi_i\left(r_2\right)\right|^2dr_1dr_2+E_{XC}\left[\rho\right]\tag{2.23}$$

And E_{XC} Definition can be obtained as

$$E_{XC}\left[\rho\right]=\left(T\left[\rho\right]-T_S\left[\rho\right]\right)+\left(E_{ee}\left[\rho\right]-J\left[\rho\right]\right)\tag{2.24}$$

According to above equation E_{XC} contains all unknown contribution to the exact total energy, first part in this equation may be considered as the kinetic correlation energy, and the second one contains both exchange and potential correlation energy.

Another question that needs to be answered is how the orbitals ϕ_i of the non-interacting reference system is defined, and to solve this question, the set of orthogonal orbitals ϕ_i which minimize the energy have to be calculated using the Lagrange method, as with the HF method.

$$L\left[\rho\right]=E_{DFT}\left[\rho\right]-\sum_{ij}^{N}\lambda_{ij}\left[\left\langle\phi_i\right|\ \left.\right\rangle\phi_i-\delta_{ij}\right]\tag{2.25}$$

Required variation of L to vanish leads to a set of equations involving the effective one-electron Kohn-Sham operator h_{KS}, similar the Fock operator in wave mechanics.

$$h_{KS}\phi_i = \sum_j^N \lambda_{ij}\phi_j \tag{2.26}$$

$$h_{KS} = -\frac{1}{2}\nabla^2 + V_{eff}(r) \tag{2.27}$$

$$V_{eff}(r) = V_{Ne}(r) + \int \frac{\rho(r_2)}{r_{12}}dr_2 + V_{XC}(r) \tag{2.28}$$

A set of canonical Kohn-Sham (KS) orbitals is obtained by apply a unitary transformation and the resulting eigenvalue equation know as KS equation

$$h_{KS}\phi_i = \varepsilon_i\phi_i \tag{2.29}$$

And the unknown orbital then may be obtained numerically or expanded in a set of basis functions, as to the HF method.

Where the Kohn-Sham (KS) one-electron operator is represented by

$$h_i^{KS} = -\frac{1}{2}\nabla_i^2 - \sum_k^{nuclei} \frac{Z_k}{|r_i - r_k|} + \int \frac{\rho(r')}{|r_i - r'|}dr' + \upsilon_{xc} \tag{2.30}$$

and

$$\upsilon_{xc} = \frac{\delta E_{xc}}{\delta\rho} \quad . \tag{2.31}$$

υ_{XC} is called the exchange-correlation potential.

Density functional theory and Hartree-Fock calculations demand similar computational costs to obtain the total energy of a molecule. At the cost of HF, DFT yields the energy of a system that includes electron correlation. This is the distinct advantage of DFT over the traditional ab initio methods [49].The Kohn Sham formulation of DFT is exact in principle but the E_{xc} term is approximated through exchange and correlation functional.

Many functionals have been designed using the Hohenberg–Kohn approach to relate the electron density to energy. The real problem is the exchange-correlation term of eqn. (2.17) and there is no way to derive this term. Therefore, numerous approximate functionals have been proposed over a period of time. There is no way to improve a functional's performance systematically as in the case of post-HF methods. In post-HF methods, results can be improved systematically by increasing the number of wave functions used to account electron correlation effect. In DFT, if a given functional does not provide an "accurate" result, then a new functional needs to be developed.

2.6.1 Exchange-Correlation Functionals

In this section we have presented s schematic structure of approximate exchange-correlation functionals. As discussed above, what we need is an approximate expression for an exchange-Correlation functional. There have been countless efforts to find suitable approximate solutions. The simplest one is known as the local density approximation (LDA), which is also the starting point for many sophisticated functionals in use today. In this approximation, the exchange correlation energy is defined as

$$E_{xc}^{LDA}[\rho] = \int \rho(\vec{r})\, \varepsilon_{xc}(\rho)\, dr \qquad (2.32)$$

According to above equation an apparent choice will be to assume $\varepsilon_{XC}(\rho)$ to be the exchange and the correlation energy of the uniform electron gas of density ρ.

This energy per particle is weighted with the probability ρ this is the local density approximation (LDA). The quantity $E_{XC}(\rho)$ can be separated into exchange and correlation contributions;

$$\varepsilon_{xc}(\rho) = \varepsilon_x(\rho) + \varepsilon_c(\rho) \qquad (2.33)$$

This functional is generally referred to as a model for a uniform homogeneous electron gas. The term E_{xc}, energy density depends on the electron density and it is expressed as an interaction between the electron density and an energy. The energy density ε_{xc} is always treated as a sum of individual exchange and correlation contributions

The Dirac form can be used for the exchange energy (ε_x).

$$\varepsilon_x = C\rho^{\frac{1}{3}}, \qquad\qquad (2.34)$$

where C is a free constant to be determined, For polarizabilities calculation, LDA and local spin density (LSD) functionals are found performing much better than the HF [50];. Nevertheless, the accuracy of these methods is insufficient for treating systems of chemical interest. These functionals generally are used in solid state physics.

2.6.2 Generalized Gradient Approximation (GGA)

In a molecular system the electron density is not uniform and that is good reason to believe that the LDA will have limitations and to overcome this limitation the best choice will be to in addition to density considering gradient of the charge density, $\nabla\rho$ in order to account for the non-homogeneity of the true electron density. This functional then defined as 'generalized gradient approximation, which is usually written as

$$E_{xc} \approx \int \rho(r)\varepsilon_{xc}(\rho, \nabla\rho)dr. \qquad\qquad (2.35)$$

It was found in our calculation for the fluorine substituted aromatic geometries that the GGA based functionals are much better in computing geometries and NMR properties than the LDA based functionals. Since early 1990, DFT is widespread accepted in theoretical chemistry community during and since then, a number of functionals within the GGA family [51-55] have been developed. The performance of these functionals will be discussed in the application part of this thesis.

2.6.3 Meta-GGA

In search of functionals that consider approximation of energy beyond GGA by taking second order gradients and the (non-interacting) kinetic energy density into account leads to a new family of functionals, which has been termed meta-generalized gradient approximation (meta-GGA) by Perdew et al., 1999 [9, 56]. They are typically represented as

$$E_{xc} \approx \int \rho(r)\varepsilon_{xc}(\rho|\nabla\rho|\nabla^2\rho, \tau)dr, \qquad\qquad (2.36)$$

Where kinetic energy τ is $\tau = \frac{1}{2}\sum_i |\nabla\varphi_i|^2$ and added kinetic energy gradient to GGA function further improve the description of the linear response of the uniform

electron gas. LDA and GGA functionals nuclei that are too deshielded and popular hybrid functionals such as B3LYP are often less accurate then GGA functional in predicting NMR chemical shifts. Zhao et al., has shown that meta-GGA produced improved ^{13}C NMR shifts as compared to GGA or LSDA. In this report we also tested some meta-GGA functionals performance in predicting ^{19}F NMR chemical shifts.

2.6.4 Hybrid Functionals

A HF hybrid functional represents a hybrid between pure density functional for exchange and exact Hartree-Fock exchange. Their development was based on the fact that instead of using an approximate functional for the exchange energy, the exact exchange from the HF method could be used. Becke adopted this approach in the definition of a new functional and he defined coefficients for exchange and correlation to fit to the observed atomization energies, ionization potentials, proton affinities and total atomic energies for a number of small molecules for example for B3LYP. The resultant (three parameter) energy functional is [57]

$$E_{xc} = E_{xc}^{LDA} + 0.2(E_X^{Fock} - E_X^{LDA}) + 0.72\Delta_X^{B88} + 0.81\Delta E_c^{LYP} \quad . \qquad (2.27)$$

Here Δ_x^{B88} and Δ_c^{LYP} are widely used GGA corrections to the LDA exchange and correlation energy, respectively. It is known as the B3LYP method, which is the most used DFT method till date [58]

3 Theoretical Background of NMR Parameters and Magnetic Coupling Constants

3.1 Introduction

This chapter discuss about the theoretical aspects of NMR chemical shifts calculation and estimation of exchange coupling constants in nitronyl-nitroxides. We discuss here basics of NMR, shielding tensors, chemical shifts and theoretical approaches that use to predict these NMR parameters. The Nuclear Magnetic Resonance (NMR) spectroscopy is one of the most powerful techniques used for the structure determination and dynamical processes [34, 59]. The recent development in NMR instrumentation and theoretical methodology provide new possibilities for chemical structural evaluation. NMR parameters, such as chemical shifts, indirect spin-spin coupling constants, and direct dipole-dipole coupling constants are the quantities determined by chemical structure. These NMR parameters are influenced by internal dynamics of the molecule and intramolecular interactions. An experimentally observed NMR chemical shifts and spin-spin coupling constants are an average over the values belonging to all geometrical isomers arising during the course of NMR experiment [60]. There is no direct description of chemical shifts dependence on either internal molecular dynamics or intermolecular interactions and therefore the coupling constants and the nuclear Overhauser effect is used to define interatomic distances and that help in an NMR molecular structure determination. Nevertheless it is strongly believed that theoretical calculation of NMR chemical shift and spin-spin coupling constants can provide in-depth chemical structural information [34] . An accurate calculation of NMR shifts is very much desired and that poses challenges for computational chemists to produce some simplified theory to predict accurate NMR chemical shifts.

In the recent past great efforts have been devoted to the development of new theoretical approaches to predict the NMR parameters[35, 61]. The aim of NMR calculations in general, is to help experimentalists to interpreting the observed NMR spectra. An accurate chemical shifts and coupling constant relationship makes the interpretation of the experimental data easier and this brings computation reliable prediction of NMR chemical shifts in high demand. To design a computational approach, that can predict experimental comparable NMR shifts and can help

resolving complex NMR experimental data, it is very much needed to understand basics theory behind the NMR experiment.

An NMR experiment involves studying a collection of interacting nuclear spins. In the simplest cases, these are the spins of nuclei in one molecule, or in a portion of one molecule; this group of spins is called the spin system. The entire (bulk) sample consists of a (statistical mechanical) ensemble of spin systems. Any theoretical treatment either of a single spin system or of a bulk collection of spin systems begins with the spin Hamiltonians. The total Hamiltonian, H, for any particular spin system is the summation of individual Hamiltonians that describe particular interactions, indicated by λ, that are present: A simplest Hamiltonian can be written as[62]

$$H = \sum_{\lambda}^{\substack{\text{inter-} \\ \text{actions}}} H_{\lambda} \tag{3.1}$$

$$H = H_Z + H_J + H_{CS} + H_{DIP} + H_{RDM} + H_{\perp} + H_2 \tag{3.2}$$

Where H_Z =Zeeman, H_J =Scalar coupling, H_{CS} =Chemical shifts, H_{DIP} =Dipole-dipole, H_{RDM} =Random field, $H_{\perp}$ = rf Field, H_2 =Relaxation

The first three interactions define the structure of a high-resolution NMR spectrum, and the last four become important when one seeks to excite a spin system to obtain the spectrum or when it is necessary to describe the return of an ensemble of spins to their equilibrium condition.

NMR phenomena are shown by any nuclei that can be expressed as

$$\mu = \gamma \hbar I \tag{3.3}$$

Where γ is the gyromagnetic ratio of the nucleus and $\hbar I$ is the spin angular momentum and in the presence of a magnetic field of flux density **B**, an interaction is set up between μ and Bo and the spin interaction energy E is given by

$$E = -\mu.B_0 \tag{3.4}$$

which will be quantized into $2I + 1$ levels. The splitting corresponds to the spin angular momentum along B_0 being restricted to one of a set of discrete values with corresponding energy Em given by

$$E_m = -m\gamma\hbar B_0 \tag{3.5}$$

Where m= I, (I-1), ….. –I. I may be integral or half-integral depending on the properties of the nucleus. The distribution of the spin states at thermal equilibrium is governed by the Boltzmann law [63]
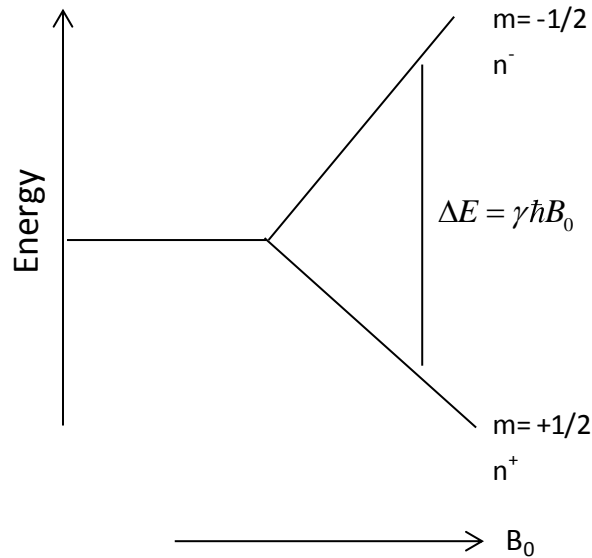
Figure 3.1 Variation of the difference in energy between spin levels as a function of magnetic flux density Bo.

 At thermal equilibrium the distribution of the number of spins, n^- and n^+, in each of the respective levels is governed by the Boltzmann law, such that the ratio $\dfrac{n^-}{n^+} = \exp\left(-\Delta E / kT\right).$

The difference in energy ΔE between the two levels is clearly

$$\Delta E = \gamma\hbar B_0 \tag{3.6}$$

 Understanding about NMR chemical shift, in NMR spectra measurement, when a molecule is placed in a magnetic field, its electrons circulate about the direction of the applied magnetic field. This circulation causes a small magnetic field at the nucleus which opposes the external applied field. The effective magnetic field experienced by the nucleus, therefore less than from the applied external field by a fraction of σ and effective magnetic field can be written as in equation.

$$B_{effective} = B_0 (1- \sigma) \tag{3.7}$$

In Equation 3.1, B_0 is an applied magnetic field and because of the electron density around each nucleus in a molecule its magnitude varies according to the types of nuclei and bonds in the molecule. The opposing field, B_0 and the effective magnetic field at each nucleus will vary and the resonance frequency of different nuclei is very much different to each other and this variation will depend on the strength of applied magnetic field, B_o. Higher the value of applied filed B_o, consequently, greater is the difference in frequencies. This relationship could make it difficult to compare NMR spectra taken on spectrometers operating at different magnetic field strengths and to avoid this problem the term NMR chemical shift δ was developed. The NMR chemical shift of a nucleus is the difference between the resonance frequency of the nucleus and a standard.

The NMR chemical shift, δ is defined in terms of the resonance frequencies, v of the sample of interest and of the reference nuclei

$$\delta = \frac{v_{sample} - v_{ref}}{v_{ref}} 10^6$$

(3.8)

The resonance frequency of a particular nucleus may be defined as

$$v = \frac{\gamma B_0}{2\pi}(1-\sigma)$$

(3.9)

Here γ is the magnetogyric ratio a characteristic of a given isotope, B_0 is the externally applied magnetic field, and σ is the nuclear magnetic shielding constant particular to the chemical environment. Substitution of equation 3.9 into equation 3.8 gives the relationship between σ and δ:

$$\delta = \frac{\sigma_{ref} - \sigma_{sample}}{1-\sigma_{ref}}$$

(3.10)

If σ_{ref} is very small as compared to unity, the above expression becomes.

$$\delta = \sigma_{ref} - \sigma_{sample}$$

(3.11)

According to above relationship, accurate prediction of chemical shifts is very much dependent on chemical shielding tensors.

3.2   The NMR Shielding Tensors

The calculation of shielding constants is difficult, even for small molecules, because it requires detailed information about the distribution of electron density in the ground and excited states energies and the excitation energies of the molecule. Although when certain approximations are used to account electron density distribution, then it is possible to calculate shielding constant for substantially large molecules. For all types of approximation, it is important to understand the different contributions to shielding tensor. Nowadays different empirical approaches are available even for the large molecules and these approaches consider that the measured shielding constant is the sum of three contributions:

$$\sigma \text{ (total)} = \sigma \text{ (local)} + \sigma(\text{neighbor}) + \sigma \text{ (solvent)} \qquad (3.12)$$

The local contribution, σ (local), is the contribution of the electrons of the atom that contains the nucleus in the study. The adjacent group contribution σ (neighbor) is an interaction to sigma from the groups of atoms that form the rest of the molecule. The solvent contribution, σ(solvent), is the contribution from the solvent molecules.

The local contribution to the shielding constant is considered as the sum of a diamagnetic contribution, σ_d and a paramagnetic contribution, σ_p

$$\sigma_{\text{local}} = \sigma_d + \sigma_p$$

A diamagnetic contribution, σ_d to opposes the applied magnetic field and shields the nucleus in study. The magnitude of the diamagnetic contribution to the shielding depends on the average distance of the electrons from the nucleus in question. The paramagnetic contribution to the shielding constant arises from the interaction of the nucleus with the field generated by the paramagnetic currents and therefore it depends on the ability of the applied field to mix excited states into the ground state A paramagnetic contribution σ_p to reinforces the applied magnetic field and de-shields the nucleus in question. The local paramagnetic contribution σ_p arises from the ability of the applied field to force electrons to circulate through the molecule by making use of orbitals that are unoccupied in the ground state.

The total local contribution is positive if the diamagnetic contribution dominates, and is negative if the paramagnetic contribution dominates. The diamagnetic contribution arises from the ability of the applied field to generate a circulation of

charge in the ground-state electron distribution of the atom. The circulation of charge generates a magnetic field that opposes the applied field and hence shields the nucleus. The magnitude of σ_d depends on the electron density close to the nucleus

The diamagnetic contribution is the only contribution to the local shielding from inner cores of atoms, for cores remain spherical even though the atom may be a component of a molecule and its valence electron distribution highly distorted. The diamagnetic contribution is broadly proportional to the electron density of the atom containing the nucleus of study.

The neighboring group contribution arises from the currents induced in nearby groups of atoms.

A solvent can influence the local magnetic field experienced by a nucleus in a variety of ways. Some of these effects arise from specific interactions between the solute and the solvent (such as hydrogen-bond formation and other forms of Lewis acid-base complex formation). The anisotropy of the magnetic susceptibility of the solvent molecules, especially if they are aromatic, can also be the source of a local magnetic field.

3.3   Chemical Shielding Tensor and Total Energy Relationship

we discuss in this chapter the nuclear shielding and spin-spin coupling constants to quantities that are obtainable from the electronic wave function [34]. The energy levels studied in NMR spectroscopy are the spin eigen-states of chemically bonded nuclei in the presence of an external magnetic field. The interactions of the magnetic moments of the NMR active nuclei (i.e. ^{1}H, ^{13}C, ^{19}F) with the magnetic field are modified by the surrounding electrons of a closed-shell electronic system. Although these interactions are rather complicated, the main features of NMR spectra may be satisfactorily accounted for by the solution of the energy equation for a simple effective spin-Hamiltonian where the electrons do not appear at all and where the nuclei are represented only by their intrinsic spins and their associated magnetic moments. This effective Hamiltonian may be written as equation 3.8 [34]

$$H = \sum_{K} \gamma_K \hbar B^T (1 - \sigma_K) I_K + \frac{1}{2} \sum_{K \neq L} \gamma_K \gamma_L \hbar^2 I_K^T (D_{KL} + K_{KL}) I_L \qquad (3.13)$$

Equation 3.8 shows a spin Hamiltonian that widely used for NMR calculation and here σ_K nuclear magnetic shielding tensors and γ_K the nuclear magnetogyric ratios and D_{KL}, which describes the direct couplings of the nuclear magnetic dipole moments; and the reduced indirect nuclear spin-spin coupling tensors K_{KL}, which describes the indirect couplings of the nuclear dipoles, mediated by the surrounding electrons. I_K the nuclear spin operators, related to the nuclear magnetic dipole μ_K as

$$\mu_K = \gamma_K \hbar I_K \tag{3.14}$$

The NMR spin Hamiltonian in equation 3.8 is effective in the sense that it's solutions reproduce the nuclear magnetic energy levels in a molecular system without reference to the electrons. It should be noted that, in the absence of the surrounding electrons (as assumed), the shielding constants and the indirect spin-spin coupling constants would vanish, leaving the NMR spectrum to be determined solely by the nuclear Zeeman term $-B^T . \mu_K$ and by the direct dipolar couplings $\mu_K^T D_{KL} \mu_L$. The magnitudes of the nuclear dipole moments μ_K are of the order of 10^{-4} atomic units and a magnetic induction B of 10 T (available in magnetic resonance experiments) corresponds to 4.3×10^{-5} atomic units.

For a restricted representation of the electronic energy in the presence of an external magnetic field and nuclear magnetic moments, we expand the electronic energy in the magnetic induction B and in the nuclear moments μ around zero field and zero magnetic moments. Actually, these interactions are small as compared to chemical bonding and over all perturbations introduced during NMR transition are small. The smallness of the effects permits the application of perturbation theory to the calculation of the NMR parameters from the electronic wave function.

Accepting the adequacy of the spin-Hamiltonian approach, we shall now establish a relationship of the nuclear shielding and spin-spin coupling constants to quantities that are obtainable from the electronic wave function. For a close representation of the electronic energy in the presence of an external magnetic field and nuclear magnetic moments, we expand the electronic energy in the magnetic induction B and in the nuclear moments μ_K around zero fields μ_K and zero magnetic moments

$$E(B,\mu) = E_0 + \frac{1}{2}B^T E^{(20)} B + \sum_K B^T E^{(11)} \mu_K + \frac{1}{2}\sum_{K \neq L} \mu_K^T E_{KL}^{02} \mu_L \tag{3.15}$$

At the expansion of above total derivatives are

$$E^{20} = \left. \frac{d^2 E(B,\mu)}{dB^2} \right|_{B=0,\ \mu=0} \tag{3.16}$$

$$E_K^{(11)} = \left. \frac{d^2 E(B,\mu)}{dB\ dM_K} \right|_{B=0,\ \mu=0} \tag{3.17}$$

$$E_{KL}^{(02)} = \left. \frac{d^2 E(B,\mu)}{d\mu_K\ d\mu_L} \right|_{B=0,\ \mu=0} \tag{3.18}$$

Here in these expressions, $\mu = \{\mu_K\}$ represents collective magnetic moments. It should be noted that for closed-shell systems, the first-order terms vanish identically and have therefore not been included in the expansion of $E(B,\mu)$ in equation 3.15 also, higher than second-order terms may be neglected, due to the smallness of the perturbations. For a rigid, nonrotating molecule, the simple expression equation 3.16 therefore gives an accurate representation of the electronic energy in the presence of an external magnetic field and magnetic nuclei. Comparing the expansion equation 3.15 with the NMR spin-Hamiltonian in equation 3.13, we identify the $E_K^{(11)}$ with the nuclear shielding tensors and $E_K^{(22)}$ with the spin-spin coupling tensors

$$\sigma_K = E_K^{(11)} + 1 \tag{3.19}$$

$$K_{KL} = E_{KL}^{(02)} - D_{KL} \tag{3.20}$$

The $E^{(20)}$ tensor represents the molecular magnetizability and does not enter the spin-Hamiltonian. We note that the absence of first-order terms in the expansion of the closed-shell energy as well as the smallness of higher-order terms serve as a justification of the effective spin Hamiltonian equation 3.13, where only terms bilinear in the external field and in the nuclear magnetic moments appear. From the point of view of molecular electronic structure theory, the shielding constants

equation 3.19 and the indirect spin-spin coupling constants equation 3.20 are particular examples of molecular properties. When a molecular electronic system is modified by a perturbation x, it's total energy changes.

$$E(x) = E^{(0)} + E^{(1)}x + \frac{1}{2}x^T E^{(2)}x + ...$$
(3.21)

The coefficients of this expansion are characteristic of the molecular system in a given quantum state and are known as molecular properties. When the perturbation is static (that is, time-independent, as for the NMR properties studied here for a homogeneous magnetic field), the molecular properties may be calculated by differentiation

$$E^{(1)} = \left.\frac{dE}{dx}\right|_{x=0}$$
(3.22)

$$E^{(2)} = \left.\frac{d^2E}{dx^2}\right|_{x=0}$$
(3.23)

Though general expression for the nuclear shielding and indirect spin-spin coupling constants were established long time before but development of ab initio methods took long time because of the problems specific to the shielding constants (the gauge dependence of the approximate results) and to the spin-spin coupling constants (the triplet nature of the perturbation. Gauge problem has been solved up to a great extent that

3.4 Different Techniques to Deal with the Gauge Origin Problem

A gauge origin problem arise when a magnetic field present in the Hamiltonian such as in the calculation of magnetic properties. The vector potential representing the external magnetic field induction $\vec{B}$ is

$$\vec{A}_O(r) = \frac{1}{2}\vec{B} \times (\vec{r} - \vec{O})$$
(3.24)

And with Hamiltonian is not uniquely defined since we may freely choose the position of the gauge origin $\vec{O}$ and still satisfy the requirement that $\vec{B} = \vec{\nabla} \times \vec{A}_O(\vec{r})$ The total energy of an atom or a molecule in a magnetic field is independent of the gauge origin and it is necessary that all derivatives of energy

should be invariant to change in gauge origin with respect to the applied magnetic field. However, the diamagnetic and paramagnetic contributions depend individually on the gauge origin. But the total nuclear shielding tensor is indeed independent of the choice of R_0

$$\sigma_{\alpha\beta}^A(R_0) - \sigma_{\alpha\beta}^A(0) = 0 \qquad (3.25)$$

Table 3.1: A Summary of Different Techniques used to Deal with the Gauge Origin Problem

Method	Description	Performance & Comments
SGO[11]	Single-gauge origin methods (SGO),Gauge origin taken as the molecular origin	Very large basis sets lead to approximate gauge invariance. Within the limit of complete basis sets, it is of no practical use.
CSGT[64]	Continuous-Set-of-Gauge Transformations (CSGT) Gauge continuously transformed back to the reference	Superior to SGO, methods, although this method still requires adequately large basis sets.
IGAIM[65]	Individual Gauges for Atoms In Molecules (IGAIM) this approach has a similar methodology used in the CSGT but it does not use interpolation to regions between two nuclei.	IGAIM approach uses real-space information to distribute gauges, provides individual gauge invariant $\square_d$ and $\square_p$ contributions and may thus be interpreted as most rewarding. Slower basis set convergence compared to GIAO.
IGLO,LORG [66]	Individual Gauge for Localized Orbital, Localized-Orbital Local Origin (LORG)	Evaluates the values of $\square$ in terms of localized MOs, whose individual gauge origins are chosen. Less computational cost enables them to be used for large systems. Needs a proper MO localization scheme.
GIAO [67, 68]	Gauge Invariant Atomic Orbitals	Convergence of calculating $\square$ is faster with the GIAO method. In particular, calculations with double zeta basis sets provide good results for organic molecules.

The variational approach is normally used to obtain wave functions in the absence of the applied magnetic field, and an exact wave function will of course give origin-independent results, as will an HF wave function if a complete basis set is employed. However for practical basis sets the gauge error depends on the distance between the wave function and the gauge origin. Therefore, only approximate wave functions are used and the shielding constant values become origin dependent. There are various theoretical approaches used to deal with the gauge origin problem and some of them are in listed in Table 3.1

Table 3. 2 Calculated ^{19}F NMR shielding for C_6F_6 obtained with different methods using UB3LYP/SVP level of theory

Method	^{19}F σ_{iso}/ppm
SGO	391
IGAIM	325
CSGT	325
GIAO	363
Experiment (Ref)	351

.

Example in table 3.2 shows ^{19}F NMR shielding tensor calculated using different approaches to overcome gauge origin. In example, ^{19}F NMR shielding of hexafluorobenzene calculated at UB3LYP/SVP level of theory and a comparison of calculated shielding with experimental values shows that SGO approach highly overestimates experimental shielding tensors, while IGAIM and CSGT underestimate it and the best result obtained with GIAO. In this thesis most of the NMR shifts were calculated using GIAO approach.

3.5 Different Factor that Influence Theoretical NMR Shift Computation

In this thesis we investigate performance of various quantum chemical schemes in predicting accurate ^{19}F NMR chemical shifts and our emphasis will be on the following topics.

1. Electron-correlation effects as treated by different quantum chemical approaches,
2. Basis-set convergence effect in NMR chemical shift calculations,

3. Influence of geometry effect on computed shift accuracy
4. Performance of different approach that use to eliminate relative errors/ computation errors

Here we didn't evaluate the effect of vibrational on nuclear magnetic shielding constants or NMR chemical shifts evaluation such influence is limited to small molecules (e.g. diatomic molecules) and our aim is to predict accurate ^{19}F shifts for fluoroaromatic.

3.5 Calculation of Exchange Coupling Constants in Spin Dimers

In the second part of this thesis, we study the magnetic exchange coupling constant, for spin dimers, bis-nitronyl nitroxide and spin coupling in diradical may be described by Heisenberg Hamiltonian, H= 2JS$_1$.S$_2$, Where J is the magnetic exchange coupling constant, the ground-state total spin (S) is S=1 for J>0 (Feeromagnetic coupling and S=0 for J<0 (antiferromagnetic coupling) and the energy difference between the two states is ΔE_{ST}=2J. Different types of quantum chemical studies have been performed to predict accurate 2J values. In this chapter we give a brief account of the theoretical background of magnetic exchange coupling and how to obtain it in practice.

3.5.1 The Heisenberg-Dirac-VanVleck Hamiltonian (HDV)

Exchange coupling constant is very interesting property and specially the magnetic coupling via bridging group make magnetic exchange interaction more interesting as the bridging molecule can be a foundation of designing low dimensional magnetic materials [59]. Anderson strategy based model, orbital model of exchange interaction is still widely used to rationalize the magnetic properties of molecules and to derive qualitative magneto-structural correlations in bridged binuclear transition metal systems or in binuclear organic radical systems. In magnetically interacting system, the magnetic electrons are rather well localized onto single paramagnetic centers called magnetic orbitals. The interactions between the magnetic orbitals therefore carry out the onset of the exchange interactions.

Exchange interactions or so called magnetic exchange coupling are mainly determined by two factors: the exchange energy between electrons of equal spin, which favors a parallel alignment of the spins between two adjacent centers

(Anderson called it as potential exchange) and the overlap between the magnetic orbitals, which gives rise to a transfer of electron density between the paramagnetic centers and favors the antiparallel alignment of the spins (Anderson called it as kinetic exchange). The interaction between magnetic orbitals can be direct (direct exchange interaction) or can occur via ligand-centered orbitals (super-exchange interaction). Qualitatively, the exchange interactions can be understood in terms of exchange pathways, which connect the magnetic and ligand orbitals interacting by symmetry, and can be regarded as the highways for the propagation of the correlation between the magnetic electrons.

The phenomenon of exchange coupling has found widespread interest in diverse research areas such as molecular magnetism, materials science and biochemistry. In bioinorganic chemistry, an understanding of the magnetic interactions between metal centers provides useful information about the coordination environment about the metal centers, and it provides information about the nature of bridging ligands, and an assessment about the distance between the metal centers

In many biochemical and material science research areas, the experimental and theoretical characterization of the exchange coupling parameter is a key point of research interest.

At a phenomenological level, the exchange coupling is modeled by the well-known Heisenberg–Dirac–Van Vleck Hamiltonian [69]. The magnetic coupling of spins localized at molecular paramagnetic sites is justified in terms of model spin Hamiltonians. For two magnetic centers with total spins S_i and S_j, it is given by the Hamiltonian in 3.21 [38, 70]

$$H_{HDV} = -J_{ij}\hat{S}_i\hat{S}_j$$

(3.26)

Where J_{ij} is the magnetic coupling constant, it depends on the energy difference between different spin states, and $\hat{S}_i$ and $\hat{S}_j$ are spin operators for the paramagnetic centers i and j. The total spin operator of the interacting system is $\hat{S} = \hat{S}_i + \hat{S}_j$. In this particular definition of H_{HDV}, J is negative for the antiferromagnetic interaction (antiparallel spins) and positive for a ferromagnetic interaction (parallel spins).

While HDVV spin Hamiltonian provides a description of exchange interactions, though it does not provide any information about the origin of these interactions, nor

does it provide a systematic procedure for the accurate calculation of magnetic coupling constants for bridged transition metal complex [13]. The above approximation can be used to calculate the energy of the spin states.

The total spin angular momentum operator expressed in terms of component operators as given in Eq. 3.23 [71]

$$\hat{S}_{tot}^2 = \left(\hat{S}_i + \hat{S}_j\right)^2 = \hat{S}_i^2 + \hat{S}_j^2 + 2\hat{S}_i \cdot \hat{S}_j$$

(3.27)

It can be written as

$$2\hat{S}_i \cdot \hat{S}_j = \frac{1}{2}\left(\hat{S}_{tot}^2 - \hat{S}_i^2 - \hat{S}_j^2\right)$$

(3.28)

Since the eigenvalue of S^2 is $S(S+1)$, the energy of the state with spin S_{Tot} resulting from interaction of species with spins S_i and S_j is given by,

$$E_{Total} = -J_{ij}\left[S_{total}(S_{total}+1) - S_i(S_i+1) - S_j(S_j+1)\right]$$

(3.29)

Hence two doublets will have resulting coupling a triplet and a singlet (multiplicity 3 and 1) and in the case of ferromagnetic coupling (e.g. $J > 0$), the energy of the triplet state ($S = 1$) is,

$$E_{S=1} = -J\left[1(1+1) - \frac{1}{2}\left(\frac{1}{2}+1\right) - \frac{1}{2}\left(\frac{1}{2}+1\right)\right] = -J\left[2 - \frac{3}{4} - \frac{3}{4}\right] = -\frac{1}{2}J$$

(3.30)

The energy of the singlet state ($S = 0$) is,

$$E_{S=0} = -J\left[0(0+1) - \frac{1}{2}\left(\frac{1}{2}+1\right) - \frac{1}{2}\left(\frac{1}{2}+1\right)\right] = -J\left[0 - \frac{3}{4} - \frac{3}{4}\right] = \frac{3}{2}J$$

(3.31)

The singlet triplet gap (E_S-E_T), is given by

$$\Delta E_{ST} = E_{S=0} - E_{S=1} = \left(\frac{3}{2}J - (-)\frac{1}{2}J\right) = 2J$$

(3.32)
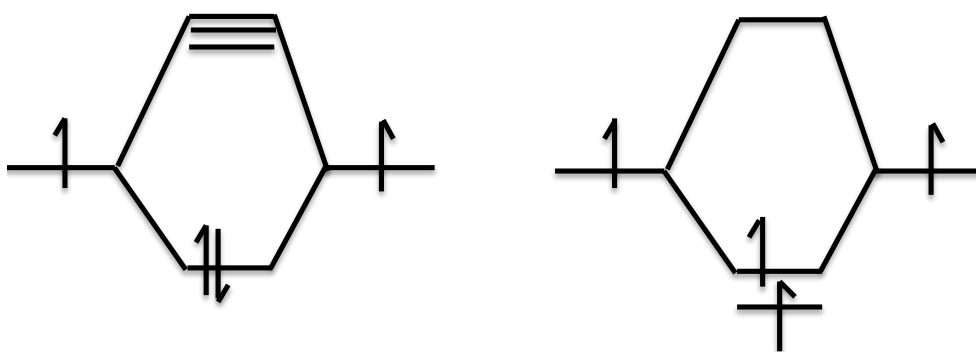
Figure 3. 1: Illustration of ΔEST resulting from antiferromagnetic and ferromagnetic interaction of spins.

3.5.2 The Broken-Symmetry Approach for Calculating *J* Values

Quantitative calculations of the magnetic exchange interactions J require an accurate description of the multiplet structure of the molecules for the ground and the lowest excited states[72]. This corresponds to the evaluation of the energies of all the spin states resulting from different occupations of a set of one-electron levels.

$$\Delta E_{ST} = E_S - E_T = E\left(\left|\uparrow\downarrow\right\rangle - \left|\downarrow\uparrow\right\rangle\right) - E\left(\left|\uparrow\uparrow\right\rangle\right) \tag{3.33}$$

For instance in equation 3.1, in the simple case of two active electrons, such as in nitronyl nitroxide diradical complexes, a correct representations of biradical singlet states needs more than one configuration $\left|\uparrow\downarrow\right\rangle$ or $\left|\downarrow\uparrow\right\rangle$, while one configuration is involved in the triplet state ($\left|\uparrow\uparrow\right\rangle$ and for singlet-triplet gap energy calculation, it is important to include all important configurations of the singlet state, and neglecting them leads to an underestimation of the singlet-triplet gap. This problem is more prominent in case of small energy gaps, loosely bound biradicals systems and in case of strongly interacting systems when there is strong antiferromagnetic couplings, the importance of this contribution decreases. This problem is minimized by the presence of strong antiferromagnetic couplings leading to large energy gaps between the ground and the excited singlet configurations. In such cases a single-determinant wave function is close to actual ground state wave function, whereas the situation is much complex in small magnetic couplings regime. A number of investigations have shown that these latter cases can be treated more effectively by computing the

energy of a fictive electronic state intermediate between high- and low-spin eigenstates. Singlet- triplet energy gap can be calculated accurately using post-HF methods such as FCI, DDCI but use of such methods is limited to very small chemical systems and cannot be used for chemically relevant systems because of very demanding computational resources, Noodleman has derived a computationally inexpensive way, the so-called broken symmetry (BS) approach to calculate J [73, 74]. Broken Symmetry calculation can be done either in unrestricted Hartree-Fock (UHF) or unrestricted density functional theory (UDFT). In BS calculation low spin open-shell molecular systems in which α and β densities are allowed to localize on different atomic centers and BS relates the energy of a broken symmetry single determinant, which is not an eigenstates of the spin operator S_2 to the energy of a pure spin state. Broken symmetry approach requires calculation of several single determinants and additionally the high spin state (HS).

According to Hay [75], the Heisenberg coupling constant J is related to the energy difference between states of spin S and (S − 1) and it can be represented as

$$- 2JS= (E(S) - E(S - 1))$$

According to Noodleman[76] approach J is proportional to the energy difference between the high spin state and the mixed spin state, E (S_{max}) - E_{BS}, while both energies are determined by SCF calculations. By the recursion relation for E(S), the energies of all the spin states can be obtained.

According Noodleman hypothesis, energies pure spin E(S) and mixed state E_B are represented as

$$E(S) =(\psi_S |H| \psi_S) =C + [n -S(S + 1)]J_F+ [n(n + 1) -S(S + 1)]J_{AF} =C' -S(S + 1)J$$

$$(3.34)$$

Here $J=J_F+J_{AF}$

$$E_B = (\psi_B |H| \psi_B) =C + \sum_{S=0}^{S_{max}} A_l(S)[n -S(S + 1)]J_F + \sum_{S=0}^{S_{max}} A_l(S)[n(n + 1) -S(S + 1)]J_{AF}$$

$$=C' - \sum_{S=0}^{S\,max} A_l(S)[S(S + 1)]J \qquad (3.35)$$

Subtracting Eq. (3.35) from Eq. (3.34) at S =S_{max} in Eq. (3.34),

$$E(S_{max}) - E_B = (-S_{max}(S_{max}+1) + \sum_{S=0}^{S_{max}} A1(S) \cdot S(S+1)) J$$

According to normalization condition

$$\sum_{S=0}^{S_{max}} A1(S) \cdot S(S+1) = n = S_{max} \tag{3.36}$$

and, therefore,

$$E(S_{max}) - E_B = -2S_{max}^2 J \tag{3.37}$$

For weakly coupled dimers $J_{AF} \gg J_F$ and the antiferromagnetic terms constitute the dominant contribution to J. Notice also that J can be calculated from Eq. (3.34) without the explicit evaluation of the individual Hamiltonian matrix elements or the overlap integrals

For a general case, when $S_i \neq S_j$,

$$J = -\frac{(E_{HS} - E_{BS})}{2S_i S_j} \tag{3.38}$$

Yamaguchi's gives scheme J_3 to calculate magnetic exchange coupling constant and this scheme is said to be applicable in all coupling range.[59]

$$J = \frac{-2(E_{HS} - E_{BS})}{\langle S \rangle_{HS}^2 - \langle S \rangle_{BS}^2} \tag{3.39}$$

Where the expectation value, $\langle S \rangle_{HS}, \langle S \rangle_{BS}$ for the high spin state and the broken symmetry state

According to Neese [70] is should be noted that expectation value of the S^2 operator depends on the overlap integrals between spin-up and spin-down electrons. For the corresponding orbitals, the expectation value over the BS wavefunction can be simplified as

$$\langle S^2 \rangle_{BS} = \left(\frac{N^\alpha - N^\beta}{2} \right) \left(\frac{N^\alpha - N^\beta}{2} + 1 \right) + N^\beta - \sum_i n_i^\alpha n_i^\beta \left| S_{ii}^{\alpha\beta} \right|^2 \tag{3.40}$$

Where N_α and N_β are the number of spin and spin-down electrons, and n_i^α and n_i^β are the occupation number and for two electrons in two-orbitals case $\langle S^2 \rangle_{BS} = 1 - S^2$ if all corresponding orbitals other than the 'magnetic pair have overlap exactly equal to 1 and the Yamaguchi 's equation then becomes

$$J = \frac{-2\left(E_{HS} - E_{BS}\right)}{1 + S^2} \tag{3.41}$$

For N_1 unpaired electrons localized on 'site 1' and N_2 unpaired electrons localized on a 'site 2' one can calculate the parameter J_{12} from two separate spin-unrestricted SCF calculations: (a) the calculation for the high-spin state with S=(N_1+N_2)/2 and (b) the `broken symmetry' calculation with Ms=(N1-N2) that features N_1 spin-up orbitals that are quasi localized on 'site 1' and N_2 spin-down electron that are quasi-localized on 'site 2' there are several formalism exists to extract J_{12}:

$$J_{12} = \frac{\left(E_{HS} - E_{BS}\right)}{\left(S_1 + S_2\right)^2} \tag{3.42}$$

$$J_{12} = \frac{\left(E_{HS} - E_{BS}\right)}{\left(S_1 + S_2\right)\left(S_1 + S_2 + 1\right)} \tag{3.43}$$

$$J_{12} = \frac{\left(E_{HS} - E_{BS}\right)}{\langle S^2 \rangle_{HS} - \langle S^2 \rangle_{BS}} \tag{3.44}$$

The last exchange coupling definition is valid approximately over the whole coupling strength regime, while the first equation implies the weak coupling limit and the second the strong coupling limit.

4. Calculation of ^{19}F NMR Shielding Tensors and Chemical Shifts of Fluoroaromatics

4.1 Introduction

According to Harding *et al.*[35], ^{19}F nuclear magnetic resonance (NMR) shieldings for small molecular systems in the gas phase can be predicted within 2 ppm accuracy, if post-Hartree-Fock(HF) methods such as CCSD(T) [77], in combination with large basis sets and high-quality molecular structures, e.g. from CCSD(T)/cc-pVTZ calculations are used [78]. When molecules with hydrogen-fluorine or carbon-fluorine bonds are considered MP2/qz2p shieldings corrected for vibrational and tempature effects at the HF-SCF/tz2p level might offer reasonable shieldings. (ref)Application of such methods, however, generally demands enormous computational resources, which makes them inefficient to apply to systems of chemically relevant sizes. Cramer *et al.*[79] have shown that the use of HF theory can produce ^{1}H and ^{13}C NMR shifts of 0.05 ppm and 5.0 ppm accuracy. Yet, HF fails to predict fluorine-chemical shifts because the non-bonding electrons of fluorine atoms can give rise to substantial electron-correlation contributions to ^{19}F NMR chemical shifts[80].

Methods based on density functional theory (DFT) offer an alternative to treat electron-correlation effects efficiently while its computational cost is of the same order as Hartree–Fock (HF) methods [78, 80-82]. However, the use of DFT methods has been criticized with respect to predicting ^{19}F shieldings as it has been found that some popular functionals such as B3LYP and BP86 were no better than HF-SCF. Interestingly, when ^{19}F NMR chemical shifts computed with DFT methods were compared with experimental data, a good agreement was observed in other work, which was interpreted in terms of favorable error cancellation [83].

In the past, the performance of a number of popular DFT functionals to predict ^{13}C NMR shifts has been investigated [10, 31]. Cheeseman *et al.* found that functionals such as BLYP and B3LYP, BPW91 and the corresponding hybrid functional B3PW91 in combination with the 6-311+G(2d,p) basis set showed significant improvement over HF, although none of the methods reached the accuracy of MP2[84]. Later Adamo and Barone showed that the hybrid functional PBE0 (also known as PBE1PBE) was able to produce shifts of comparable quality to MP2 results. Their conclusion was based on a comparison between calculated absolute ^{13}C shieldings with experimental values [82].

Additionally, various DFT approaches have been designed and tested to reproduce experimental ^{1}H, ^{13}C and ^{19}F NMR chemical shifts [9, 78, 84-86]. Unlike for post-HF based approaches, in DFT there is no systematic way to improve the results. The only choice to identify a suitable method for a set of systems under study is to try different functionals in combination with different basis sets for optimum performance. So far, large basis sets (cc-pVTZ, cc-pVQZ) in combination with post-HF methods have been recommended to compute ^{19}F shieldings [35, 86].

Our motivation is to identify a computational approach which would be computationally inexpensive, easy to use, and able to predict the relative ^{19}F NMR shifts for perfluorinated aromatic compounds within a target accuracy of about 4 ppm. In this chapter, various functionals and different basis sets are systematically tested for their performance in this respect. We will also discuss the quality of computed C-F bond lengths and we will examine the correlation between the quality of computed C-F bond lengths and ^{19}F NMR shifts.

4.2 Computational Details

All calculations reported in this chapter were carried out with the Gaussian 09 program [87]. DFT methods used are listed in Table 3.1.

We used 6 Minnesota-type functionals (M05[88], M05-2X[89], M06[89], M06-2X[89], M06-L[9, 90], M06HF[90]) and 17 other functionals commonly in use for various applications (LSDA [91], BP86[52, 92], BLYP[55, 92], BPW91[52, 53], B3P86[51, 52], B3PW91[51], BHandHLYP[51, 55], B3LYP[51, 55], PBE[54], PBE1PBE[54], B97-1[56], B97-2[56], OLYP[55, 81], O3LYP[55, 81, 93], TPSS[94, 95] TPSSh[94, 95], B97D[96]).

Unless mentioned otherwise, all DFT, HF and MP2 NMR calculations were performed using fully optimized geometries obtained at the same level of theory and the Gauge Invariant Atomic Orbitals (GIAO) approach was employed [34]. In this chapter, different types of basis sets were employed including the IGLO-II and IGLO-III basis sets specifically designed for NMR calculations [97], as well as several standard Pople-style basis sets ranging from 6-31G(d,p) to 6-311++G(2d,p).[98-101].

Table 4. 1: List of exchange-correlation functionals used in this chapter.

Method	[a]X_{HF}	Year	[b]Type	Exchange/correlation functional	References
LSDA	0	1980	LDA	S/VWN	[102]
BP86	0	1988	GGA	B/P86	[51, 52]
BLYP	0	1988	GGA	B/LYP	[51, 55]
BPW91	0	1992	GGA	B88/PW91	[52, 53]
B3P86	20	1993	HGGA	B/P86	[51, 52]
B3PW91	20	1993	HGGA	B/PW91	[51]
BHandH	50	1993	HGGA	B/LYP	[51, 55]
B3LYP	20	1994	HGGA	B/LYP	[51, 55]
PBE	0	1996	HGGA	PBE/PBE	[54]
PBE1PBE	25	1996	HGGA	PBE/PBE	[54]
B97-1	21	1998	HGGA	B97-1/PW91	[56]
B97-2	21	2001	HGGA	B97-2/B97-2	[56]
OLYP	0	2001	GGA	O/LYP	[55, 81]
O3LYP	12	2001	HGGA	O/LYP	[55, 81, 93]
TPSS	0	2003	MGGA	TPSS	[94, 95]
TPSSh	10	2003	HMGGA	TPSS	[94, 95]
B97D	0	2006	GGA	B97	[96]
M05	28	2005	MGGA	M05	[88]
M05-2X	56	2006	HMGGA	M05-2X	[89]
M06	27	2008	HMGGA	M06	[89]
M06-2X	54	2008	HMGGA	M06-2X	[89]
M06-L	0	2006	MGGA	M06-L	[9, 90]
M06HF	100	2006	HMGGA	M06-HF	[90]

B = Becke88, P = Perdew86, LYP = Lee−Yang−Parr, PW91 = Perdew-Wang91, O = OPTX, a X_{HF} = amount of Fock-exchange admixture. b LDA = Local Density Approximation, GGA = Generalized gradient approximation, HGGA = Hybrid generalized gradient approximation, MGGA = Meta generalized gradient approximation, HMGGA = Hybrid meta generalized gradient approximation.

The correlation-consistent basis sets developed by Dunning and co-workers, cc-pVXZ (X=D,T,Q,5) [103, 104] are also included in the test. The performance of the extrapolation scheme devised by Petersson and co-workers [105, 106] was also assessed for the prediction of ^{1}H, ^{13}C NMR shifts [98, 99]. We have tested Jensson pcS basis sets for our selected test systems, and as the quality of extracted ^{19}F NMR

shifts were not to good and consistent, so we did not include the data in thesis. Performance here we tested this scheme for the prediction ^{19}F NMR shifts.

Sanders *et al.* [86] reported that ^{19}F NMR isotopic shielding tensors are sensitive to geometrical parameter variation, specially to C-F bond lengths. We have therefore tested the performance of various functionals for the prediction of molecular structures (especially C-F bond lengths) and its influence on predicted ^{19}F NMR shifts.

4.3   Results and Discussion

4.3.1   Prediction of C-F Bond Lengths

We used various functionals and basis sets for geometry optimizations on a set of simple fluorobenzenes and compared the computed C-F bond lengths with experimental data available in the literature [107-109].
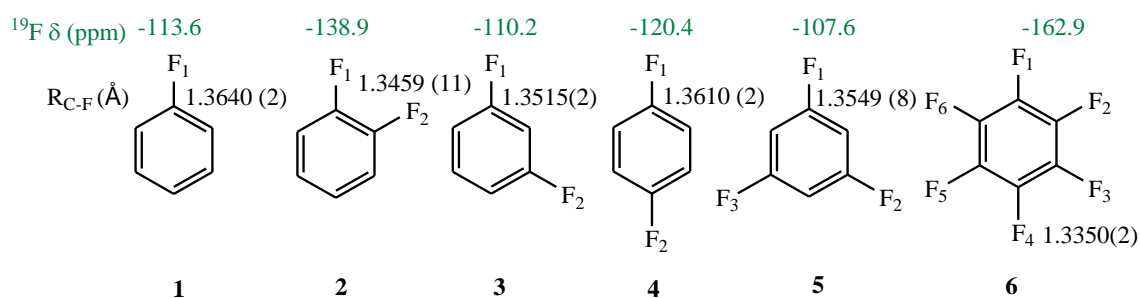
Figure 4. 1: Structure set I, experimental 19F NMR shifts (ppm)[110-112] and C-F bond lengths (Å) [18, 108, 109].

The resulting mean signed errors (MSEs) for the individual functional/basis set combinations for C-F bond lengths (cf. Fig 4.1) were computed according to Equation 4.1 and the results obtained with Pople-style basis sets are displayed in Figure 4.2.
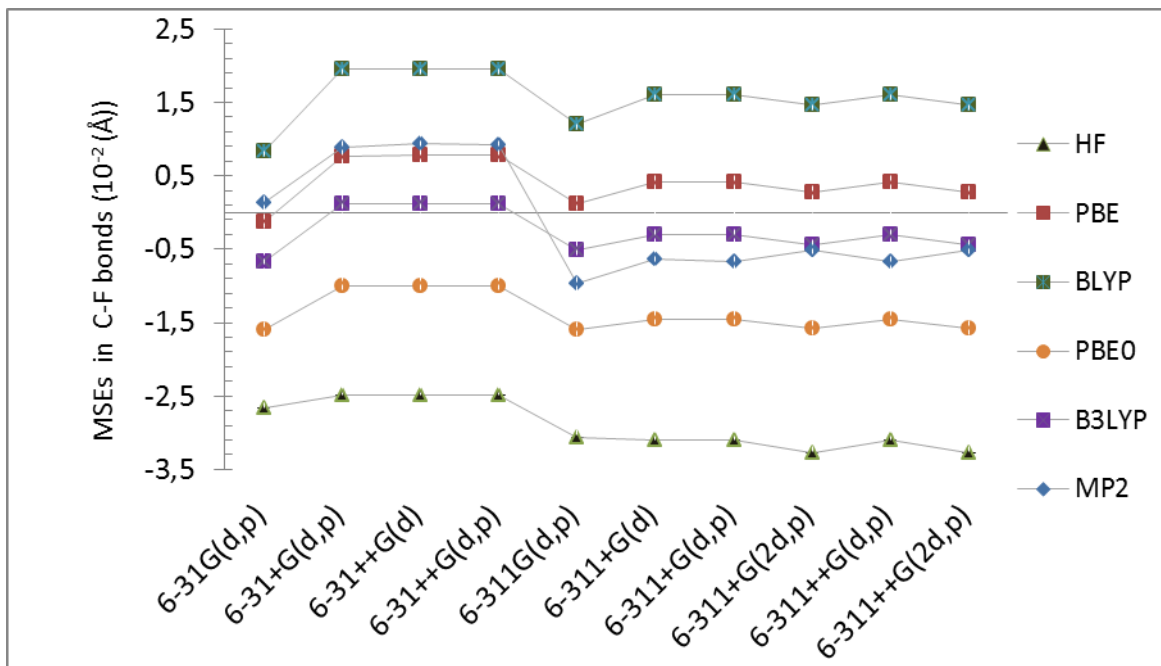
Figure 4. 2: Mean signed errors of the calculated C-F bond-lengths from the experimental data for structure set I. The average experimental uncertainty is ± 0.0007 (Å) (i.e. the error bar).

Assuming an experimental uncertainty of 3σ for C-F bonds for each structure in Figure 4.1 we calculate an average experimental uncertainty in the structure set I according to the error-propagation formula proposed by Andraos [113] (Eq. 4.1).

$$\Delta \overline{R}_{CF}^{Expt} = \pm \frac{1}{6}\sqrt{\sum_{i=1}^{6}\left(3\sigma_i\right)^2} \qquad (4.1)$$

In Equation 4.1, σ represents the standard deviation and $\Delta \overline{R}_{CF}^{Expt}$ represents the average experimental uncertainty in C-F bond lengths in figure 3.1. The mean signed errors for computed C-F bond lengths are calculated using equation 3.2,

$$MSE^{Calc} = \sum_{1}^{6} \frac{\left(R_{CF}\right)_{calc} - \left(R_{CF}\right)_{exp}}{6} \qquad (4.2)$$

Here $(R_{CF})_{calc}$ and $(R_{CF})_{exp}$ are the computed and experimental C-F bond-lengths for structure set I, respectively.

The data displayed in Figure 4.2 indicate a few general trends: The perception that HF generally gives too short bond lengths holds true also for C-F bond lengths in fluorobenzenes, irrespective of the basis set applied. Conversely, MP2 in combination with double-zeta basis sets overestimates C-F bond lengths, while its

use $_{in}$ combination with triple-zeta basis sets slightly underestimates C-F bond lengths.

The overall performance of the MP2 method can be understood in terms of inclusion of electron correlation when compared to HF. Not so good performance of MP2 with higher basis set, 6-311G++(d,p) is because MP2 at the basis set limit overestimates electron correlation, and the excellent performance of MP2/6-31G(d,p) is thus a consequence of fortuitous error compensation [114-116].

The pure GGAs PBE and BLYP overestimate C-F bond lengths on average by 0.004 Å and 0.016 Å, respectively. The admixture of HF exchange in the hybrid functionals PBE0 (25% HF) and B3LYP (20% HF) leads to an underestimation of C-F bond lengths on average by -0.014 Å and -0.003 Å respectively. At this point these results provide evidence that, independent of the basis set, the HF admixture in PBE0 does not improve the agreement with experiment compared to the PBE-GGA, whereas B3LYP is found generally superior over BLYP.

With respect to the basis-set influence on the computed C-F bond lengths, we note a decrease in the computed C-F bond lengths upon increasing the basis-set size from double-zeta to triple-zeta for HF and MP2, while a slight increase with the basis-set size results for DFT methods. For example, with HF an average shortening of C-F bonds by 0.004 Å and with BLYP an average increase of C-F bond by 0.004 Å is found upon the increase of the basis set quality from double to triple zeta. Upon augmentation of basis sets with diffuse functions, an overall increase in C-F bond lengths is found and this effect is more pronounced with double zeta than with triple-zeta basis sets.

4.3.2 Correlation between C-F Bond Lengths and ^{19}F Chemical Shifts

For example, BLYP in combination with double-zeta basis sets results in an average elongation of C-F bonds by 0.011 Å (e.g. 6-31G(d,p) to 6-311+G(d,p)) whereas augmentation of triple-zeta basis sets results in an average elongation of C-F bonds by only 0.004 Å (e.g. 6-311G(d,p) to 6-311++G(2d,p))

Two schemes, namely P_1 and P_2, are used to investigate the correlation between C-F bond-lengths and chemical shifts. In scheme P_1, the NMR parameters are calculated at geometries optimized at the respective level of theory using the 6-311+G(2d,p) basis set recommended for ^{13}C and ^{1}H NMR shift calculation by Cheeseman [84]. For geometry optimization in scheme P_2, the PBE/6-311G(d,p) level was selected based

on its good performance in Sect. 4.3.1. Table 4.2 lists the functionals, the mean signed errors (MSEs) in C-F bond lengths, and the MSEs of ^{19}F NMR shifts for the fluorobenzenes of structure test set I.

A closer inspection of the data reveals a few general trends: (1) The PBE, OPBE, OLYP and B3LYP functionals all yield very good C-F bond lengths but large MSEs for computed NMR shifts. Also, an increase from 20% HF in B3LYP to 50% in BHandHLYP results in a substantial deterioration in the quality of computed C-F bond. Nonetheless, within scheme P_1, BHandH and BHandHLYP in combination with the 6-311+G(2d,p) basis set furnish impressively accurate NMR shifts (cf. Table 3.3). (2) Pure functionals in general produce larger MSEs for ^{19}F NMR shifts as compared to their hybrid-exchange counterparts (e.g., MSEs for PBE and PBE0 are -27.4, ppm and -6.7, ppm). (3) Replacing traditional B88 exchange with OPTX exchange leads to further improvements in shift calculations (e.g. MSEs for PBE and OPBE in combination with the 6-311+G (2d,p) basis set are -22.9 ppm and -10.9 ppm, respectively). (4) Except for HF and BLYP, Scheme P_2 yields inferior shifts compared to P_1.

In this section we found the PBE0, BHandH, BHandHLYP, B97-2 and M06-L functionals to be reasonably good in predicting ^{19}F shifts for simple fluorobenzene (within scheme P_1). As our ultimate goal is to identify a scheme which can be applied pragmatically to produce accurate shifts for extended substituted fluorine systems, we re-assessed the performance of M06-L, B97-2, BHandH and BHandHLYP to predict ^{19}F shifts for the extended structure set II, which includes thirty ^{19}F NMR shifts in different chemical environments (Figure 4.3).

Table 4. 2: Mean signed errors (MSEs, in ppm) and maximum errors (max, in ppm) for ^{19}F chemical shifts (δ) according to schemes P_1^a/ P_2^b. Those species from structure set I, for which the largest deviations occur, are specified in parentheses.

Methods	P_1^a MSE (R_{C-F}) (Å)	MSE (δ) (ppm)	$\Delta\delta$(max) (ppm)	P_2^b MSE (δ) (ppm)	$\Delta\delta$(max) (ppm)
HF	-0.027	18.0	19.9 (**5**)	10.4	15.9 (**6**)
LSDA	-0.018	-22.9	-30.6 (**6**)	-33.0	-37.9 (**6**)
PBE	0.001	-27.4	-32.0 (**6**)	-28.0	-31.7 (**6**)
PBE0	-0.014	-6.9	-14.4 (**6**)	-14.1	-15.3 (**4**)
OPBE	-0.007	-10.5	-9.4 (**6**)	-17.5	-20.2 (**6**)
BLYP	0.011	-37.2	-39.6 (**6**)	-29.8	-31.9 (**6**)
OLYP	0.001	-20.5	-23.6 (**6**)	-22.1	-24.3 (**6**)
B3LYP	-0.004	-17.3	-18.4 (**6**)	-18.5	-20.0 (**4**)
O3LYP	-0.008	-11.9	-14.0 (**6**)	-16.5	-17.5 (**4**)
BP86	-0.218	-29.3	-33.0 (**5**)	-28.4	-31.2 (**6**)
OP86	-0.228	-13.9	-18.3 (**5**)	-20.4	-23.4 (**6**)
BHandH	-0.032	0.7	5.0 (**6**)	-11.8	-13.3 (**4**)
BHandHLYP	-0.240	0.5	1.6 (**6**)	-6.3	-9.8 (**1**)
TPSS	-0.218	-20.4	-21.8 (**6**)	-20.4	-21.7 (**4**)
TPSSh	-0.224	-12.4	-13.5 (**6**)	-15.3	-17.2 (**4**)
OPW91	-0.228	-10.5	-14.3 (**6**)	-17.6	-20.0 (**6**)
B3PW91	-0.232	-10.1	-11.8 (**6**)	-14.8	-16.3 (**4**)
B3P86	-0.233	-10.1	-12.1 (**6**)	-16.3	-17.7 (**4**)
B97-1	-0.221	-12.8	-14.4 (**6**)	-16.3	-17.7 (**4**)
B97-2	-0.229	-6.7	-7.9 (**6**)	-13.0	-14.9 (**4**)
B97D	-0.454	-27.2	-29.0 (**6**)	-24.6	-25.7 (**4**)
M05	-0.018	-16.0	-19.1(**6**)	-25.4	-26.9 (**4**)
M05-2X	-0.011	-15.1	-20.1(**6**)	-20.0	-22.3 (**6**)
M06	-0.021	-7.5	-8.6 (**6**)	-16.4	-19.2 (**1**)
M06-2X	-0.015	-7.2	11.4 (**6**)	-13.7	-15.3 (**6**)
M06-L	-0.014	-2.5	4.6 (**6**)	-3.7	-7.1 (**4**)
M06HF	-0.009	-15.3	-25.4 (**6**)	-15.9	-22.2 (**6**)

Figure 4. 3: Structure set II, experimental ^{19}F shifts (ppm)[117].

Table 4. 3: Mean signed errors (MSEs) and maximum deviations ($\Delta\delta_{max}$) in ^{19}F NMR chemical shifts for structure set II. Those species from structure set II for which the largest deviations occur are specified in parentheses.

	P_1			P_2	
δ_{MSE} (ppm)	$\Delta\delta_{max}$ (ppm)	$\Delta\delta_{max}$ (ppm)	δ_{MSE} (ppm)	$\Delta\delta_{max}$ (ppm)
B97-2	-6.4	21.9 (**9**)	-12.8	-20.8 (**9**)
PBE0	-6.5	-12.0 (**9**)	-13.9	-21.6 (**9**)
BHandH	1.3	21.9 (**6**)	-11.9	-19.8 (**9**)
BHandHLYP	0.9	16.8 (**4**)	-6.3	-15.1 (**9**)
M06-L	3.0	18.4 (**4**)	-3.5	-12.5 (**4**)

Table 4.3 presents MSEs in computed ^{19}F shifts. Again scheme P_1 produces overall better NMR shifts compared to P_2. By and large, the performance of the methods noted for structure set I carry over to the much larger structure set II. Although clearly the BHandH and BHandHLYP hybrid functionals show an excellent overall performance, the good performance of the M06-L functional is interesting because this meta-GGA can be used in combination with the RI approximation for calculations on large systems with significantly reduced computational costs.

4.3.3   Assessment of Basis Sets

4.3.3.1   Pople Style Basis Sets

In the previous test, NMR single-point calculations and geometry optimizations were performed in combination with the 6-311+G(2d,p) basis set. Here, we will assess the series of Pople-style basis sets for use with the M06-L, PBE0, BHandH and BHandHLYP functionals to compute NMR shifts. Table 4.5 presents MSEs and maximum errors obtained with the best functionals identified so far, in combination with 10 different standard Pople-style basis sets.

Table 4. 4: Mean Signed Errors (MSE) and maximum errors for calculated ^{19}F chemical shifts for structure set I

Basis Set [a]	M06-L MSE	Δδ (max)	PBE0 MSE	Δδ (max)	BHandH MSE	Δδ (max)	BHandHLYP MSE	Δδ(mx)
BS1	8.7	10.4(**2**)	3.0	7.1(**4**)	13.0	18.2(**5**)	12.1	14.3(**5**)
BS2	5.9	10.6(**6**)	-2.6	-3.9(**4**)	6.5	8.2(**5**)	5.5	8.9(**6**)
BS3	4.6	10.6(**6**)	-3.6	-5.6(**4**)	5.7	6.9(**5**)	5.8	8.9(**6**)
BS4	5.2	10.6(**6**)	-3.2	-5.0(**4**)	6.0	7.5(**5**)	-5.3	-10.4(**6**)
BS5	-3.1	-7.1(**6**)	-13.5	-21.5(**6**)	-4.9	-14.1(**6**)	-1.9	-4.2(**4**)
BS6	1.2	3.7(**6**)	-9.9	-11.2(**6**)	-2.0	-4.8(**6**)	6.2	8.9(**6**)
BS7	1.9	4.2(**2**)	-9.3	-11.2(**6**)	-1.4	-4.8(**6**)	-1.3	-3.3(**4**)
BS8	2.5	4.5(**2**)	-6.9	-9.8(**6**)	0.7	-3.4(**6**)	0.5	-1.5(**4**)
BS9	2.6	4.6(**2**)	-7.1	-9.8(**6**)	-1.2	-4.7(**6**)	0.2	-1.5(**4**)
BS10	1.8	4.2(**2**)	-9.0	-11.1(**6**)	0.6	5.0(**6**)	-0.9	-2.7(**2**)

[a] BS1 = 6-31G(d,p), BS2 = 6-31+G(d,p), BS3 = 6-31+G(d), BS4 = 6-31++G(d,p), BS5 = 6-311G(d,p), BS6 = 6-311+G(d), BS7 = 6-311+G(d,p), BS8 = 6-311+G(2d,p), BS9 = 6-311++G(d,p), BS10 = 6-311++G(2d,p),

First, we note a good performance of PBE0 in combination with all double-zeta basis sets (BS1 to BS4). The M06-L, BHandH and BHandHLYP functionals on the other hand produce generally lower errors in combination with triple zeta basis sets. While augmentation of non-hydrogen atoms with diffuse function generally leads to lower errors, replacement of one d polarization function by two d polarization functions leads an increase of MSEs for M06-L and to lower MSEs for the other functionals.

4.3.3.2 Huzinaga-Kutze (IGLO-Type) Basis Sets

In this series of benchmark calculations, we used the IGLO-II and IGLO-III basis sets of Huzinaga, which have been devised explicitly to calculate magnetic properties [59]. Being computationally inexpensive, these basis sets are suitable to calculate NMR shifts for larger chemical systems [118]. As NMR shifts generally profit from error compensation, it is always advisable to compare computed shifts with experiment rather than shielding constants. The calculated shifts were then compared with individual experimental values and the corresponding mean signed errors (MSEs), and maximum errors are given in Table 4.5.

Table 4. 5: Mean signed errors (MSEs) and maximum deviations ($\Delta\delta_{max}$) in ^{19}F NMR chemical shifts for structure set I. Those species from structure set I, for which the largest deviations occur are specified in parentheses.

	IGLO-II		IGLO-III	
Method	**MSE (δ)**	**$\Delta\delta$ (max.)**	**MSE(δ)**	**$\Delta\delta$ (max.)**
HF	25.4	27.4(**5**)	14.6	18.3(**6**)
BLYP	-24.2	-29.3(**4**)	-32.9	-35.9(**6**)
PBE	-13.9	-22.7(**6**)	-24.4	-29.6(**6**)
B3LYP	-6.0	-9.1(**6**)	-14.6	-16.4(**6**)
PBE0	2.7	6.0(**6**)	-4.8	-7.9(**6**)
MP2	-0.1	2.0(**5**)	-6.7	-8.2(**6**)

We note that all density functionals yield lower MSEs with IGLO-II compared to IGLO-III and the PBE0 and B3LYP produced lowest MSEs. These results suggest the preferential use of the IGLO-II basis set. The performance of various functionals is further assessed in combination with the IGLO-II basis set.

Table 4. 6: Mean signed errors (MSEs) and maximum deviations ($\Delta\delta_{max}$) in ^{19}F NMR chemical shifts for structure set I. Those species from structure set I for which the largest deviations occur are specified in parentheses. In all calculations the IGLO-II basis set was used.

	% HF	**MSE(δ)**	**$\Delta\delta$ (max.)**
HF		19.9	23.5(**6**)
LSDA	0	-12.9	-22.9(**6**)
OPBE	0	-0.2	-5.9(**6**)
B971	21	-2.6	-5.9(**6**)
B972	21	2.4	4.5(**5**)
B97D	0	-17.1	-20.8(**6**)
OLYP	0	-7.3	-12.7(**6**)
O3LYP	12	0.2	-3.8(**6**)
OP86	0	-3.3	-9.2(**6**)
M05	27	-6.8	-11.7(**6**)
M05-2X	54	-2.8	-8.2(**6**)
M06	28	-5.1	-7.6(**6**)

M06-2X	56	2.6	6.7(**5**)
M06HF	100	5.6	15.0(**5**)
M06-L	0	2.7	4.1(**2**)
BP86	0	-19.6	-25.4(**6**)
BHandH	50	10.5	15.2(**5**)
BHandHLYP	50	10.2	12.0(**5**)
OB97-1	0	-5.9	-11.4(**6**)
OB97-2	0	-11.2	-16.2(**6**)

In Table 4.6 statistical errors, the mean signed error (MSE), and maximum errors $\Delta\delta$ (max) for the structure sets I are presented. It is clearly seen that the functionals that include HF exchange produce significantly improved ^{19}F NMR shifts compared to pure GGA functionals. Judging on the basis of mean signed errors, the best performing functionals from this study are M06-L (2.7 ppm), B97-1 (-2.6 ppm), B97-2 (2.4 ppm) and PBE0 (2.7 ppm). Addition of Hartree-Fock exchange plays an important role in improving the results. As a possible explanation we point out that HF exchange introduces some correlation contributions [119], which might improve the agreement with experiment.

For the cases tested here, the functionals M06-L, OPBE, PBE0, B972 and O3LYP in combination with IGLO-II basis set are able to predict ^{19}F shifts within 4 ppm accuracy.

4.3.3.3 Dunning's Basis Sets

Dunning's correlation-consistent basis sets are specifically designed for high quality energy calculations using post-HF methods [103]. Further, basis sets were devised to allow for an efficient extrapolation to the complete basis-set limit [120]. Let these basis sets are generally computationally expensive and thus their use is limited to smaller chemical systems. However, the medium-sized cc-pVDZ and cc-pVTZ basis sets are affordable in combination with density functionals and can be applied to larger molecules with 50 to 100 atoms. In this test, correlation-consistent basis sets have been used in combination with several functionals to predict ^{19}F NMR shifts for fluoroaromatics.

As illustrated in figure 4.6 all tested functionals show convergence for the computed shielding constant already with cc-pVTZ basis set and the use of larger basis sets does not improve the results.
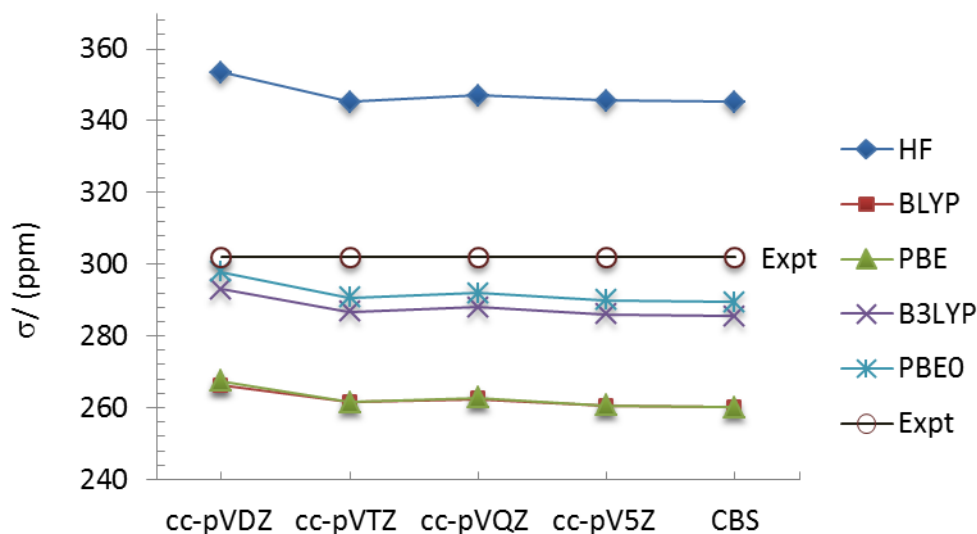
Figure 4. 4: Convergence of computed ^{19}F NMR shielding constants (σ) only for fluorobenzene.

Table 4. 7: Mean signed errors (MSEs, ppm) and maximum deviations ($\Delta\delta_{max}$) in ^{19}F NMR chemical shifts for structure set I. Those species from structure set I for which the largest deviations occur are specified in parentheses.

	HF		BLYP		PBE		B3LYP		PBE0	
Basis Set	MSE	$\Delta\delta$max	MSE	$\Delta\delta$max	MSE	$\Delta\delta$max	MSE	$\Delta\delta$max	MSE	$\Delta\delta$max
cc-VDZ	27.5	30.5	-14.8	-24.8	-7.3	-19.5	1.8	-5.4	8.7	11.5
cc-VTZ	23.9	27.8	-24.9	-31.6	-15.1	-24.4	-7.0	-11.6	2.9	5.6
cc-VQZ	20.6	24.4	-30.9	-36.3	-21.0	-28.9	-12.5	-15.9	-1.7	-6.8
cc-V5Z	20.1	23.6	-32.8	-37.0	-22.8	-29.9	-13.7	-16.2	-3.1	-7.3
CBS	18.5	22.2	-34.7	-39.1	-24.7	-31.8	-15.9	-18.6	-4.7	-9.2
		(5)		**(6)**		**(6)**		**(6)**		**(3)**

The errors for computed ^{19}F NMR shifts for structure set I are displayed in Table 3.8 and a few general trends become obvious: (1) HF in combination with cc-pVXZ correlation-consistent basis set appears to predict better shifts upon moving from smaller to larger basis set. (2) The pure functionals BLYP, PBE and the hybrid functional B3LYP in combination with the cc-pVDZ basis set produce the lowest MSEs whereas larger errors result upon enlargement of the basis set. (3) The PBE0 functional in combination with the cc-pVTZ and cc-pVQZ basis sets produces

moderately low MSEs, while a larger error results om the CBS limit. Obviously these basis sets offer no advantage over Pople- or IGLO- type basis sets.

We further assessed the performance of several other functionals in predicting ^{19}F NMR shifts with the cc-pVTZ basis set and the resulting statistical errors are presented in Table 4.9.

The functionals OPBE, PBE0, O3LYP and B972-2 produced the lowest MSEs. The results clearly indicate that replacement of B88 or PBE exchange with OPTX exchange reduces the errors in all cases. Replacement of P86 by PW91 in B3PW91 does not produce any appreciable change. The B97-2 functional produces the lowest maximum error. The best performing functionals were further tested to reproduce ^{19}F shifts for structure set II and all functionals yield very low MSEs but substantial maximum errors

Table 4. 8: Mean signed errors (MSEs, ppm) and maximum deviations ($\Delta\delta_{max}$) in ^{19}F NMR chemical shifts for structure set I computed with various functionals and the cc-pVTZ basis set. Those species for which the largest deviations occur are specified in parentheses.

	% HF	MSE(δ)	$\Delta\delta$(max)
HF		24.2	27.7(**6**)
LSDA	0	-13.2	-23.2(**6**)
PBE	0	-17.3	-24.4(**6**)
OPBE	0	-1.0	-7.2(**6**)
PBE0	25	1.2	5.3(**5**)
BLYP	0	-27.1	-32.3(**6**)
B3LYP	20	-8.4	-12.0 (**6**)
OLYP	0	-10.3	-16.2(**6**)
O3LYP	12	-2.6	-7.2(**6**)
BP86	0	-20.4	-26.4(**6**)
OP86	0	-4.6	-11.2(**6**)
B97-1	21	-4.9	-8.6(**6**)
B97-2	21	1.4	4.3(**5**)
B97D	0	-17.9	-21.9(**6**)
TPSS	0	-10.3	-13.9(**6**)
TPSSh	15	-3.2	-6.4(**6**)
BHandH	50	8.6	14.5(**5**)

BHandHLYP	50	7.9	10.7(**5**)
M06-L	0	5.4	6.8(**2**)
B3BP86	20	-2.4	-6.3(**6**)
B3PW91	20	-2.0	-5.8(**5**)

Table 4. 9: Mean signed errors (MSEs, ppm) and maximum deviation ($\Delta\delta_{max}$) in ^{19}F NMR chemical shifts for structure set II.computed with cc-pVTZ basis set. Those species from structure set I for which the largest deviations occur are specified in parenthesis.

	MSE(δ)	$\Delta\delta$(max)
OPBE	-0.8	-8.9(**9**)
PBE0	1.0	7.6(**13**)
O3LYP	-2.8	-11.1(**11**)
B972	1.1	7.0(**13**)

4.4 Conclusions

The geometry evaluation for structure set I reveal that PBE in combination with the 6-31G(d,p) basis set, and B3LYP in combination with either the 6-31+G(d,p), the 6-31++G(d) or the 6-31++G(d,p) basis sets produce accurate C-F bonds for fluorobenzene. However NMR calculations performed with methods that yield better structures (as judged based on the comparison of computed C-F bond lengths with experimental data above) do not generally yield better NMR shifts than methods that yield worse structures.

According to Table 4.3, NMR calculations with the M06-L/6-311+G(d), PBE0/6-31+G(d,p), BHandH/6-311+G(2d,p) and BHandHLPY/6-311+G(2d,p) methods produce low MSEs for ^{19}F shifts in fluorobenzenes. For all functionals tested on structure set I we found that the smaller IGLO-II basis set outperforms over the IGLO-III basis sets, the first-one has been found a better performer. The functionals, PBE0, B97-2, O3LYP, M06-L in combination with the IGLO-II basis set produce within MSEs of 3 ppm and with a low maximum errors.

PBE0 and B97-2 in combination with the cc-pVTZ basis set yield ^{19}F shifts with low MSEs. However, enlargement of the basis set does not improve accuracy. Hence, these basis sets do not offer any advantage over the Pople or IGLO type basis sets.

Based on the MSEs for structure set I, we conclude that the functionals M06-L and PBE0 in combination with 6-311+G(d) and 6-31+G(d,p) basis sets, respectively, are good choices to calculate ^{19}F shifts for fluorobenzenes.

Although, selected functionals and basis sets ^{19}F shifts were identified that can yield within the required accuracy, still a more accurate and less method-dependent approach is desireable. In the next chapter we will analyze the performance of various schemes that can generally be used to correct computed ^{19}F NMR chemical shifts.

5. Correction Schemes for Computed ^{19}F Chemical Shifts

5.1 Introduction

In chapter 4, an extensive benchmark calculation was presented to identify the best functional and basis set combination to predict accurate ^{19}F NMR chemical shifts for fluorobenzenes. In last chapter was shown that the BHandH, BHandHLYP and M06-L functionals in combination with a triple-ζ quality basis set (e.g. 6-311+G(2d,p)) produced the good results. By using above level of theory an acceptable accuracy of about 2-4 ppm in ^{19}F shifts can be achieved but it will be computationally expensive when it aimed to apply three-four fused-ring system, and therefore a computationally less demanding method that easily applicable to large chemical systems.

It was found, that the errors in the calculated shifts at least in part were systematic in nature. Therefore, they could be minimized by using a correction scheme. Several correction schemes are available in the literature and these schemes are applied frequently to correct the computed ^{13}C and ^{1}H NMR chemical shifts [31, 121-124]. Unfortunately, the sources of error and the correction approach are not related in a one-to-one fashion. Some schemes are designed to deal with specific problems such as conformational and solvent effects and vibrational averaging [13, 125]. There are other schemes that are more general in nature and are effective in reducing systematic errors from several sources at once [15, 122, 124]. Among of these approaches are the linear regression correction (LRC), empirically parameterized DFT methods, and the use of a corrected reference [15, 31, 126].

In this chapter we evaluate the applicability of various available correction schemes for the calculated ^{19}F NMR chemical shifts for fluorobenzenes and fluorine substituted fused ring systems. During synthesis our experimentalist collaborator got several issues in identifying isomers that are very similar and solution NMR spectra are not able to conclude because the differences in ^{19}F NMR chemical shifts is very small (i.e. 2-4 pm) . So to resolve above isomers a correction is desired that can predict ^{19}F chemical shifts within 2-4 ppm accuracy for fluoroaromatic and polycyclic fluoro-aromatic compounds (e.g. perfluoro-anthracene, methoxy-, and dimethyl- and thiol-substituted fluoroanthracenes) at a modest computational cost. In this chapter each scheme is tested on three structure sets of fluororobenzne.

5.2 Multi reference standard (MSTD) Scheme

The multi-standard scheme is based on the assumption that in the calculation of NMR chemical shifts, the choice of a reference standard is arbitrary, and in principle, any chemical molecule can be used as reference standard. The idea behind this approach is the assumption that a major source of error in computed NMR chemical shifts is the difference in the chemical nature of the test and reference molecules. Pellegrinet and co-workers used the similar scheme to minimize such errors for ^{13}C & ^{1}H NMR chemical shifts [122, 127]. It was reported that the tetramethylesilane (TMS) is an inappropriate computational reference for calculating ^{13}C NMR chemical shifts for aromatic systems [128]. Timmons and co-workers used sp^2-hybridized carbons as a reference for ^{13}C shifts calculation for benzene [129]. So far, this scheme has been applied for ^{1}H and ^{13}C shifts.

We note that plenty of experimental ^{19}F NMR chemical shift data are available in the literature and most of it was recorded using $CFCl_3$ as a reference standard [130-132]. It is assumed that $CFCl_3$ does not influence the measured shifts. Though reference standard in NMR shift calculation is virtual and essentially there should be no effect of reference standard on computed chemical shifts its true only when test molecule and reference standards have similar chemical nature and this is not true always, for example computing ^{19}F NMR chemical shift for fluorobenzene using $CFCL_3$ as a reference standard. Therefore, a difference in the chemical nature of the test and the reference molecule could be a source of large errors in NMR shift computations.

According to the MSTD approach, a molecule can be used as a reference standard with the condition that its experimental chemical shift must be known with respect to the main reference standards. For example, TMS would be considered as the main reference for ^{13}C and similarly $CFCl_3$ would be the main reference standard for ^{19}F shift calculation. Calculated ^{19}F shifts can be computed as well using the equation (5.1) [11, 122, 123]

$$\delta^x_{calc} = \sigma_{ref} - \sigma_x + \delta_{ref}, \tag{5.1}$$

where σ_{ref} and σ_x are the values of the NMR isotropic magnetic shielding constant for the reference and the tested molecule, respectively, computed at the same level of theory, and δ_{ref} is the experimental chemical shift of the secondary reference compound (in the case of fluorobenzene, δ_{ref} -113.2 ppm). Multi reference approach has additional benefit when it is being used in combination with DFT functional, as functional error cancellation will improve quality of NMR chemical shift.

5.3   Linear Regression Correction (LRC) Scheme

Forsyth and Sebag applied a simple empirical correction to calculate ^{13}C NMR shifts [15] this linear scaling approach, notify here a linear regression schema significant improvement were noted even with calculated shifts with a comparatively small basis set. Forsyth *et* al [15] compared a wide variety of abinitio methods combined with small to moderately large basis sets to determine potentially useful methods for computing ^{13}C NMR chemical shifts. This approach has been used to study the conformations and configurations of several organic molecules [31, 133]. Among different scheme use to correct calculated NMR chemical shifts perhaps the most general approach is Linear Regression Correction (LRC). When aplenty experimental data is available, plots of several varieties may be generated; these include computed chemical shifts vs experimental chemical shifts, computed isotropic shielding constants vs experimental chemical shifts. Linear fits are looked at for all types of such regression plots and the quality of these linear fit indicates the extent to which a computational method is able to produce data free from random error. The extent to which the slope of the correlation line deviates from unity is a measure of the overall systematic error. The primary benefit to this procedure is that the slope can be used as a scaling factor to correct the computed chemical shifts for systematic error. The other benefit of linear regression correction (LRC) that this scheme is more accurate and less dependent on the level of theory [122, 134-136].It has been noted that such a procedure is able to reduce error from different sources at once. It is observed that linear scaling is able to reduce error occur from solvation effects, rovibratory effects, and other method limitations, all at one time [137].The linear regression correction is an efficient way to correct systematic errors across the whole ^{13}C, ^{1}H and ^{19}F spectra.

We applied it for computing ^{19}F NMR chemical shifts and instead of using calculated shifts relative to $CFCl_3$, the computed isotropic shielding tensors were used and that carried advantage of eliminating errors introduced from computed shifts of the reference standard. In linear regression correction scheme it is not straight forward to choose appropriate regression parameters as theses parameters depend strongly on the test set molecules.

In this work, we tested the applicability of the LRC scheme to correct ^{19}F shift of fluorobenzenes.

5.4   Computational Details:

All calculations were performed using the Gaussian09 suite of programs and the NMR chemical shift calculations were carried out with the optimized geometry (no imaginary frequency was found for each structure) imaginary frequency means is that geometry is not fully converged and a zero imaginary frequency means that geometry is already converged to an energy minimum. Both structure sets investigated in chapter 4 (Figure, 4.1 and 4.2) were used for the test calculations. The structure set I contained a set of fluorobenzenes and the structure set II contained fluorobenzenes substituted with different groups such as -OH, -NH$_2$, -OMe and -Cl. The structure set III (figure 4.4) consisted of perfluoroanthracene and its precursors. The performance of various DFT functionals and various Pople basis sets were evaluated.

5.5   Results and Discussion

5.5.1   Multi-Reference Standard (MSTD) Scheme

In Table 5.1, we illustrate the advantage of using fluorobenzene as secondary reference standards comply with multi-standard scheme. The fifth column in Table 5.1 shows a deviation ($\Delta\delta$) of 24-32 ppm in the calculated shift from the experimental value. However, by the use of fluorobenzene as a secondary reference, the deviation reduces significantly to a range of 0-8 ppm. The improvement in the predicted values is due to a similarity in the chemical nature of the reference standard and the test molecules.

Table 5. 1: ^{19}F NMR chemical shift of the proposed reference in CDCl$_3$ (CFCl$_3$) computed using the functional PBE and 6-311+G (2d, p) basis set.

CFCl$_3$ (Ref.)	^{19}F Shielding (σ, ppm)	^{19}F Shifts (δ, ppm)		
	Calc.	Calc.	Expt.	Error
Fluorobenzene	262.7	-138.0	-113.6	-24.4
1,2 difluorobenzene	289.7	-165.0	-138.9	-26.1
1,3 difluorobenzene	258.9	-134.2	-110.4	-23.8
1,4 difluorobenzene	271.6	-146.9	-120.4	-26.5
1,3,5 difluorobenzene	256.6	-131.8	-107.6	-24.2

perfluorobenzene	319.9	-195.1	-162.9	-32.2
CFCl$_3$	124.7	0.0	0.0	

Fluorobenzene (FB) (Ref.)

Fluorobenzene	262.7		-113.6	0.0
1,2 difluorobenzene	289.7	-140.6	-138.9	-1.7
1,3 difluorobenzene	258.9	-109.8	-110.4	0.6
1,4 difluorobenzene	271.6	-122.5	-120.4	-2.1
1,3,5 difluorobenzene	256.6	-107.5	-107.6	0.1
hexafluorobenzene	319.9	-170.8	-162.9	-7.9

5.5.3   Linear Regression Correction (LCR) to the Computed Shift

The LRC scheme emerges as an efficient tool to reduce systematic errors significantly [15, 124, 133, 138, 139]. It proved to be very practical to obtain calculated shifts within acceptable error limit (ca. 2 ppm) for fluorobenzene and related systems at low computational cost [10-12]. The computational cost equals that of the method used to produce the original data. But error will be less then original computed shifts.
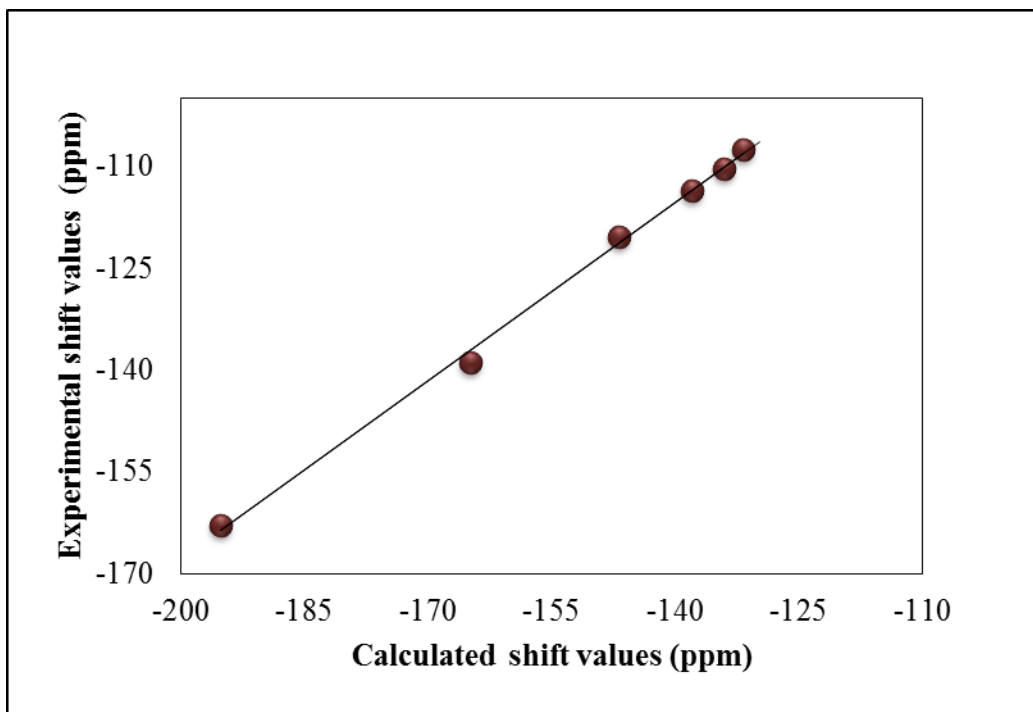
Figure 5. 1: Correlation between the experimental and calculated values of the chemical shifts for fluorobenzenes [112, 132,].

Table 5. 2: A Comparison of the calculated (PBE/6-311+G(d,p)) and corrected values of the chemical shift (using equation $\delta_{corr.}=$ slope*δ_{calc}+intercept, where values of slope and intercept are 0.87 and 6.70 respectively.

	^{19}F NMR chemical shifts (δ, ppm)		
	Calc.($\Delta\delta$)	**Corr ($\Delta\delta$)**	**Expt.**
Fluorobenzene	-138.0 (-24.4)	-113.4 (0.2)	-113.6
1,2 difluorobenzene	-165.0 (-26.1)	-136.9 (2.0)	-138.9
1,3 difluorobenzene	-134.2 (-23.8)	-110.1 (0.3)	-110.4
1,4 difluorobenzene	-146.9 (-26.5)	-121.2 (-0.8)	-120.4
1,3,5 difluorobenzene	-131.8 (-24.2)	-108.1 (-0.5)	-107.6
Perfluorobenzene	-195.1 (-32.2)	-163.2 (-0.3)	-162.9

The slope and the intercept of the linear regression line could be used to "scale" the results in such a way that systematic errors were removed significantly and the two parameters for a given computational method could easily be used to correct calculated chemical shift values for similar molecules. Table 5.4 shows a comparison of the computed, corrected and the experimental values of the chemical shift. The equation (5.7) was used to correct the calculated shift values, where the correction parameters (slope and intercept) were dependent on the level of theory.

$$\delta_{corr.} = \text{Slope}*\delta_{calc} + \text{Intercept} \qquad\qquad (5.7)$$

It is evident from Table 5.4 that the calculated values of ^{19}F chemical shift computed produces error in the range of 24-32 ppm, while, after applying linear regression correction, it reduce to 0.2 to 2 ppm.

Based on different schemes assessment to predict ^{19}F NMR shifts for fluorine substituted benzenes, we observed that multi standard and corrected reference standard (CRS) schemed are very much test system dependent and both produce similar errors and errors magnitude vary from 1 to 7 ppm from fluorobenzene to hexafluorobenzene, nevertheless based on limited set of molecules and single quantum chemical method we cannot conclude about these schemes, so we further assess the influence basis set and functional.

5.6 Assessment of Different Correction Schemes

Table 5.5 shows the performance of the different functionals along with the 6-311+G (2d, p) basis set to predict ^{19}F chemical shift values for the structure set II (Figure 4.2). It is seen that without correction the PBE0 and B97-2 functionals yield large errors (MSE, -7.2 ppm). The DFT methods with a higher percentage of exact Hartree-Fock exchange, BHandH (50% HF) and BHandHLYP produce significantly improved results, with MSE = 0.4 and -0.2, respectively.

Table 5. 3: A comparison of different correction schemes with statistical parameters (in ppm) for the structure set II.

	NC		MSTD		LRC
	MSE	$\Delta\delta_{max}$	MSE	$\Delta\delta_{max}$	$\Delta\delta_{max}$
B97D	-7.2	-30.6 (20-F1)	-0.7	-24.2	-5.4(20-F1)
PBE0	-7.2	-32.0 (20-F1)	-1.7	-26.5	-5.1(20-F1)
BH	0.4	-26.5(20-F1)	-2.7	-29.6	-3.5(20-F1)
BHL	-0.2	-23.6(20-F1)	0.2	-23.2	-5.1(20-F1)
M06-L	2.1	-18.7(20-F1)	1.2	-19.6	-6.7(20-F1)

For LRC correction below given slope and intercept were used.

	BHandHLYP	PBE	M06-L	B97D	BHandH	PBE0
Slope	0.90	0.79	0.91	0.89	0.80	0.85
Intercept	-21.0	-12.0	-19.8	20.8	-33.1	-19.0

NC=No correction, MSTD=Multi reference standandard correction, LRC=Linear Regression Correction.

It can be seen clearly that each of the correction schemes makes a significant improvement to the predicted chemical shift values. The MSTD and CRS approaches show a significant improvement in the values of the calculated chemical shift, producing an MSE in the range of 2-3 ppm. The LRC scheme was found to be the best among the three schemes used.

Furthermore, to assess the influence of the basis set on the predicted values of the chemical shift the performance of ten different Pople-style basis sets was tested. Table 5.6 lists mean unsigned errors from the experimental values of the ^{19}F the NMR chemical shift for the structure set I. Clearly, if no correction is applied to the

calculated values the 6-31G (d, p) basis set produces the lowest error. While adding the diffuse functions to the double-ζ basis set and also on going from the double-ζ to the triple-ζ basis set, the error increases.

Table 5. 4: Mean Signed Error (MSE), (in ppm) in ^{19}F NMR chemical shift (PBE functional is used in all the calculation) for the structure set I.

	NC		MSTD		LRC*	
Basis set	MSE	$\Delta\delta$ max	MSE	$\Delta\delta$ max	MSE	$\Delta\delta$ max
6-31G(d,p)	-15.9	-25.5	-4.2	-13.8	0.3	-1.5
6-31+G(d,p)	-23.0	-24.8	-0.4	-2.2	0.1	-0.6
6-31++G(d)	-24.2	-25.1	0.0	-0.8	0.0	-0.9
6-31++G(d,p)	-23.6	-24.8	-0.3	-1.5	0.1	-0.8
6-311G(d,p)	-32.7	-46.7	-6.2	-20.2	0.3	-1.5
6-311+G(d)	-30.6	-34.6	-1.3	-5.3	0.1	-1.0
6-311+G(d,p)	-29.7	-34.6	-1.8	-6.7	0.1	-0.9
6-311+G(2d,p)	-26.6	-32.2	-2.2	-7.9	0.2	-0.8
6-311++G(d,p)	-29.3	-34.4	-1.9	-7.1	0.1	-0.8
6-311++G(2d,p)	-26.5	-32.2	-2.2	-8.0	0.2	-0.8

*For LRC correction below given slope and intercept were used.

PBE	Slope	Intercept
6-31G(d,p)	0.80	-12.7
6-31+G(d,p)	0.96	17.2
6-31++G(d)	0.99	22.9
6-31++G(d,p)	0.98	20.2
6-311G(d,p)	0.73	-10.9
6-311+G(d)	0.90	15.6
6-311+G(d,p)	0.88	11.6
6-311+G(2d,p)	0.87	6.7
6-311++G(d,p)	0.88	10.6
6-311++G(2d,p)	0.87	6.3

However, by adding diffuse functions to the triple-ζ basis set and replacing "d" by "2d" reduces the error. With MSTD and CRS scheme, basis sets 6-31+G (d, p), 6-31++G (d, p), 6-311+G(d) and 6-311++G (d, p) were found to be the best ones, and with the LRC scheme, all the basis sets gave MUE values less than 1 ppm. Among all the correction approaches, the LRC scheme was found to be the best, and also its performance was seen to be independent of the basis set used.

Table 5.7 presents the results for the structure set II of 26 benchmark ^{19}F chemical shift values in the substituted fluorobenzene. All basis set that produce good results for structure set I, were then chosen to calculate ^{19}F NMR shifts for structure set II. [19]F chemical shift calculated for structure set II in table 5.7 shows that MSTD and CRS produce similar quality ^{19}F NMR chemical shift and the mean signed error and maximum errors in shift conclude that basis sets with diffuse function produce good results.

Table 5. 5: Mean signed error (MSE), (in ppm) in ^{19}F NMR chemical shift values obtained using PBE functional for the structure set II.

	NC		MSTD		LRC
Basis Set	**MSE**	$\Delta\delta_{max}$	**MSE**	$\Delta\delta_{max}$	$\Delta\delta_{max}$
6-31G(d,p)	-17.9	-27.3 **(9)**	-5.0	-14.4**(9)**	-6.9**(9)**
6-31+G(d,p)	-24.0	-31.5**(9)**	-0.3	-7.7**(9)**	-5.6**(9)**
6-311G(d,p)	-35.9	-47.7**(9)**	-9.4	-21.1**(9)**	-8.0 **(9)**
6-311+G(d,p)	-30.8	-38.4**(9)**	-2.9	-10.6**(9)**	-6.4 **(9)**
6-311+G(2d,p)	-27.6	-34.4**(9)**	-3.2	-10.0**(9)**	-5.6 **(9)**

When the LRC scheme is used any basis set varying from 6-31G(d, p) to 6-311+G(2d,p) reduce errors about to 2 ppm. For the given test structure the change in the MSE value with a change in the size of the basis set can reach up to 17.4 ppm if without any correction, 7.3 ppm for the MSTD scheme, 7.2 ppm for the CRS scheme and 0.5 ppm for the LRC scheme. For used test structures set, the linear regression correction scheme produced best ^{19}F NMR chemical shifts values and resulted shifts show minimal method dependencies thus, it can be deduced that the LRC scheme is applicable regardless of the used theoretical method.

5.7 Application of the Correction Schemes for the Structure Set III.

In our collaborated project we planned to synthesize extended perfluoroacenes that are potential candidates for electron-transport materials. Regioselective substitution on perfluoroanthrance is the way to get extended perfluoroacenes and experimentalist are intended to find better ways to synthesize perfluoroanthrance. HALEX [140] reaction is well known procedure for synthesizing perfluoranthracene but this reaction needs harassing conditions and final product output of reaction is low. Tefort and coworkers were looked various reaction path-ways to synthesize perfluoroanthrance and in that process he obtained some intermediate products that were not easy to identify on the basis of experimental data. So to help them out in resolving these intermediate we evaluated various theoretical strategies to resolve these intermediate and final products.

In this chapter different correction schemes are evaluated for predicting ^{19}F NMR chemical shift and as in previous sections LRC scheme was concluded best scheme for predicting ^{19}F NMR chemical shifts for structure set I and II. To confirm it in this section we evaluate the performance of LRC scheme in predicting the ^{19}F NMR chemical shift values of structure set III (in figure 5.3).

Table 5.8 presents the results for 13 benchmark values for five fluorine substituted anthracene. It was observed that if no corrections were applied, MSE values obtained using the functional PBE in combination with the basis set ranging from 6-31G (d, p) to 6-311+G (2d, p) varied between 22 and 31.8 ppm. Once the LRC scheme was applied, the MUE values are reducing to ~1.5 ppm. With LRC correction 6-311+G (2d,p) produced standard errors SEE,0.7 ppm and with theory level a required chemical accuracy ^{19}F NMR shift can be achieved for perfluoranthracene .
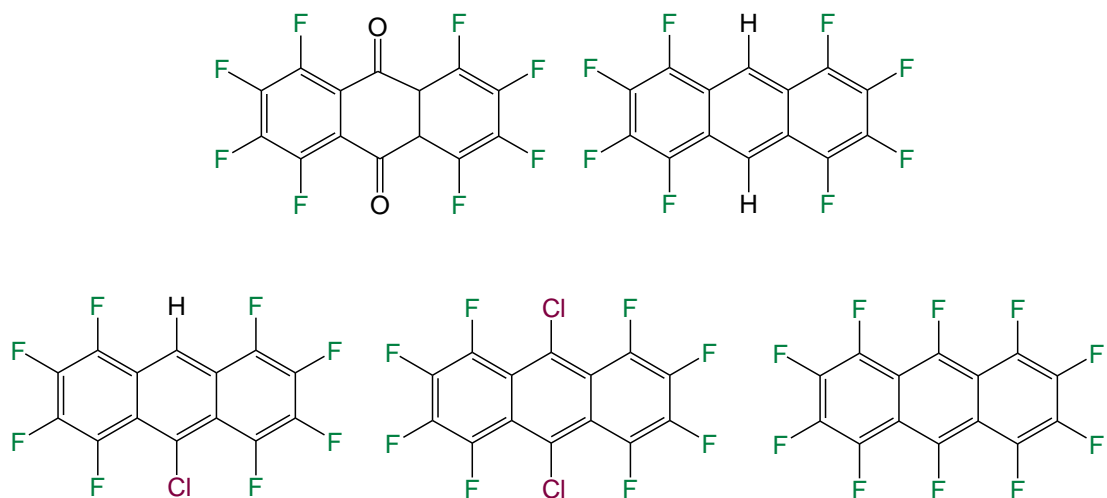
Figure 5. 2: Chemical structural formulas of perfluoranthracene and related molecules (structure set III).

Table 5. 6: Performance of PBE and PBE0 Density Functional in predicting ^{19}F chemical shifts of structural set III.

	Unscaled			Scaled		Regression Data		
	MSE	MUE	δ_{max}	MUE	δ_{max}	Slope	Intercept	SEE
PBE								
6-31G(d,p)	-22.0	22.0	25.9	1.4	4.4	0.91	6.9	2.0
6-311+G(d,p)	-30.0	30.0	31.8	0.6	1.3	0.88	8.1	0.8
6-311+G(2d,p)	-27.0	27.0	28.8	0.5	1.2	0.87	3.9	0.7
PBE0								
6-31G(d,p)	-0.2	1.5	3.8(2, F-1)	1.3	3.7	0.98	-3.4	2.0
6-311+G(d,p)	-9.0	9.0	10.9 (1, F-2)	0.9	2.8	0.94	-0.9	1.1
6-311+G(2d,p)	-7.0	7.0	8.9(1, F-2)	0.8	2.9	0.93	-3.8	1.2

To evaluate further accuracy dependence on hybrid functional we evaluate the performance of PBE0 in combination with 6-31G (d,p), 6-311+g(d,p), 6-311+G(2d,p) without correction 6-31G(d,p) basis set produced lowest error (MUE, 1.5 ppm). LRC correction further improves shifts.

In summary, out of three schemes on three different test sets we note that the LRC scheme produces best results than any other scheme evaluated. Without LRC correction the PBE0 functional performs better than PBE with used basis.

5.8 Predicting shifts for unknown molecules.

We aimed here to resolve the ^{19}F NMR spectra of four fluoroanthracenes intermediates products that our experimental collaborator obtained while scrutinizing reaction path ways to synthesizing perfluoranthracene. According to inconclusive experimental ^{19}F NMR NMR spectra, ^{19}F δ -127.3 -148.4 (1), -127.1,-150.0 (2) -127.0 -150.0 (3), -135.1, -150.8 (4) probable structures are given in figure 5.8.

.
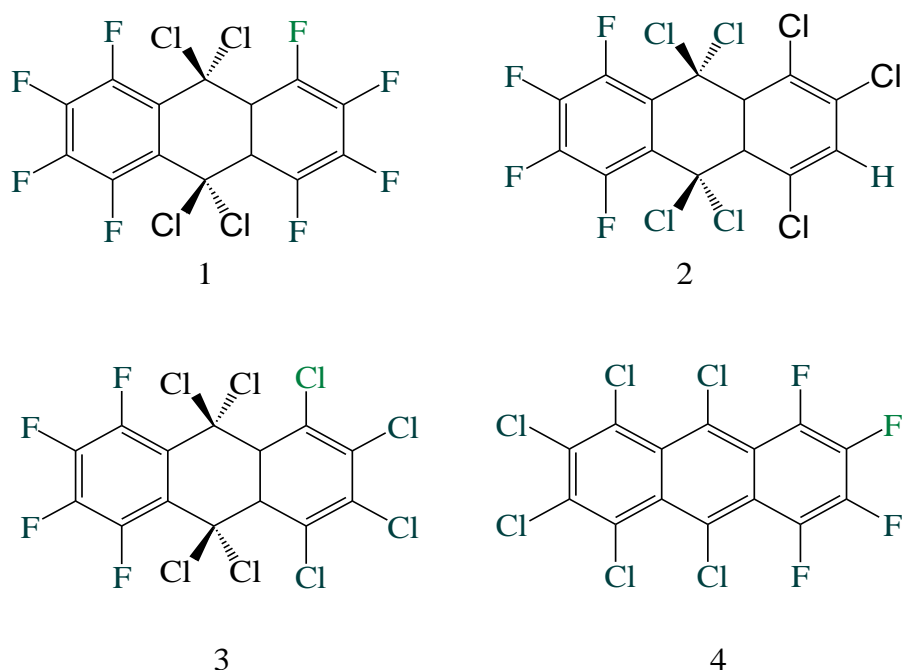
Figure 5. 3: Newly synthesized fluoroanathrances [141].

Table 5. 7: LRC corrected ^{19}F chemical shift values, for newly synthesized fluoroanthracenes   in Figure 5.8. The functional PBE0 is used in all calculations. Regression data from Str.set III given in table 5.9 used in calculations Maximum deviation is given in parenthesis

	^{19}F NMR chemical shifts (δ, ppm)			
	6-31G(d,p)	6-311+G(d,p)	6-311+G(2d,p)	Expt.
1-F1	-122.5 **(4.8)**	-125.0	-124.8	-127.3
1-F2	-150.8	-151.9	-151.6	-148.4
3-F1	-123.2	-125.1	-124.9	-127.0
3-F2	-151.9	-153.2	-152.9	-150.0
2-F1	-122.8	-124.8	-124.7	-127.1
2-F2	-151.7	-153.1	-152.8	-150.0
4-F1	-134.9	-131.8 **(3.3)**	-130.5 **(4.6)**	-135.1
4-F2	-149.8	-151.0	-150.2	-150.8

LRC corrected ^{19}F NMR shifts are given in table 5.10 and for all molecules PBE0/6-311+G (d, p) are in line with experimentalist observation and with other basis set large deviation are observed.

5.9 Conclusion

As concluded in previous chapter a desired accuracy 2-4 ppm in predicting ^{19}F NMR shift can be achieved with the PBE0, BHandH, BHandHLYP, and M06-L functionals in combination with the 6-311+G(2d, p) basis set but here we would like to emphasize that this conclusion is valid only for the planar fluorine substituted benzenes. Predicted shift based calculation with and without correction schemes shows that a correction scheme is necessary to predict accurate ^{19}F NMR chemical shift values for substituted fluorobenzenes and fluoroarenes. In this chapter used two correction schemes (MSTD, and LRC) improve the results significantly for all fluorine substituted compounds studied. The improvement in predicting ^{19}F chemical shift values using MSTD is qualitatively good but this scheme stayed behind to predicts shifts within required accuracy. The linear regression correction (LRC) scheme is found to the best and it produces ^{19}F chemical shift values within 2-3 ppm for fluoroanthrance and it is also nearly independent of the theoretical method and the basis set employed. Further improvement can be made when regression parameters in use, are obtained from similar structure sets. To predict accurate ^{19}F chemical shift values for unknown compounds, the LRC scheme in combination with BHandH and PBE0 functional in combination with any Pople basis sets with at least diffuse functions, 6-31+G(d,p), 6-311+G (d, p), or 6-311+G (2d,p) basis sets is recommended.

6. Studies on the Regioselective Nucleophilic Aromatic Substitution (S$_N$Ar) Reaction of Perfluoroanthracene

6.1 Introduction

The research in the field of organic semiconductors is driven by its potential use in the design of smaller and faster computers, photovoltaics and organic light emitting diodes (OLED)[142]. Many conjugated organic systems, such as anthracene have a low electron affinity and behave as p-type semiconductors [143]. Perfluorination of anthracene converts it into a n-type semiconductor [144] and extended perfluoroacenes are a potentially useful class of efficient electron-transport materials. These compounds retain many of the attractive physical properties of the parent hydrocarbons due to the small size difference between fluorine and hydrogen. Therefore, perfluorination is the most effective way to convert a p-type semiconductor (e.g anthracene) to an n-type semiconductor (e.g. perfluoranthracene) without changing the size of the molecule drastically. Although the synthesis process for perfluoroanthracene (PFA) is known (from tetrachlorophthalic anhydride)
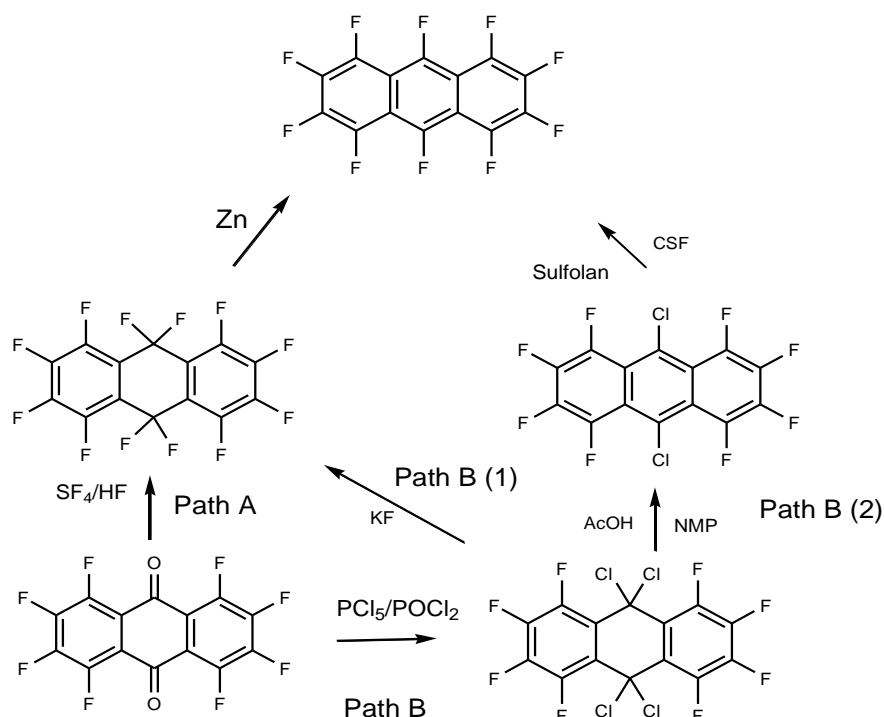

Figure 6.1 Different reaction paths to synthesize perfluoroanthracene[144].

[3], it requires drastic conditions and proceeds with 20-25 % product yield [145]. Production of PFA at industrial scale needs an inexpensive and high yield route [146].

In a perfluoro polyaromatic compound with topologically distinct fluorine atoms, substitution may occur at one position preferably. Thus, a nucleophilic substitution on perfluoroanthracene opens up ways to generate new fluorinated arenes. The products obtained from nucleophilic substitution on PFA, (i.e. perfluoro polycyclic aromatic hydrocarbons (PAHs) (i.e. methoxy ($-OCH_3$) substituted fluoro anthracene) are seen as basic building blocks to design fascinating organic semiconductor materials [145, 147, 148].

Terfort and coworkers encountered problems for assigning right substitution site on perfluoroanthracene using NMR spectra, while examined different reactions and routes to synthesizing PFA [149]. They have tried to synthesizing perfluoroanthracene from octafluoro-9,10 anthraquinone, tetrachlorophthalic anhydride,perfluoro-9,10-dihydroanthracene,etc. Max muir showed previously that stability of meisenheimer complex, a reaction intermediate complex that obtained in nucleophilic aromatic substitution and it can be used for qualitative prediction of nucleophilic substitution in fluoroaromatic compounds. Calculating accurate NMR chemical shift can also be helpful for predicting nucleophilic substitution. But this scheme very much depends on NMR shift accuracy and used quantum chemical methods.as in previous chapters we did benchmarks study to find best quantum chemical methods that can predict accurate ^{19}F NMR chemical shifts.

In this chapter, we evaluate meisenheimer stability and NMR shifts prediction schemes, which can be applied to predict the outcome of these types of nucleophilic aromatic substitution reactions. A general nucleophilic aromatic substitution reaction may follow different reaction pathways. One possible pathway is via transition metal catalyzed substitution, for example, with osmium or potassium as catalysts [150, 151]. An aromatic nucleophilic substitution reaction can proceed via a two-step addition–elimination mechanism, where the active nucleophile is added to a substituted aromatic carbon atom, followed by the departure of the leaving group. In between, a stable intermediate that is composed of both the nucleophile and the leaving group is formed and is known as Meisenheimer complex (Mc)[152]. As depicted simple example in figure 6.1, a negative charge on the Meisenheimer complex is delocalized in the aromatic π-system.
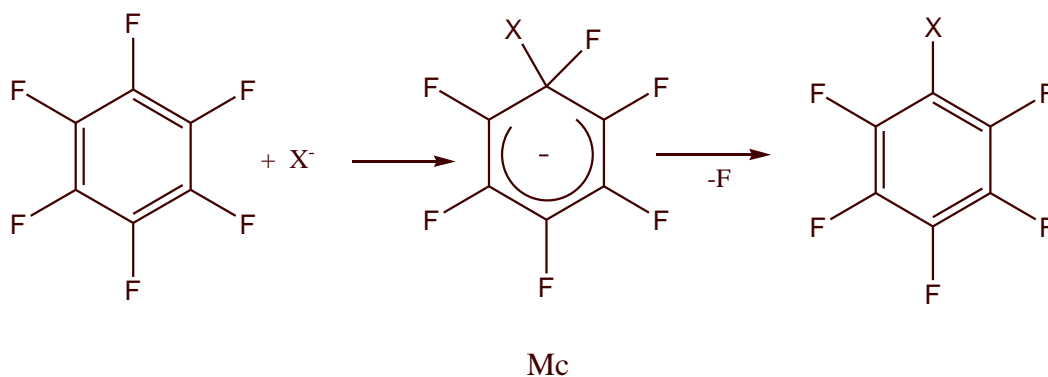
Figure 6. 2*: **Depicted mechanism of a nulceophilic substitution reaction on perfluorobenzene via the Meisenheimer complex (Mc).**

This Mc complex plays a decisive role in defining the orientation of the nucleophilic attack on polyfluoroaromatic and related species. One possible model to account for this is to consider the calculation of relative stabilities of all possible Meisenheimer complexes. As the most stable complex would lead directly to the most probable substitution site and method that can predict accurate Mc complexes stabilities will be very useful in determining region-selectivity in nucleophilic substitution reaction. There are some other models that are also used to predict the orientation of the nucleophilic substitution in polyfluoroaromatic and related species [152-154] such as I_π repulsion theory. This theory is based on the calculation of partial charges using the Hückel approach. I_π repulsion theory was very initial approach used to rationalize substitution sites [152] and according to this theory repulsion between electro negative atom and π-system destabilizes the hybrid system formed during substitution and qualitatively this theory predicts accurate nulceophilic substitution in naphthalene, fluoroanthracene and many other related systems [146]. The transition state theory is also good for making semi quantitative predictions about preferred substitution sites and intermediate products [155]. One way to make quantitative predictions of the selectivity pattern in S_NAr reactions is obviously to calculate the potential energy profile in each case, including the transition states, and theoretical investigations of the potential energy profile in vacuo have recently been performed within the DFT framework At present, however, modeling of the potential energy profile is bit complex to be routinely used in synthetic route design. Therefore, a simplified method for the prediction of selectivity in S_NAr reactions would be highly valuable[153].

In this chapter, we investigate the possibilities for the use of simplified computational approaches for a qualitative prediction of the orientation of the

aromatic nucleophilic substitution reaction (S_NAr) in fluorobenzene,fluoronapthalene and fluoroanthracenes. Here following approaches are tested: (i) comparing relative stabilities of all possible Meisenheimer complexes, previously Muir used to qualitative prediction of aromatic nucleophilic substitution reaction (S_NAr) [153]. (ii) Computing isomers ratios and (iii) comparing the computed and the observed chemical shifts for the resulting products. These computational approaches are sought to assist the synthetic planning in lab, by answering questions such as, will this reaction give predominantly the desired product or an undesired product isomer, or the reaction outcome is uncertain?

In this chapter we used selected quantum chemical schemes from previous chapter to predict ^{19}F NMR chemical shifts for possible reaction products and intermediates and compared them with observed shifts. To predict the orientation of nucleophilic substitution, we have compared the relative stabilities of two possible Mc complexes of PFN and three possible Mc complexes of PFA.

For example a schematic scheme given in figure 6.3, when compound A is treated with TBAF in 20%HCl at room temperature, it was expected to obtain compound (B) but instead, a mixture of two products was obtained and identification of these products was not possible, based on experimental evidence e.g. ^{19}F, ^{1}H, NMR experimental spectra and mass spectral elucidation. In this chapter in the later section we have shown NMR predicted shifts using linear regression correction scheme helped in resolving the outcome of this reaction.
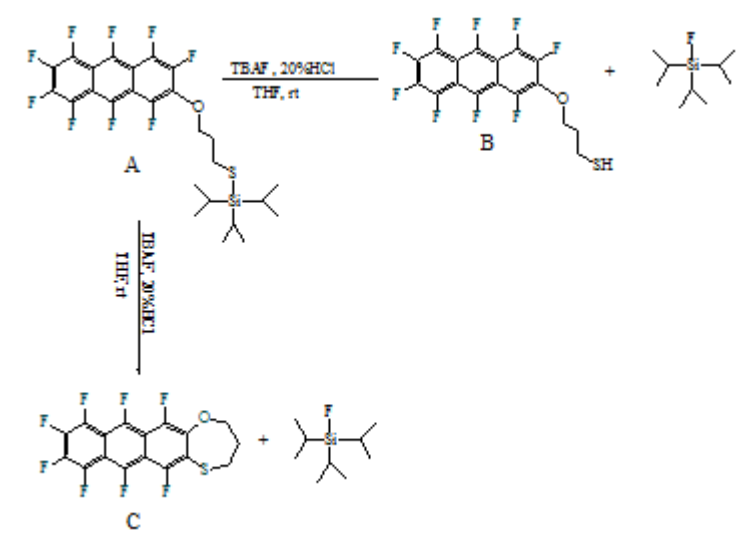
Figure 6. 3: Illustration of the expected compound B and the actual compound C obtained from A.

6.2 Computational Details

In this chapter linear regression correction scheme is used for ^{19}F NMR shift correction. DFT functional OPBE, B97D, PBE0, B3LYP, BHandH in combination with 6-31+G (d, p) were used. As concluded in previous chapters linear regression corrections is also used to correct calculated shifts. All ^{19}F NMR shifts were in the gas phase and for Meisenheimer complex calculation PCM methods and 6-311++G (d,p) basis set is used.

Experimental values of ^{19}F NMR chemical shift were taken from Tamara, Burdon and co-workers [143, 156] for PFN and for PFA shifts were taken from the Terfort and coworker[157]. The relative stabilities of possible Meisenheimer complexes were calculated using the fluoride ion as a model nucleophile. Frequency calculations were carried out for all the Mcs complexes and no imaginary frequency values were obtained. All NMR calculations were performed for the minimum energy geometries with no imaginary frequency. Each calculated ^{19}F NMR chemical shift was corrected using equation (6.1).

$$\delta_{predicted} = Slope.\delta_{calc} + Intercept \qquad (6.1)$$

The regression parameters that are used in this chapter were taken from structure set II, discussed in chapter 4.

6.3 Results and Discussion

6.3.1 Predicting the site for $S_N Ar$ Reaction

Relative energies of all possible Mc complexes for both perfluoronapthalene and perfluoroanthracene are listed in Table 6.1 and a lowest energy structure in each case was taken as the reference. Under the experimental column, P denotes the experimentally observed substitution site (i.e. 100% selectivity) methoxide ion as the nucleophile in methanol as the solvent.[153]

Table 6. 1: Relative stability energies (in kcal/mol) of various Meisenheimer complexes. All calculations used PCM (CH_3OH)/6-311++G(d,p).

Molecule	Relative stability (kcal/mol)				
	OPBE	**PBE0**	**B3LYP**	**B97D**	**Expt.**
Perfluoronaphthalene					
F_1	0.0	0.0	0.0	0.0	
F_2	-1.6	-1.3	-1.4	-1.2	P
Perfluoroanthracene					
F_1	0.0	0.0	0.0	0.0	
F_2	-1.8	-1.5	-1.6	-1.5	P
F_9	-6.0	-7.1	-6.5	-6.7	

P = experimentally preferred site for nucleophilic substitution in (kcal/mol)

We compared the relative stabilities of various Mc complexes by computing Gibbs free energy values (ΔG, in kcal/mol) for each possible isomer in Table 6.1. Gibbs free energy value obtained for 1-F for 2-F substitution on perfluoroanthracene for all DFT functionals shows that 2-substition value is lower than 1-substitution that means 2-F substituted complex is more stable and that is in-line with experimentally observed results for perfluoronapthalene, a 2-fluorine as the preferred substitution site, but same methods contradict the experimentally observed substitution site for perfluoranthracene (2-fluorine substitution is preferred). Literature shows the amplified version of ''I_π-repulsion'' theory predict 9-fluoroine substitution [153] on perfluoroanthracene. I_π-repulsion'' theory is based on the destabilization by a bonded fluorine of a negative charge on a carbon atom when that charge is part of a I_π-system and the degree of destabilization is calculated from HOMO Huckel charge densities in meisenheimer complexes [143], this theory predict correct position of nucleophilic attack on perfluoronapthalene, phenanthrene, pyrene and related systems. What we see above is that meisenheimer complexes stablitiy alone cannot be use to define nucleophilic substitutions in fluoro-substituted compounds.

6.3.2 Nucleophilic Attack on Perfluoroanthracene

Decafluoroantracene was synthesized about 2 decades before and its nucleophilic replacement has been studied several times [158]. Although so far there is no method that correctly predicts accurate nucleophilic substitution for perfluoroaromatic

compounds. Terfort group have studied the nucleophilic substitution on perfluoroanthracene using to different reaction scheme and the structure of the mono-replacement of products was deduced from their ^{19}F NMR spectra (Referance). perfluoroanthracene itself shows three ^{19}F signals [(in p.p.m. up field from CFCl3): 144.1 (1,4,5,8-F}; 153.8 (2,3,6,7-F); 122.5 (9,10-F); intensity ratios 4: 4: 2] with those from the (1,4,5,8) and (9,10) fluorine atoms showing a strong and typical peri-coupling (J ca. 75 Hz). In nonafluoromonomethoxyanthracene there were peaks at 122.9 (2F), 140.5 (1F), 145.1 (3F), 147.3 (1F), 153.8(2F) the down-field shift of about 5-7 p.p.m. for 1-F and 3-F is usual for the fluorine atoms ortho to a methoxy-group when this has replaced fluorine. Furthermore, the large peri-couplings were all still distinct although unexpressed; this shows that the 1, 4,5,8,9, and 10 fluorine atoms were still present. Based on above fact experimentalist jump on conclusion, that nucleophilic replacement in decafluoro- anthracene has taken place mainly or entirely in the 2-position (Scheme 1). As we saw above amplified π repulsion theory predicts 9-position substitution in case if there is a nucleophilic substitution on perfluoroanthracene.

1-OMe   2-OMe   9-OMe
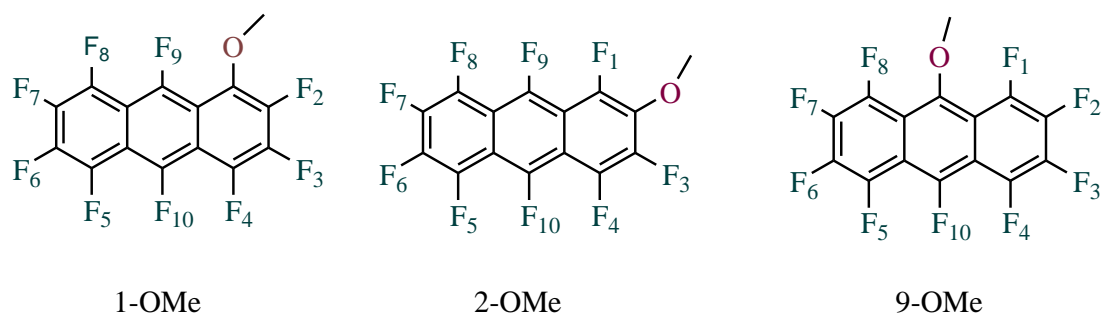
Figure 6.1: Three possible isomers from a S_NAr reaction on perfluoroanthracene with -OMe as the nucleophile.

Shows that π repulsion theory correctly gives the position of nucleophilic attack on perfluoro-naphthalene, phenanthrene, naphthylene, -pyrene, and fluoroanthene it does not do so for octafluorobiphenylene but strain in octafluorobiphenylene provides an obvious reason for. The perfluoroanthracene results here are not in line with amplified pie-repulsion theory and to confirm experimental observation. we computed ^{19}F NMR shifts for all three possible isomers using best benchmark selected functions.

Table 6. 2: Deviation (Δδ, ppm) in the computed ^{19}F chemical shifts for three possible isomers arising from a nucleophilic substitution of perfluoroanthracene with -OMe as the nucleophile (All calculations used the 6-31+G (d, p) basis set)

Deviation Δδ (ppm)									
1-OMe			2-OMe			9-OMe			$(\delta_{expt.}$ (ppm)
PBE0	BHandH		PBE0	BHandH		PBE0	BHandH		
8.5	-6.4	(F_{10})	1.4	-0.9	(F_9)	3.0	0.4	(F_{10})	-122.9
0.4	-2.4	(F_9)	-0.2	-2.6	(F_{10})	-19.8	-21.4	(F_4)	-122.9
-2.5	-3.9	(F_8)	-3.1	-4.3	(F_5)	-2.2	-3.8	(F_5)	-140.5
1.0	-0.2	(F_5)	0.7	-0.9	(F_8)	-2.6	-2.5	(F_8)	-145.1
-7.3	-7.0	(F_3)	-0.7	-1.7	(F_4)	-2.6	-2.6	(F_1)	-145.1
-6.2	-7.5	(F_4)	-0.4	-1.6	(F_3)	-8.2	-8.6	(F_2)	-145.1
-6.7	-6.9	(F_6)	-1.5	-3.4	(F_1)	-6.0	-6.4	(F_7)	-147.3
-0.9	-1.4	(F_7)	0.1	-0.4	(F_7)	0.3	-0.4	(F_3)	-153.8
3.5	-11.2	(F_2)	-1.2	-1.7	(F_6)	0.3	-0.4	(F_6)	-153.8

Products spectra of ^{19}F NMR from the nucleophilic substitution on PFA, shows that 2 fluorine atoms are detected of δ -122.9 ppm, which clearly indicates that no substitution took place at 9- or 10- position. As benchmark studies shows in previous chapter PBE0 and BHandH can predict ^{19}F chemical shifts within 4 ppm accuracy, such accuracy is required to help in resolving complex ^{19}F NMR spectra. An accurate prediction of chemical shift is crucial for identifying the actual product. We calculated ^{19}F NMR shifts for all three possible isomers using PBE0 and BHandH DFT functionals. Deviation in shift from experimental values are given in table 6.3 and it shows that both PBE0 and BHandH both functions consistently give very large deviation on F3, F4, F6 and F10 for 1-OMe and F2, F4 and F7 for 9-OMe these deviation from experimentally observed values clearly eliminate 1-OMe and 9-OMe substitution. Table shows a good agreement for all ^{19}F shifts in case 2-OMe substitution. Consistently agreement by both functionalwith experimentally observed spectra, strongly suggest that substitution is taken place on perfluoroanthracene at 2-position.

6.3.3 Calculation of Boltzmann Isomers ratios:

To confirm substitution at the 2- position in PFA, the abundance ratios of the all possible isomers that can be formed when a nucleophilic substitution take place on perfluoroanthracene, three different isomers are 1, 2, or 9-position substitution. The computed free energies along with a temperature value are fed into the Boltzmann equation [79, 159]

$$\text{Isomer ratio (\%)} = 100 \times \frac{P_i}{P_{total}} = e^{\frac{(G_i - G_j)}{k_B T}} \qquad (6.1)$$

Equation 6.1 expresses the abundance ratio of conformer i relative to conformer j using the computed free energies (Gi and Gj on a per-particle basis), the temperature, and the Boltzmann constant. The computed ratios are listed in Table 6.4 and based on isomer ratios, it can be concluded that 2-methoxy substitution was took place in nucleophilic substitution on decafluoroanthracene.

Table 6. 3: Calculated percentage of each isomer, All calculations used 6-311++G (d, p) basis sets.

	Functional					
Isomer	**BHandHLYP**	**PBE**	**M06-L**	**B97D**	**BHandH**	**PBE0**
1-OMe	0.0	0.0	0.1	0.2	0.1	0.1
2-OMe	100.0	100.0	99.9	99.8	99.9	99.9
9-OMe	0.0	0.0	0.0	0.0	0.0	0.0

6.3.4 Nucleophilic Substitution in Perfluoroanthrance by a Dimethyl amino group
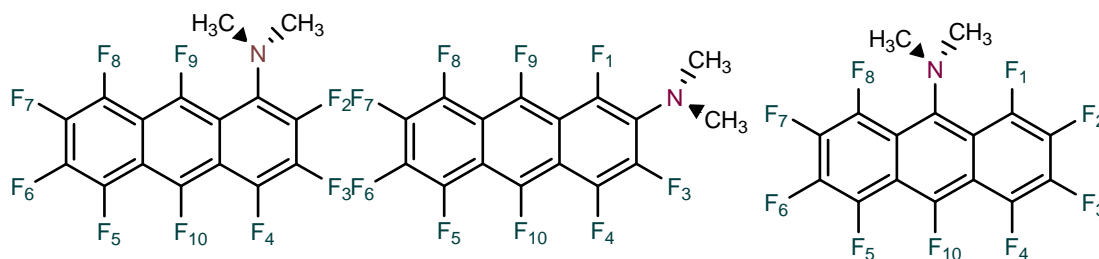
Figure 6. 2: Three possible isomers from an S_NAr reaction of perfluoroanthracene with -N(Me)$_2$ as the nucleophile.

The ^{19}F NMR spectrum of the dimethylaminononafluoroanthracene showed a similar pattern A nucleophilic substitution in PFA by a dimethyl amine group as the nucleophile, is interesting because of NNMe$_2$ steric effect and interaction with neighboring fluorine atoms. it is assumed that the 2- substituted product would be obtained preferentially. The experimental[149] ^{19}F NMR spectrum of the product shows nine different signals, which is rule out the possibility of substitution in the 9th position. However, it is not obvious from the spectrum to clearly say whether the 1-F or the 2-F substituted product was formed.

Table 6. 4: Deviations *(Δδ, ppm)* in the computed ^{19}F chemical shifts for three possible isomers a from nucleophilic substitution of perfluoroanthracene by a dimethyl amine group (All calculations used the 6-31+G (d, p) basis set)

Δδ (ppm)									δ (ppm)
1-(NMe)$_2$			2-(NMe)$_2$			9-(NMe)$_2$			
PBE0	BHandH		PBE0	BHandH		PBE0	BHandH		Expt
4.1	1.1	(F$_9$)	3.4	2.6	(F$_9$)	4.1	2.5	(F$_9$)	-124.0
3.6	4.3	(F$_{10}$)	4.2	4.1	(F$_{10}$)	-17.6	-18.8	(F$_4$)	-125.1
-7.5	-7.6	(F$_2$)	-2	-2	(F$_1$)	-8.3	-9.5	(F$_5$)	-134.4
-4.3	-6.6	(F$_4$)	1	0.3	(F$_3$)	-15.1	-14.7	(F$_7$)	-140.3
1.5	0.1	(F$_8$)	1.1	2.5	(F$_5$)	-10.1	-9.7	(F$_2$)	-145.3
2.4	1.1	(F$_5$)	1.4	2.4	(F$_8$)	-5.9	-4.8	(F$_8$)	-145.9
-5	-5.1	(F$_3$)	1.4	2.5	(F$_4$)	-3.4	-2.3	(F$_1$)	-148.4
0.4	0.1	(F$_7$)	0.2	0.6	(F$_7$)	0.1	-0.3	(F$_6$)	-154.9
-0.3	-0.6	(F$_6$)	-1.4	-1.6	(F$_6$)	-0.3	-0.7	(F$_3$)	-154.5

To identify the substitution product, we did ^{19}F NMR chemical shifts calculation using our best approach, we concluded in last chapters. DFT Functionals, PBE0, BHandH were considered for calculating ^{19}F chemical shifts for perfluoroanthracene. All calculated values were corrected using LRC scheme. The predicted ^{19}F chemical shift values for all three possible isomers are compared with the experimental values in Table 6.4. Deviation in shift from experimental values in table 6.4 shows that both PBE0 and BHandH both functions consistently give large deviation on F2, F3, F4 and F10 for 1-(NMe)^2 and F2, F4, F5, F7 and F8 for 9--(NMe)^2 these large deviation from experimentally observed values clearly eliminate 1-(NMe)^2 and 9-

(NMe)^2 substitution. Table shows a good agreement for all ^{19}F shifts in case 2-(NMe)^2 substitution. Consistently agreement by both functional with experimentally observed spectra, strongly suggest that substitution is taken place on perfluoroanthracene at 2-position.

6.3.7 Synthesis of SH-terminated Fluoroanthracenes (FA)

2-SH substituted fluororanthracene is interesting , a further substitution on it will lead interesting chain product. Terfort group did nucleophilic substitution on 2-SH terminated fluoroanthrancene and resulted product ^{19}F spectra in figure 6.6 is inconclusive. To resolve these ^{19}F spectra, we did ^{19}F NMR shift calculations for all possible products that can be obtained in nucleophilic substitution on 2-SH terminated fluoroanthrancene for these calculations we used our benchmarked functions PBE0. High deviation in computed shifts for FA (1O, 2S), FA (3O, 4S) and FA (9O, 10S), and FA (2O, 1S), FA (4O, 3S) and FA (10O, 9S), ring closed confirmers from experimental values eliminate the possibility that nucleophilic substitution resulted any of the above product. Calculations shows the observed spectrum could be interpreted in terms of the chain and the twist form of the compound C. The deviation of the computed ^{19}F chemical shift values from the experimental values, for the FA (2O, 3S) ring closed chair conformer is given in table 6.5.

6.3.7 Synthesis of SH-terminated Fluoroanthracene (FA)
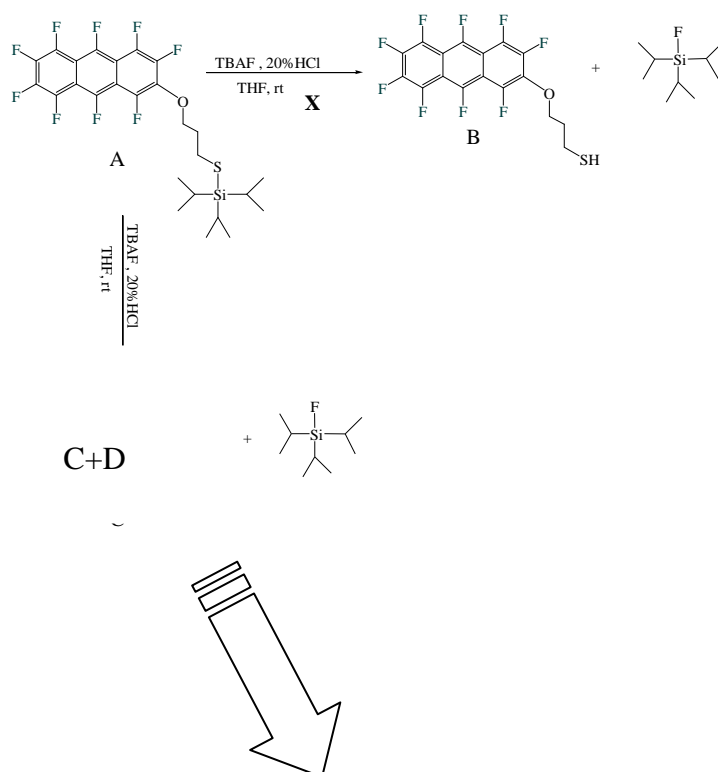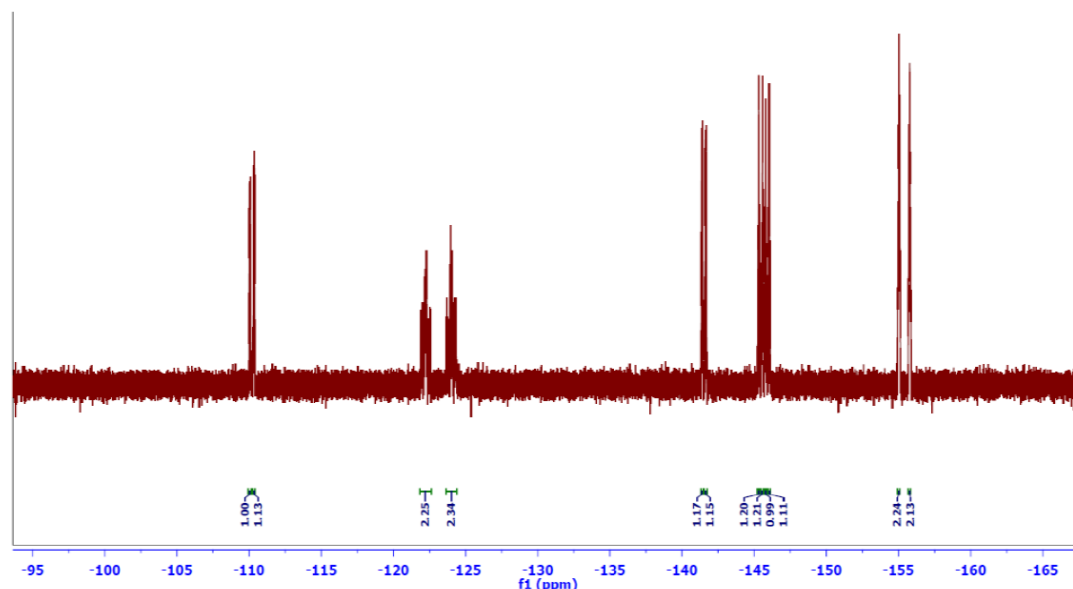
Figure 6.6 [19]**F NMR spectra of product from above reaction,** [19]**F spectra is provided by Terfort group [157]**

O2-S3-Chair (C)   O2-S3-Twist (D)
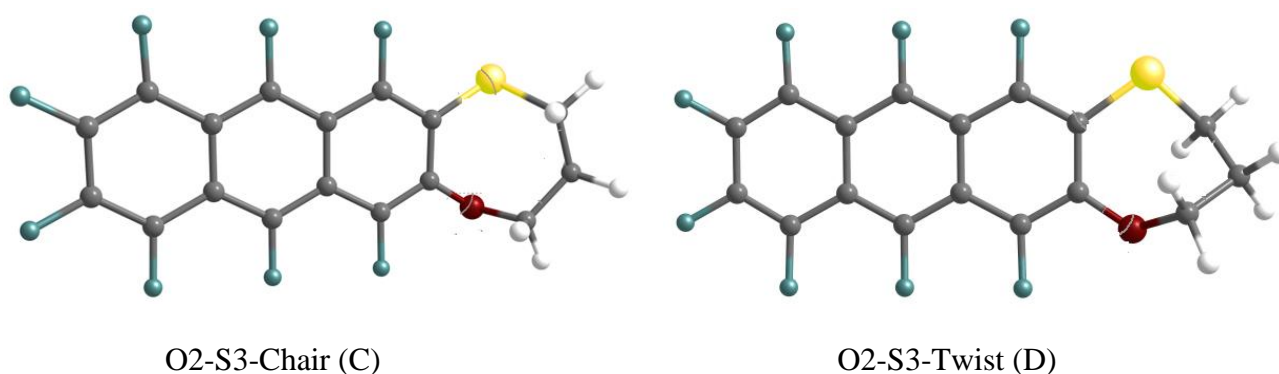
Figure 6. Structure of the products obtained during nucleophilic substitution given in figure 6.3 ring closed 2-3 substituted structures one is O2-S3-Chair (C) separated with small energy from O2-S3-Twist (D)

When synthesizing a disubtituted fluoroanthracene according to scheme given figure 6.3, the resulted product ^{19}F NMR experimental spectra reveals that a mixture of two compounds were obtained, though based on this spectra, it is not possible to determine that which substitution has occurred, and we see various possibilities as it may be 2,3 or 1,2 or 1,4 or 1,9 substitutions. To resolve the above spectra we computed ^{19}F NMR chemical shifts of all possible substituted molecules. Among all possibility, according to predicted ^{19}F NMR shifts for these possible model molecules we conclude that corresponding spectra is for 2, 3 substitution and obtained product is mixture of twist and chair conformation (i.e. compound C and D) separated with small energy barrier.

Table 6.5 Deviations (Δδ, ppm) in the computed ^{19}F chemical shifts for product obtained from nucleophilic substitution on 2-orthofluoroanthracene (All calculation with PBE0/6-311+G (2d, p) basis set) (all calculated ^{19}F NMR shifts were corrected using LRC

	O2-S3-Chair (C)	O2-S3-Twist (D)	Experimental
	δ (Δδ)	**δ(Δδ)**	**δ**
F-4	-106.0(4.0)	-111.8 (-1.8)	-110.0
F-10	-118.3(4.0)	-121.1 (1.2)	-122.3
F-9	-121.2(2.7)	-122.4(1.5)	-123.9
F-1	-138.6(2.9)	-141.3 (0.2)	-141.5
F-5	-143.3(2.1)	-144.1 (1.3)	-145.4
F-8	-144.1(1.9)	-144.6 (1.4)	-146.0
F-7	-153.7(1.3)	-154.8(0.2)	-155.0
F-6	-154.9(0.9)	-155.7(0.1)	-155.8

6.3.8 S$_N$Ar Substitution on nonafluoromonomethoxyanthracene

To the best of our knowledge, no methoxy disubtituted fluoroanthracene product has been reported so far. Some fluoro naphthalene disubtituted products were identified with the (2, 6) isomer as the major product [160-162]. It was reported recently that diamination of perfluoronapthalene yields a mixture of (1, 6), (1, 7), (2, 6), and (2,7)-diaminohexafluoronaphthalenes as products with a considerable prevalence of the (2,7)-isomer (70%). This was the first reported example of the predominant substitution occurring at position (2,7) in nucleophilic substitution of perfluoronapthalene[163]. Terfort group tried a di-nucleophilic substitution reaction on (1);

2-(2-chloroethoxy)-1,3,4,5,6,7,8,9,10-nonafluoroanthracene (1)

2,7-bis(2-chloroethoxy)-1,3,4,5,6,8,9,10-octafluoroanthracene (2)

2,6-bis(2-chloroethoxy)-1,3,4,5,7,8,9,10-octafluoroanthracene (3)
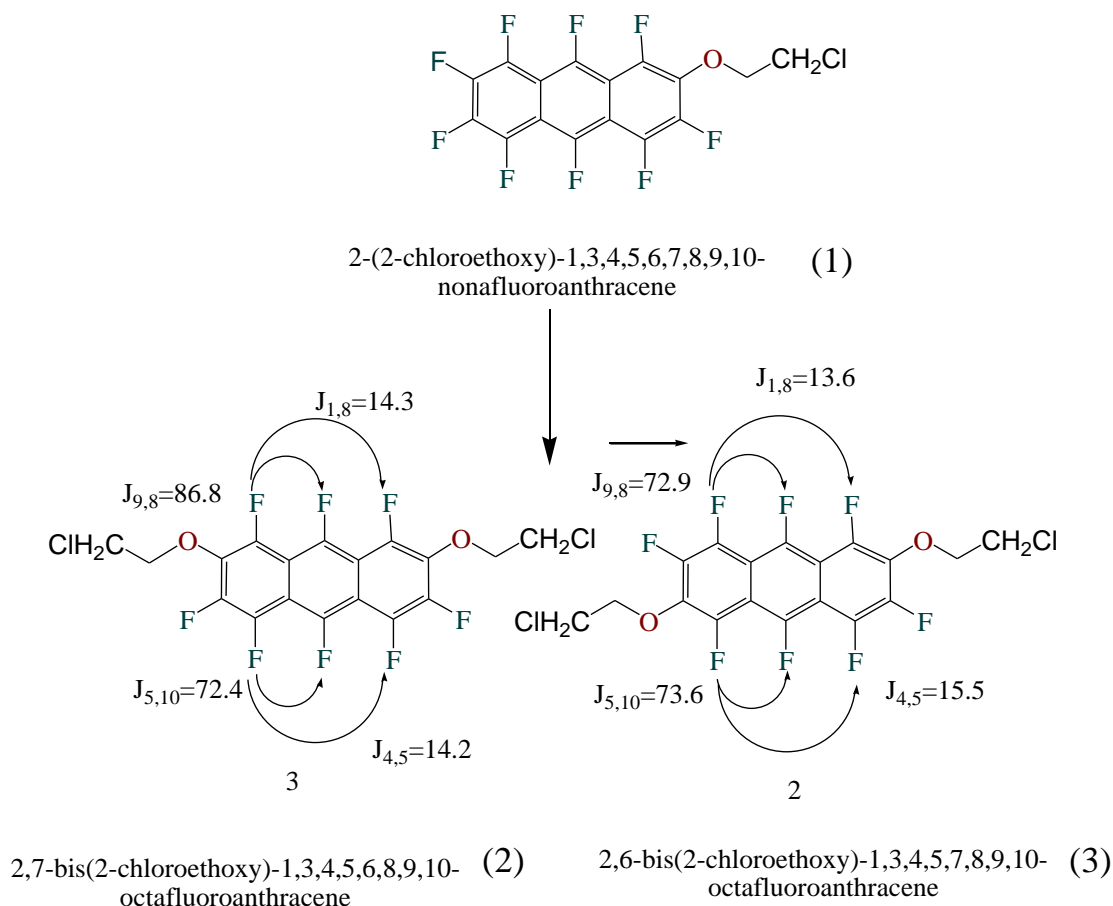
Figure 6.7: Two possible isomers arising from disubstitution on 2- (methoxy) fluoro anthracene (1), J couplings were calculated with M06-L using Jenison basis set pcJ-2[164] .

the resulted product NMR spectrum (given in Appendix) does not lead to any conclusion whether it is corresponding to 2,6-PFA (2) or 2,7-PFA (3) substitution. Both substitutions have four, ^{19}F-NMR (CDCl$_3$) signals : δ = -124.06 (m, 2F, F-9,F-10), - 139.58 (m, 2F, F-1,F-5), -147.50 (m, 2F, ?), -148.50 (m, 2F ?) ppm. A sharp peak at -148.5 ppm indicates two equivalent atoms and a peak at -147.5 ppm splits into two. This shows the possibility of 2-7 substitution and the two-methoxy substituent are in different conformations.

To determining whether the obtained product is 2, 6 or 2, 7, we computed the ^{19}F NMR chemical shift values for 2,6-PFA (2) and 2,7-PFA (3) and compared them with the experimental values. The deviations in the computed shift values for the corresponding isomers are shown in Table 6.6. The deviation corresponding to the two isomers are very much similar and only slight better comparison were found with 2,7-PFA (3) isomer.

Table 6. 6: Deviation ($\Delta\delta$, ppm) in the computed ^{19}F chemical shift values for two possible isomers from disubstitution on 2-fluoroanthracene with (-OCH$_2$CH$_2$-Cl) as the nucleophile. All calculation used 6-31+G (d, p) basis set

	$\Delta\delta$ (ppm)					δ(ppm)
2,6-PFA			**2,7-PFA**			
Position	**PBE0**	**BHandH**	**Atom**	**PBE0**	**BHandH**	**Expt**
F$_{9,10}$	2.6	-0.2	F$_{9,10}$	1.8	-0.6	-124.1
F$_{1,5}$	1.2	-2.3	F$_{1,8}$	1.4	-2.6	-139.3
F$_{4,8}$	0.5	-0.7	F$_{4,5}$	0.3	-0.6	-147.0
F$_{3,7}$	0.0	0.7	F$_{3,6}$	0.3	0.6	-148.6

Therefore it is difficult to say whether 2, 6 or 2,7 substitution occurred.

6.4   Conclusions

As we concluded in last chapter that functional PBE0 in combination with the 6-311+G (d,p) 6-311+G(2d,p) or any moderate pople type basis set is adequate to predict chemical shift values, when linear regression scheme is used to correct them. In this chapter a detailed study of the regioselectivity of the nucleophilic aromatic substitution in perfluoroanthrance has been carried out using selected DFT functionals and basis sets. Here we confirmed that the stability of the Meisenheimer complex helps in predicting aromatic nucleophilic substitution in fluoronapthalene, OPBE, PBE0, B3LYP, B97D in combination with 6-311+G(d,p) favors 2-substitution that is in-line with experiments but this approach fails to predict accurate substitution in perfluoroanthrance. A comparison of the computed (using PBE0 and BHandH functionals in combination with the 6-31+G(d,p) basis set) and experimental ^{19}F NMR chemical shift values shows that aromatic nucleophilic substitution on perfluoranthracene always results in 2-substitution as the major product. Both functionals PBE0 and BHandH predicted 2-substitution as the major product with –OMe, -N(Me)$_2$. A nucleophilic substitution on 2-OMe nonafluoroanthracene has produced a mixture of 2-3 disubtituted twist and chair ring-closed products. A disubstitution on nonafluoromonomethoxyanthracene has produced (2, 7) as major product.

7. Effective Computational Strategies for the Calculation of Exchange Coupling Constants

7.1 Introduction

One of the exciting research topics in the field of modern molecular science is the accurate determination of the magnetic exchange interaction between two spins in a single molecule or in solid state molecular magnetic systems, experimentally as well as theoretically [87, 165, 166]. The "molecule-to-material" approach is recognized to design materials with desired properties.

To generate novel magnetic materials by using the molecular approach, the magnetic exchange coupling (J) should be optimized, starting from the molecular level aiming at calculating macroscopic magnetic properties. Transition metal complexes, stable organic diradicals and metal-mono organic radical complexes are considered to be promising building blocks. So far, only a few stable organic diradicals like nitronyl nitroxide and iminio-nitroxide and copper (II) complexes are found to be the best candidates for designing fascinating magnetic materials [71, 167]. To synthesize magnetic materials based on organic molecules, it is important to gain an understanding of the key structural and electronic factors that control the exchange coupling between two nitronyl nitroxide units (units bearing two unpaired electrons) [168]. Therefore, reliable and quantitative prediction of magnetic coupling constants (J) using quantum chemical methods is of primary importance. The major obstacle in the prediction of accurate J accounts is that these diradical systems have various low-lying nearly degenerate electronic states and also each state has a different chemical behavior [169]. Therefore, one has to account for the multi-reference character of such systems while computing magnetic couplings, J.

Density functional theory has been used widely for studying organic and transition metal complexes of relevant molecular size [42]. [170]. In recent years, DFT has become a pivotal tool to predict magnetic exchange coupling constants (J) values for large molecular systems [171] and these calculations are usually done within the spin-polarized unrestricted formalism, which represents α and β spin orbitals by two different spatial parts.
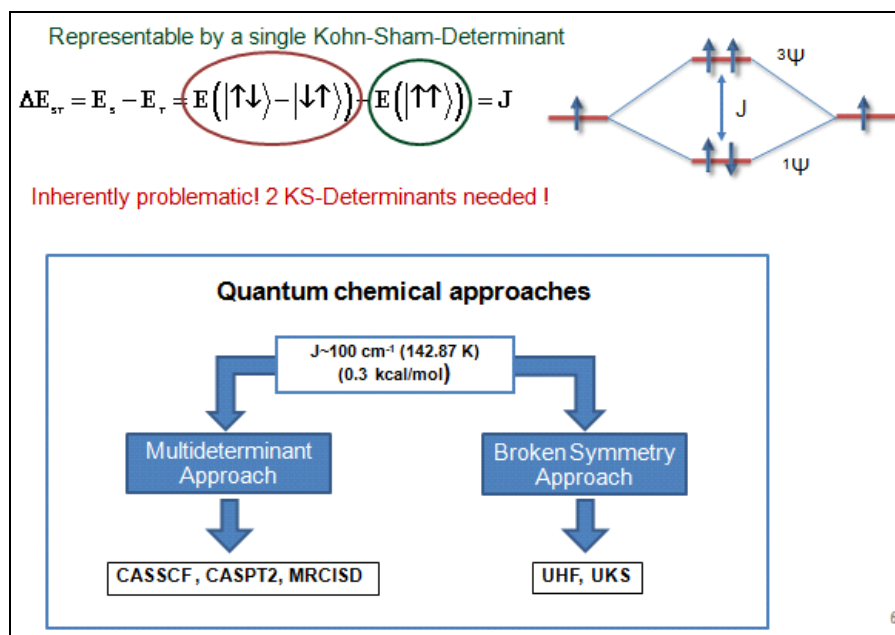
Figure 7. 1: Schematic illustration of quantum chemical interpretation of the J coupling.

Conceptual problems arise due to the single-determinant nature of modern DFT implementations within the Kohn-Sham (KS) framework, as depicted in Figure 7.1. While the ferromagnetic high-spin states are well represented by a single determinant, but this is generally not possible for lower spin states as the resulting orbitals are no longer pure spin eigenfunctions. A single configuration model containing non orthogonal magnetic orbital were proposed to represent the important features of the antiferromagnetic state of a spin dimer[76]. A spin state of lowered space symmetry (broken symmetry) was constructed. Both UHF and spin polarized DFT theory can be used to generate the mixed spin state wave function. The most important consequence of such a theory is that the Heisenberg exchange coupling constant J can be calculated simply from the energy of the mixed spin state and that of the highest spin multiplet. The extraordinary progress in this field is made due to the development of improved functional and a systematic benchmarking of available economic methods applied to transition metal compounds against selected experimental data [38, 172].

The aim of this work is to complement and to guide the preparative work on the development of molecular building blocks used to form extended coordination polymers. We aim at the understanding and control of the magnetic properties of the resulting materials. The first class of building blocks contains antiferromagnetically coupled nitronyl nitroxide (NN) as the spin carrier. The second class contains

coordination complexes of copper (II) ions as the spin carrier bridged by quinoid bridging ligands as shown in the TK91 [170, 173]

For a system containing two [40, 174, 175] magnetic centers with spins S_1 and S_2, the energy of the broken symmetry (BS) state is a weighted average of the energy values of the spin multiplets, detailed is given the theory chapters. In this chapter various strategies used to calculate the J coupling in the H-He system are discussed. Performances of both post-HF methods and broken symmetry approaches for predicting J by are compared. The application of the best methods for extended systems is reported in Chapter 8.

7.2 Computational Details

All DFT calculations were carried out using the GAUSSIAN09 [87] and the ORCA 2.7.0 computer programs and full CI calculations were carried out using the MOLPRO program [176]. The DFT functionals chosen for the benchmark study were BLYP, B3LYP [58, 92], PBE, PBE0 (dubbed PBE1PBE in Gaussian 03) [7, 52-54] BHandH, BHandHLYP [177] B97D, B971 and B972 [96].

All the calculations using the ORCA were carried out with the additional keywords TightSCF, NoFinalGrid and Grid4. The RIJONX approach was used along with the cc-pVXZ/J auxiliary basis set [70, 174]. The correlation-consistent basis sets of Dunning and co-workers, cc-pVXZ were employed. Single-point energy values were obtained using the cc-pVXZ basis sets. An extrapolation to the complete basis set limit (CBS) was obtained using the scheme of Peterson and co-workers [178, 179]. The extrapolated values were chosen as the reference for checking the values obtained using the DFT method for the small systems. Originally, Feller et. al. [180] proposed the following scheme for correlation-consistent basis set extrapolation:

$$E(X) = E(\infty) + Be^{-CX}$$

(6.2)

where X represents the cardinal number of the correlation-consistent basis set, i.e. X = 4 and 5 for the cc-pVQZ and cc-pV5Z basis sets, respectively. $E(\infty)$ is the energy at the CBS limit, B and C are fitting parameters. Equation (6.3) is used for FCI energy extrapolation.

$$E_{xtra}(XY) = E_Y^{HF} + \frac{\left(X^3 \cdot E_X^{corr} - Y^3 \cdot E_Y^{corr}\right)}{X^3 - Y^3}$$

(6.3)

HF and DFT energy values were extrapolated using a two point extrapolation scheme:

$$E_L^{HF} = E_\infty^{HF} + A^{HF}(L+1)e^{-B\sqrt{L}}$$

(6.4)

L is the highest angular momentum of the used basis set. By solving equation (6.4) the following explicit expression to extrapolate total electronic energies was yielded [180, 181].

$$E_{xtra}(Q,5) = \frac{E_Q + (E_Q - E_5)}{\left(4\dfrac{\left(9\left(\sqrt{(4)} - \sqrt{(3)}\right)\right)}{5} - 1\right)}$$

(6.5)

7.3 Results and Discussions

7.3.1 Broken Symmetry Approach

For two interacting spins the Heisenberg spin Hamiltonian [182] is given as:

$$H = -2J\hat{S}_1 \cdot \hat{S}_2$$

(6.6)

where S_1 and S_2 are the local spin operators for each of the paramagnetic centers in a system with two unpaired electrons. The exchange coupling constant J is given by

$$2J = (E_S - E_T).$$

(6.7)

Here E_S and E_T are the energies of the singlet and triplet spin states. In principle, this can be calculated accurately using high levels of theory such as the FCI and DDCI but application of such method on relevant system is not possible. It must be noted that to obtain the magnetic exchange coupling constant one has to calculate energy differences that is very usually less than 100 cm^{-1} (0. 3 kcal/mol) and in the DFG project we aimed at is even less about 25 cm^{-1}, which is very small when compared to the total energy. Such small singlet-triplet state gaps have a spin contamination of the triplet state from higher spin states .Therefore, multi-determinant approaches are needed to obtain a high accuracy.

However, such multi-determinant methodologies are computationally demanding and usually a simplified model structure is required to reduce the number of atoms in a calculation [183, 184]. An alternative method is provided by the broken symmetry (BS) approach given by Noodleman et al [76]. This approach consists of performing either an unrestricted Hartree-Fock (UHF) or a density functional theory (DFT) calculation.

7.3.2 Model System H-He-H

A popular model system, H-He-H was used to test the performance of various quantum chemical methods. This model system has two unpaired electrons (one on each H atom) coupled through a super exchange pathway (via He spacer). The

exchange interaction between two magnetic orbitals in magnetic compounds arises through the bridging atom situated between the magnetic orbitals and is called super exchange interaction.The coupling strength changes along the He-H bond length[175, 185].On H-He-H system, in which two hydrogen atoms are bridge via He atom is crucial test system on which FCI calculations can be performed. Estimation of bridging group effect on magnetic interaction in this system can be useful, it will help for designing approach to calculate magnetic interactions in organic diradicals mediated with bringing molecule. The one-electron orbital scheme for H-He-H spin is shown in Figure 7.2. The interactions arise from a distribution of four electrons in three orbitals. The low-lying singlet state is $^1\sum_g^+$ and the triplet is $^3\sum_u^+$ the singlet-triplet energy gap (E_S-E_T) computed and it is called magnetic moment. To describe the influence of bridging atom on J, a number of theoretical methods were tried.
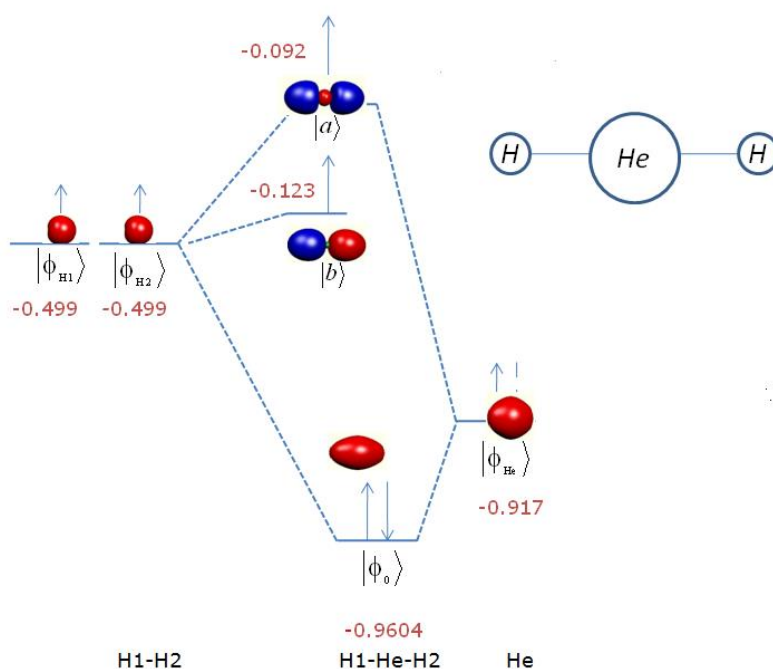
Figure 7. 2: Interaction in H-He-H system

7.3.3 Effect of a Bridge (Spacer) on Exchange Coupling (J)

To analyze the bridging atom effect on magnetic coupling, a H_2 model molecular system was chosen. In H_2 two molecular orbitals arise when two hydrogen atoms are brought together. A second model system we used was H-He-H, a three center, four electron systems consisting of three separated atoms. Similar to H-He-H model

system, Nitronyl nitroxide (BNN) bridged through an aromatic ring, conjugated π-systems and metal mediated diradical complexes [175, 186, 187].

The added neutral bridging atom increases the strength of the coupling. This can be explained by the super exchange mechanism [187, 188]. An understanding of the effect of the bridging group on *J* is crucial to calculate accurate exchange couplings accuratly in systems where two interacting spins are coupled via a bridging group, for example, nitronyl nitroxide-benzene-nitronyl nitroxide (NN-Ph-NN).

7.3.4   Effect of the Bridge Angle $^{(\theta)}$ on J for the Model Molecule,

H-He-H

Bridging group angle effect on magnetic exchange couplings was also tested and to investigate the effect of the H–He–H angle the bridge angle was changed from 110.0° to 180.0° with the H–He distance fixed at 1.25 Å.

An accurate description of magnetic exchange between two bridged magnetic spins (i.e H-He-H) need a proper treatment of the charge transfer between the bridging atom and the side atoms.

Also the performance of different difference dedicated CI (DDCI) and FCI, are compared however, these methods are computationally too expensive to apply to chemically relevant systems and alternate inexpensive methods are needed. Methods such as the difference dedicated CI (DDCI) method has been proposed for the determination of the bridging ligand orbitals involved in charge transfer excitations. The DDCI method was classified as single excitation (DDCI1), double excitation (DDCI2) and triplet excitation (DDCI3) based on the excitation. Table 7.2 lists the variation in *J* with the variation in θ. The performance of different methods was compared to the values obtained using the FCI method. It was observed that *J* was sensitive to θ

Table 7. 1: Variation in J with a variation in θ for the H-He-H model molecule system.

θ/°	DDCI1	DDCI2	DDCI3	FCI
110	-192,5	-206	-217,5	-224
120	-298	-372,5	-363	-363,5
130	-813	-959,5	-967	-963,5
140	-1273	-1479	-1497,5	-1490
150	-1643	-1888	-1919,5	-1909,5
160	-1911	-2184	-2223	-2210,5
170	-2072	-2360,5	-2404,5	-2391
180	-2068,5	-2392	-2555,5	-2451

It is clear that DDCI1 method underestimates the 2J value when compared to the FCI and does not show any improvement over CASSCF. However, the DDCI2 method shows a significant improvement over DDCI1 and produces a 2J value that is in good agreement with that compared from the FCI method. In contrast, the DDCI3 method overestimates the value of 2J. The deviations in 2J values obtained by different methods are plotted in Figure 7.7. The lowest deviation was seen for the DDCI2 and DDCI3 methods. The DDCI2 can be considered the best method according to cost and accuracy.

7.3.5   The Effect of Varying the H-He Bond Distance on J

We aimed at compare the performance of different approaches to predict accurate J value for existing systems. The crucial part of this study was to predict the J values within 25 cm^{-1} for spin-dimers synthesized or to be synthesized in the laboratory.

A few studies have been carried out previously to understand the relationship between J and the distance between interacting spins [40, 189-191]. As the distance between two atoms increases, the overlap between two adjacent magnetic orbital decreases, resulting in a lower J value. The magnetic exchange coupling constant values in Table 7.3 implies that the value of J depends strongly on the H-He distance. We tested the performance of some other methods (DDCI (I-III), CASPT2 and NEVPT2) in predicting J at various values of the H-He distance, as listed in Table 7.3.

Table 7. 2: Performance of different abinito methods in predicting *J* values at various H-He bond distances. The cc-pVTZ basis set was used in all the calculation.

$d_{H\text{-}He}$ / Å	1.25	1.625	2.00
CAS(2,2)	-2080.5	-235.5	-22.5
DDCI1	-2068.5	-233.5	-22.5
DDCI2	-2392.0	-260.0	-23.5
DDCI3	-2555.5	-284.0	-25.5
FCI	-2451.0	-274.5	-25.5

As table shows DDCI2 predict values that qualitatively comparable with FCI .Above studies reflect the effect on magnetic couplings of changing distance of two spins, bridging group effect or bridging atom effect on J. these cannot be used to predict practically usable systems. So we have to find out cheaper alternate to predict above mentioned effects on magnetic exchange couplings. Further we did a benchmark study of various methods to predict

magnetic exchange couplings.

7.3.6 Benchmark Study of QM methods and Basis Sets to Calculate J

7.3.6.1 Application of the Broken Symmetry Approach

Another inexpensive approach to predict the J value was found to be the Broken Symmetry (BS) approach proposed by Noodleman [76]. It can be applied within the UHF method or the density functional theory (DFT), which requires modest computational cost. The BS approach has been tested on various spin dimer systems of different magnetic coupling strengths and various sub-approaches have been proposed. They are successful for some systems. But they fail for some. Various DFT methods and the basis sets have been tested recently and the search is still on to find the best DFT method and basis set combination to predict the J value. *Here,* we tested various density functionals in combination with different basis sets to reproduce the J value obtained by the FCI method.

7.3.6.2 Validation of the Methods

Various DFT functionals and basis sets were tested to calculate J in the H-He-H spin dimer. The results obtained from the DFT calculation were compared with that of the FCI. For the H-He-H model, following bond-distances were chosen to calculate J: 1.25 Å (strongly coupled) 1.625 Å (moderately coupled) and 2.50 Å (weakly coupled). We further compared the performance of CASSCF, CASPT2 and B3LYP methods in predicting J values for H-He-H model system at various H-He distances. The results are listed in Table 7.5. It is seen that the CASSCF method underestimates the J value. This may be due to the reason that the CASSCF method does not account for dynamic correlation. The CASPT2 method underestimates J slightly, when compared to the FCI value. Similar trends were reported for the calculation J [192, 193].

Table 7. 3: Exchange coupling constant J (cm^{-1}) for the H-----He----H system at different H–He distances deduced from calculated energies of triplet, broken-symmetry and singlet states. Basis set: cc-pVTZ

	H-He-H			
	J_2	$J=(E_S-E_T(cm^{-1}))/2$		
H-He(Å)	B3LYP-BS	CAS(3,4)	CASPT2	FCI/CBS
1.250	-2156.6	-2123.7	-2432.4	-2450.8
1.625	-254.4	-238.6	-274.5	-274.7
2.000	-28.1	-23.0	-25.6	-25.3
2.500	-1.3	-0.9	-1.0	-0.9

The CASPT2 method can be a good choice for calculating J. In the medium coupling strength region the B3LYP method underestimates the J value, while in the weak coupling strength region it overestimates J.

7.3.6.5 Basis Set Selection

To assess the influence of different types of basis sets on the computed value of J, the errors are listed in percentages in Table 7.4. The BLYP functional in combination

with different basis sets, ranging from the minimum split valence double zeta to polarized triple zeta quality were used. The use of the 6-311++G(d, p) basis set produced a minimum deviation. The basis sets 6-31++G (d, p) and aug-cc-pVTZ were found to be the second best and third best in the list. The computational cost for the use of the aug-cc-pVTZ basis set is relatively high. Moving from double zeta to triple zeta basis sets, improve the accuracy and addition to that use of diffuse functions, and improve J value further.

Table 7. 4: The influence of the basis set influence on the value of J calculated using the BLYP functional for H-He-H for various H-He bond distances.

	d_{H-He}/Å		
	1. 25	**1.625**	**2.0**
Basis set	**% ΔJ**		
SVP	-624.0 (12.6)	-63.0 (11.0)	-16.0 (29.1)
TZVP	-412.0 (8.3)	-31.0 (5.4)	-11.0 (20.0)
6-31G (d, p)	-693.0 (14.0)	-86.0 (15.0)	-20.0 (36.4)
6-31++G (d, p)	-178.0 (3.6)	-18.0 (3.1)	-14.0 (18.2)
6-311G (d, p)	-431.0 (8.7)	-46.0 (8.0)	-10.0 (25.5)
6-311++G (d, p)	-130.0 (2.6)	-11.0 (1.9)	-14.0 (18.2)
cc-pVDZ	-605.0 (12.2)	-48.0 (8.3)	-10.0 (25.5)
cc-pVTZ	-341.0 (6.9)	-37.0 (6.4)	-13.0 (23.6)
aug-cc-pVTZ	-155.0 (3.1)	-25.0 (4.3)	-13.0 (23.6)

$\%\Delta J=(J-J_{FCI})*100/J$

7.3.6.7 The performance of the different DFT functional in calculating the *J* value.

Table 7.5, present DFT functional performance comparisons for predicting J value for H-He-H system at various distance. We note that a pure functional like BLYP produced a lower % error as compared to its hybrid counterpart B3LYP. It was seen that the amount of % HF exchange plays an important role in predicting *J*, but only if it was added in low quantity

.

Table 7. 5: The performance of different functional to calculate the J value for He-He-H at various H-He bond distances. In all calculations the 6-311++G (d, p) basis set was used. [a] H-He distance in atomic uni

Functionals	1. 25[a]	1.625[a]	2.0[a]
		% ΔJ	
BLYP	2.6	1.9	18.2
PBE	-13.7	-22.8	-23.6
OPBE	-13.6	-25.4	-21.8
PBE0	-30.1	-35.0	-34.5
B3LYP	-16.1	-14.6	-1.8
B97D	40.5	-20.0	-61.8
B971	-25.2	-44.9	-60.0
B972	-21.8	-47.8	-65.5
BhandH	-29.5	-25.7	-14.5
BHandHLYP	-33.0	-30.8	-21.8

The hybrid functional with large % HF quantity show a large deviation. For example, the B3LYP (20% HF) performed better than PBE0 (25% HF) and BHandHLYP (50% HF). The overall best suited functionals were BLYP and B3LYP at H-He distance 2. In conclusion, either a pure functional or a hybrid functional with a small amount of Hartree-Fock exchange is best suited to calculate the J value for the H-He-H system.

7.4 Conclusions

In this chapter we have discussed the effect of changing bond distances, bridging atom and bridging angle on the magnetic coupling constant of H-He-H as a model spin dimer. Our results show that an increase in the distance between the two interacting spins lowers the *J* values and if a bridging atom (or a π-conjugated system) is added, it helps in spin propagation which would certainly increase the coupling strength. To predict the value of J accurately, the effect of such a mediating group must be accounted for properly in the calculations.

For comparisons the performance of various post-HF methods in predicting the J values was tested in three different magnetic coupling ranges and among all post-HF methods, DDCI-3 was found to be the best alternative to FCI as per computational cost and accuracy. The DDCI-2 and CASPT2 method in combination with the cc-pVTZ basis was found to be an alternative.

All DFT calculations were done using broken symmetry approach. The Broken symmetry approach is considered a suitable method in terms of computational cost and accuracy however prediction consistency is not visible in coupling strength range. Among tested DFT functional we have not found any functional that predicts accurate coupling among in all coupling strength. The pure functional BLYP in combination with the 6-311++G (d, p) basis set was found be the best performer in strong and medium coupling range strength and on other hand in for week coupling strength B3LYP found best performer. A double zeta function with at least one diffuse function is necessary to predict qualitative J value for H-He systems.

8. Calculation of Magnetic Exchange Coupling Constant for BNN and its Analogues

8.1 Introduction

The accurate calculation of magnetic exchange couplings in bis nitronyl nitroxides (BNN) and its analogues is part of the collaborative TR-SFB49 project title rational design with input from DFT calculations and preparation of coordination polymer-based quantum magnets. In this project three research teams were directly involved, two experimentalist groups and one theoretical team. Both experimental teams are much advanced in synthesizing BNN and metal based organic diradicals. The groups of Wagner [170] and Baumgarten group have expertise in the preparation of low-dimensional solids from soluble precursor molecules. Baumgartn group already synthesized various BNN based molecules[194]. Max Hotlhausen group had expertise in DFT for calculating structural properties. Calculation of accurate magnetic exchange couplings for BNN molecules was very much crucial for this collaborative project.This chapter main focus is on finding best approach to calculate magnetic exchange couplings for BNN and application of selected approach to calculate exchange coupling in bigger BNN. The design of magnetic materials using a 'molecule-to-material approach' is an active research area. An organic material designed on a molecular basis seems to be promising candidates for optical and low weight electronic devices [195-197]. The organic diradicals are frequently recognized as interesting building blocks for molecule-based magnetic materials. These materials being light in weight have a very good scope in the design of low weight computer hard disk. The basic requirement is the stability stable organic

diradical .So far only a few stable organic diradicals Nitronyl nitroxides(NNO), bis-nitronyl nitroxide (BNN) and imino nitroxide (IN) have been identify [198, 199]. Many diradical entities have been synthesized using these basic units and a large number of them are antiferromagnetically coupled[194, 200]. The intermolecular magnetic interaction in these entities depends on the structure and the nature of the molecular crystal which controls the total magnetic moment of the material [201].

Our main focus is on deep understanding about A detailed quantum chemical study of such diradical molecules is essential to guide a rational design of new magnetic materials. An accurate estimate of the intermolecular and intra-molecular exchange coupling constant of basic building blocks is a prerequisite to identify a novel magnetic material.

In chapter 6, the effect of the bridge angle and He-H distance on J was investigated for the model spin dimer (H-He-H). The performance of various density functionals and basis sets in calculating J was also evaluated. In this chapter, we discuss a benchmark study to find the best method to predict J accurately for BNN diradicals and its analogues. Various models and synthesized molecules with different coupling strength were used in the benchmark data.

8.2   Computational details

All DFT calculations were performed using GAUSSIAN 09 and ORCA programs. Full-CI calculations were carried out with MOLPRO 09 and for visualization the Chemcraft, Molekel and GaussView5.0 programs were used. Most of the organic radical geometries were fully optimized at the ROHF/6-311++G (d, p) level unless theory or mentioned otherwise. The CASSCF and N Electron Valence State Perturbation Theory (NEVPT2) calculations were performed using the ORCA program. *ORCA* has implemented the strongly contracted version of the NEVPT2. Strongly contracted NEVPT2 is an internally contracted multireference perturbation theory which applies to CASSCF type wave functions. It is therefore an alternative to the popular CASPT2 method[202].

For all DFT calculations, the broken symmetry (BS) approach was used to compute *J.* The BS calculations were performed using the geometries obtained with the spin multiplicity either triplet or singlet. In some cases the geometry was optimized using the ROHF method. The "gauss=mix" keyword was used to obtain the BS state. In

cases where, there was no convergence reached, the "SCF=QC" was used. The overlapping integral between two magnetic orbitals was calculated as suggested by Neese [70].

$$S_{AB} = 1 - \langle S_{BS} \rangle^2 \quad . \tag{7.1}$$

Functional BLYP, PBE, PBE0, OPBE, B3LYP, BHandHLYP, M06, M06-2 and M06-L were used in this study. The double-hybrid functionals B2-PLYP and B2GP-PLYP (which differ by the amount of Fock-exchange and perturbative correlation) were also included in the test. A dispersion corrected DSD-LYP functional which uses only the double hybrid density functional part of DSD-BLYP [203, 204] was also tested.

Functional	Keyword in Gaussian09
B2GP-PLYP	B2PLYP/ iop (3/125=03600036003/76=0350006500,3/78=0640006400)
DSD-BLYP	B2PLYP/ iop (3/125=04000046003/76=0300007000,3/78=0560005600)

8.3 Results and Discussion

Bis-nitronyl nitroxide (BNN) is a stable organic diradical and it has been studied extensively as the basic building block to design an array of antiferromagnetically coupled pairs of $S_z=1/2$ ions. Much effort has given into understanding the magnetic properties of these biradicals.
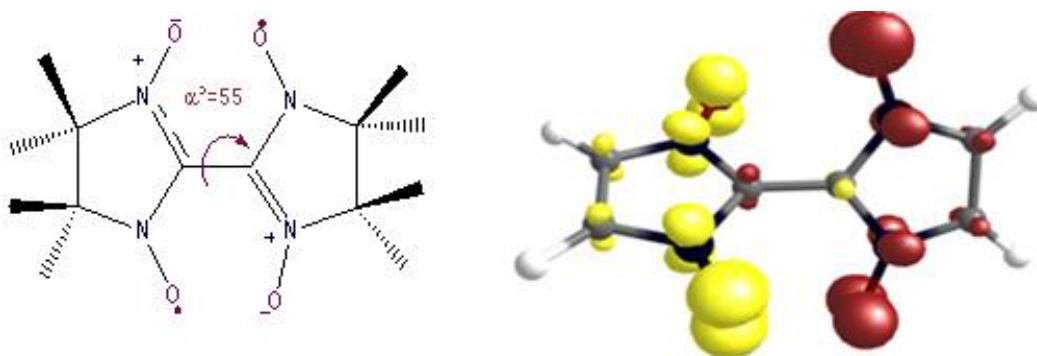

Figure 8. 1: Molecular structure of bis nitronyl nitroxide(BNN) and broken symmetry spin density plot(Red: α ,Yellow :β).

In BNN, the two radicals are connected by a C-C bond (Figure 8.1) and Table 8.1 presents the calculated *J* values and dihedral angles between the two NCN planes ($N_1C_5N_2$ and $N_3C_6N_4$). It was found that all functionals suggest the open-shell singlet

state to be slightly more stable than the triplet state. It was also found by that the ground state of BNN is significantly governed by the conformation of the molecule, particularly the torsion angle between the two five membered rings (ref). If the geometry of BNN is fully optimized in the triplet state, a higher dihedral angle ($\alpha \sim 90°$) was found. It is to be noted that the magnetic interaction in BNN depends strongly on the torsion angle of the C-C unit (i.e N-C-C-N). A small change in the torsion angle leads higher magnetic orbitals coupling between two NNOs and that add to a significant change in the magnetic coupling.

8.3.1 Predicting *J* at various Dihedral angle ($\alpha°$)

The performance of various density functionals in predicting J the value of *J* for different dihedral angles is illustrated in Figure 8.2. The results show that BNN remains antiferromagnetically coupled while changing the dihedral angle. (BNN Twisted with 55 $\alpha°$, at this torsion, the BLYP functional method with 16% HF exchange predicts the J value to be -160/cm^{-1} and that is a good agreement with the experimental value [205]. The PBE functional underestimates J (-78/cm^{-1}). On the other hand the CASSCF (6,6) method overestimates the J (-254/cm^{-1}) significantly and the NEVPT2 (6,6) which includes dynamic correlation, gave slightly improved results with J -230/cm^{-1}.
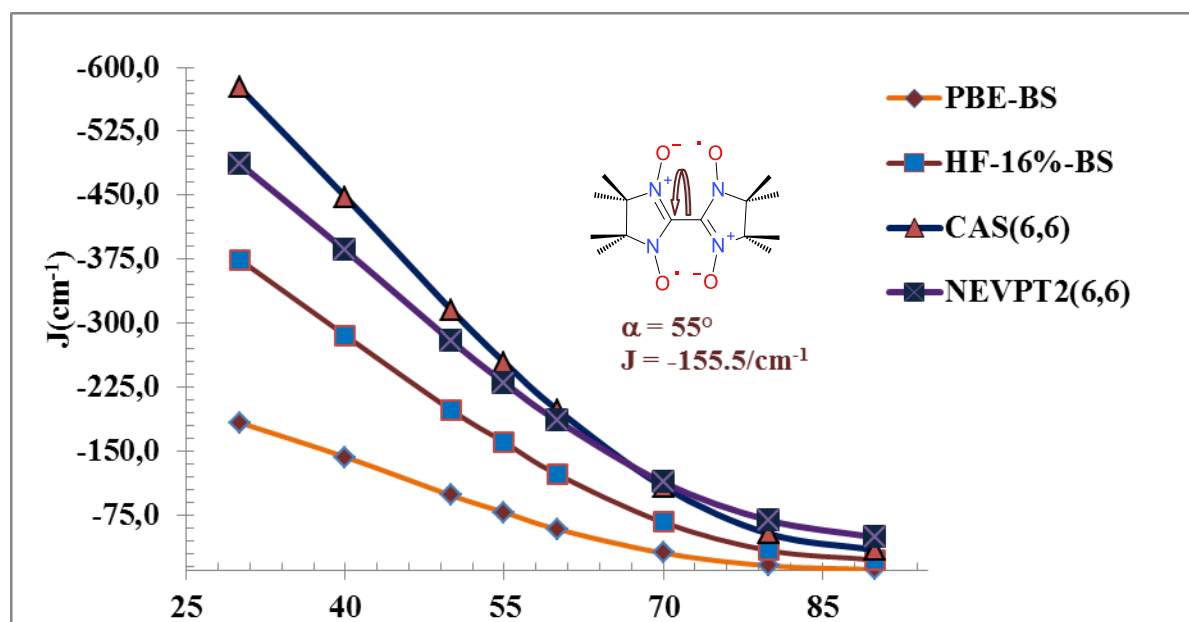
Figure 8. 2: Comparison of the variation of J with $\alpha°$ for the BNN model (BS was used with the cc-pVTZ basis set).

8.3.2 The Effect of Geometry Optimization on α and J

To guide a synthetic chemist for designing a molecule with desired property, the value of α for the most stable geometry must be known. We need a method that can predict α accurately or the dihedral angle units. To arrive of an optimal method, we carried out a benchmark study.

Geometry optimization was carried out with singlet and triplet spin states in the restricted open shell HF (ROHF) formalism. The results obtained are summarized in Table 8.1. For the singlet state the BLYP functional led to the most accurate torsion angle (α= 51.2 °). The other two functionals, which gave fairly well α values were PBE (α = 48.9°) and B3LYP (α = 48.2°). Overall, the DFT method underestimates the torsion angle for the most stable geometry in the single state. The M06-L functional produced the best result of J/cm^{-1}, = -179. The two other pure functionals BLYP and PBE also gave reasonable J values. It was found that all the functional used functionals overestimated the α value for the triplet state, when compared to the experimental result. Only two functionals, the M06-L and M06, could predict a reasonably accurate torsion angle (M06-L: α= 62.0°, M06-2X: α= 64.0°). For the triplet state, none of the functionals was found to be reliable. In summary, the BLYP functional for the singlet state and the M06-L functional for the triplet state produced the best value of α. In the singlet state, a higher percentage of HF exchange resulted in a lowering of the dihedral angle, while an opposite trend was observed in the triplet state.

Table 8. 1: The optimized value of the torsion angle (α/°) and a comparison of the J values calculated using different functional for BNN. All calculations were performed using the 6-311++G (d, p) basis set.

Singlet	α°	$<S^2>_T$	$<S^2>_{BS}$	J_2
Singlet				
BLYP	51.2	2.02	1.01	-113
PBE	48.9	2.02	1.00	-127
M06-L	45.1	2.04	1.05	-179
B3LYP	48.2	2.09	1.13	-303
PBE0	46.6	2.11	1.17	-391
M06	44.9	2.08	1.11	-301
M06-2X	43.3	2.16	1.23	-584

BHandH	42.0	2.21	1.31	-781
BHandHLYP	46.4	2.26	1.36	-727
Triplet				
BLYP	89.7	2.02	1.03	-12
PBE	89.2	2.02	1.02	-12
M06-L	62.0	2.04	1.06	-71
B3LYP	89.3	2.1	1.11	-31
PBE0	90.0	2.13	1.14	-39
M06	64.0	2.09	1.11	-112
M06-2X	78.0	2.19	1.20	-60
BHandH	90.3	2.25	1.26	-70
BHandHLYP	90.6	2.31	1.33	-86
Expt	55.0			-156

8.3.3   Assessment of Various DFT Functionals used in Calculations

In this section, we report on the performance of DFT functionals with varying amount of Hartree–Fock exchange in predicting J value for the BNN diradical at the fixed torsion angle (α=55°, an experimental value from BNN x-ray structure) [205]. The deviation in the calculated value of J from the experimental value is depicted in figure 8.3.
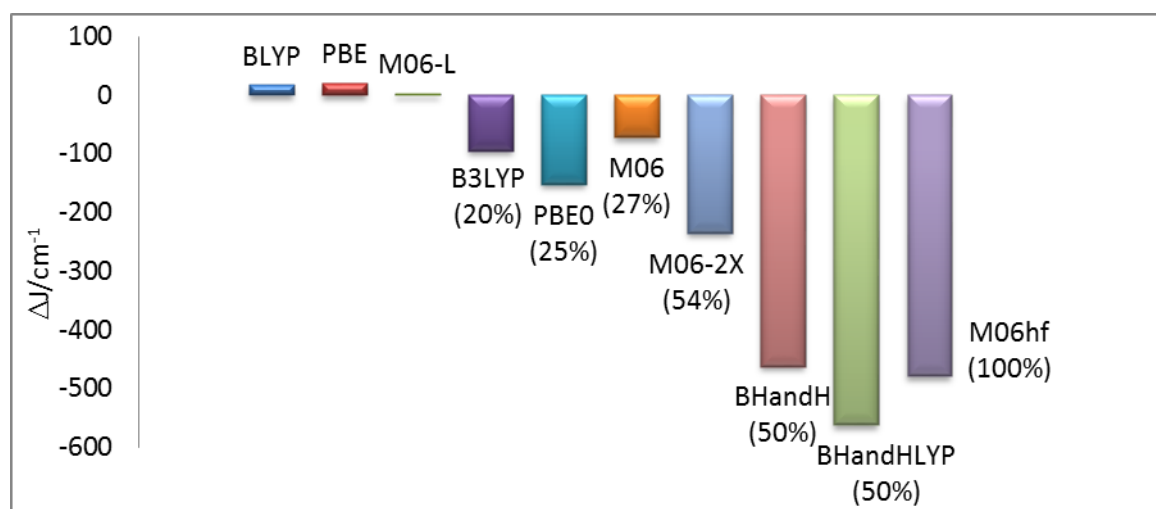
Figure 8. 3: Deviations in J (in cm^{-1}) for BNN. Broken symmetry calculation were done using 6-311+ (G, d,p) Basis set at ROHF/6-311++G (d, p) geometry (where α°=55 (N-C-C-N) kept fixed).

It can be seen clearly that the pure functionals underestimate the J value, while hybrid functionals overestimate it. If we meta GGA, M06 family functions, deviation in predicted J increase with increasing %HF and among these M06 family functions, M06-L functionals turned out to be the best for predicting J for BNN among this category functions. For Becke functions, BLYP and B3LYP deviation increase with increasing %HF. As shown in figure 8.3 value of the coupling constant increases with an increase in the amount of Hartree–Fock exchange. The large deviations obtained when a higher percentage of HF-exchange was used within similar functions.

## 8.3.4   Correcting the J value using the Linear Regression

The performance of DFT functionals in predicting the J value was previously evaluated by Zein et al [197]. In this section we have investigated the applicability of linear scaling to correct the calculated magnetic coupling constant values for H-He-H and BNN.

For the initial test, H-He-H model was chosen and the J value was calculated at various H-He distances in the range of 1.625 to 2.20 Å, 10 points as given in Table 8.2. This range corresponds to medium to weak coupling strength (ca: -275 to -7.0, cm^{-1}). The FCI results on H-He-H system shows that the couplings for the two limiting cases; that is H-He bond length = 1.625 Å J = -275 cm^{-1} and H-He bond length = 2.2 Å J = -7 cm^{-1}) which lies in the range of our interest of magnetic coupling strength. Table 8.2 presents the calculated J values (J=E_{BS}-E_T/2) at various H-He distances. In previous chapter study we found 6-311++G(d,p) basis set as a good performer for calculating J value for H-He-H system. In this study we used same basis set Our main propose in this study is find a functional that can predict accurate couplings between high coupling strength to low coupling strength and addition to that the performance of double-hybrids B2-PLYP and B2GP-PLYP are included in this study, these function differ by the amount of Fock-exchange and perturbative correlation and DSDB-LYP, a dispersion corrected functional without the additional perturbation correction was assessed, and recently Grimme and coworkers showed that these functions perform better than regularly used functions, B3LYP,BHandH and M06 [206]. There have been several studies on the use of linear regression correction scheme to improve the calculated magnetic exchange couplings values [172, 207]. In this study, calculated couplings were corrected using

equation (8.1) in which self-regression correction parameters (Slope and Intercept) were used.

$$J_{Predicted} = Slope * J_{Calculated} + Intercept. \qquad (8.1)$$

Linear regression correction scheme leads to a standard error (SE), which in general is used as a parameter to define the quality of the method used. The regression plot between the calculated and the FCI values are illustrated in Figure 8.4.
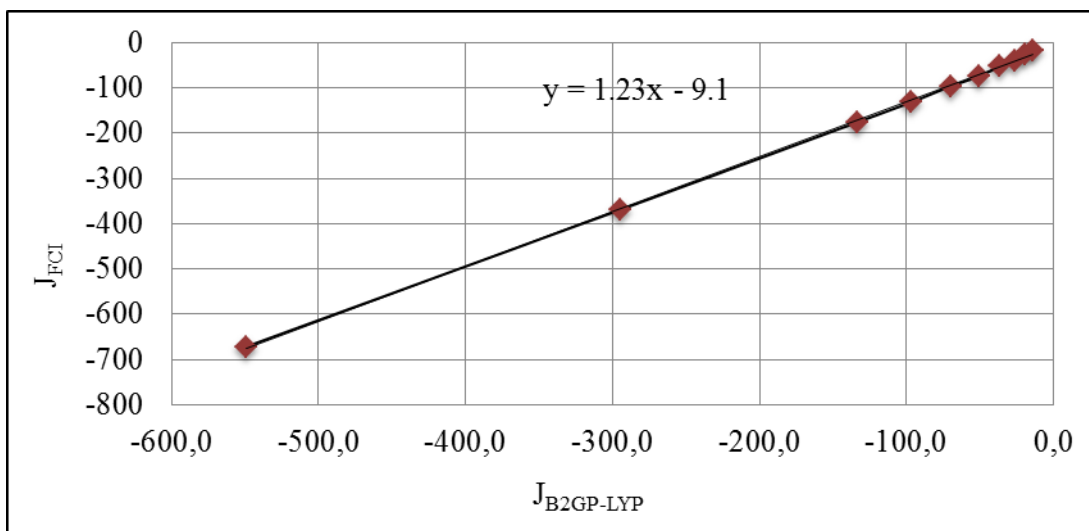
Figure 8. 4: Regression line for JFCI, values with respect to DFTvalues obtained using the B2GP-PLYP functionals the and 6-311+G (d,p) basis set.

Table 8. 2: Linear regression parameters from DFT vs. FCI H-He bond distance varies from 1.625 Å to 2.20Å.

Functionals	Slope	Intercept	R^2	SE /cm^{-1}
BLYP	0.47	4.0	0.999	2.0
B3-LYP	0.57	3.9	0.999	2.1
BHandH-LYP	0.69	3.1	1.000	2.1
B2-PLYP	0.77	3.2	0.999	1.9
DSDB-LYP	0.94	14.5	1.000	26.2
B2GP-PLYP	0.82	2.8	0.997	2.1
M06-L	0.90	-17.2	0.942	8.4
PBE	0.62	0.8	1.000	0.3
PBE0	0.74	0.7	1.000	0.4

A significant improvement in magnetic exchange coupling constants was obtained by using the linear regression correction scheme. Each of the functionals used shows an improvement in J.

Table 8. 3: Magnetic coupling constant J (in cm^{-1}) for H-He-H at various He-H distance. In all calculations the 6-311++G(d,p) basis set was used.

$d_{H\text{-}He(Å)}$	B-LYP	B3-LYP	BHandH-LYP	B2-PLYP	DSD-LYP	B2GP-PLYP	M06-L	PBE	PBE0	J_{FCI}
1.625	-586	-491	-398	-360	-295.6	-336	-291	-444	-374	-275
1.725	-326	-273	-222	-200	-163.1	-184	-135	-238	-201	-147
1.850	-157	-131	-106	-94	-154.2	-88	-43	-109	-92	-67
1.900	-117	-98	-79	-70	-114.0	-66	-22	-80	-67	-48
1.950	-87	-73	-58	-53	-84.3	-48	-10	-58	-49	-35
2.000	-65	-54	-43	-40	-62.3	-37	-5	-42	-36	-25
2.050	-49	-41	-32	-29	-46.0	-26	-2	-31	-26	-18
2.100	-36	-30	-24	-20	-33.9	-20	0	-22	-19	-13
2.150	-27	-22	-17	-15	-24.9	-13	1	-16	-14	-10
2.200	-20	-17	-13	-13	-18.3	-9	1	-12	-10	-7

Amongst the used functionals, PBE0, DSDB-LYP and B2GP-PLYP were found to be the best performers. On comparing the results obtained using the BLYP, B3LYP and BHandHLYP, it was inferred that the added Hartree-Fock exchange improves the results as B3LYP functional with 20% HF exchange shows less deviation than BLYP does. A further improvement was seen with the BHandHLYP method which has 50% HF. In summary, DSDB-LYP, B2GP-PLYP, PBE0 in combination with the 6-311++G (d,p) basis set could predict the coupling constant value accurately within 8-30% of the FCI results.

8.3.5 Linear Regression Correction to Nitronyl Nitroxides analogues

After correcting the J value successfully for the H-He-H model spin dimer, the performance of the linear regression correction approach was applied to the case of nitronyl nitroxides and its analogues. The DFT functions, DSDB-LYP, B2GP-PLYP, and PBE0 that showed good performance for predicting J for H-He-H system.

Table 8. 4: Regression parameters used to correct the calculated J value (in Table 7.10) for NNO radicals.

S_1(NNO)	BLYP	M06-L	PBE
Slope	1.29	0.97	1.32
Intercept	-3.72	-10.06	-18.39
S_2(H-He-H)			
Slope	0.47	0.90	0.62
Intercept	8.02	-34.30	1.60

NNOs = for regression data Nitronyl nitroxide set is used

Table 8. 5: Application to extended nitronyl nitroxide structures, using two S_1 and S_2 are two regression parameters: S_1 from NNOs and S_2 from H-He-H.

	NN-NN	NN-Thio-NN	NN-eth-NN	NN-3eth-NN	NN-Ph-Ph-NN	NN-m-Ph-NN	NN-Py-NN
				BLYP			
$J_{calculated}$	-138.5	-53.2	-89.1	-6.7	-3.4	3.7	1.1
$J_{corrected}(S_1)$	-156.4	-54.9	-97.6	0.6	4.5	12.9	9.8
$J_{corrected}(S_2)$	-64.6	-24.5	-41.4	-2.7	-1.1	2.2	1.0
				M06-L			
$J_{calculated}$	-151.5	-100.9	-164.8	-5.2	-6.3	10.1	3.3
$J_{corrected}(S_1)$	-112.7	-72.9	-123.2	2.5	1.6	14.5	9.2
$J_{corrected}(S_2)$	-135.5	-89.9	-147.5	-3.8	-4.8	10.0	3.8
				PBE			
$J_{calculated}$	-135.0	-52.9	-90.6	-6.1	-3.4	4.1	1.3
$J_{corrected}(S_1)$	-154.9	-55.4	-101.0	1.4	4.7	13.8	10.3
$J_{corrected}(S_2)$	-83.1	-32.2	-55.6	-3.2	-1.5	3.2	1.4
Exp [21]	-156.0	-78.5	-175.0	-33.0	-9.0	10.0	3.5

J values were corrected using Equation (8.1) and to correct it the self-regression (S1) and the parameters (S2) obtained from the H-He-H models were used.

We tried to use same functions for calculating J for NNO and on its analogues but our calculations haven' not converged and we were not able to calculate the J value for these entire molecule.

So for testing linear regression correction applicability on NNO and its analogues we used BLYP M06-L and PBE. For these function we didn't get the geometry conversion problems. Regression parameters given in Table 8.4 were used to correct J given in Table 8.5.
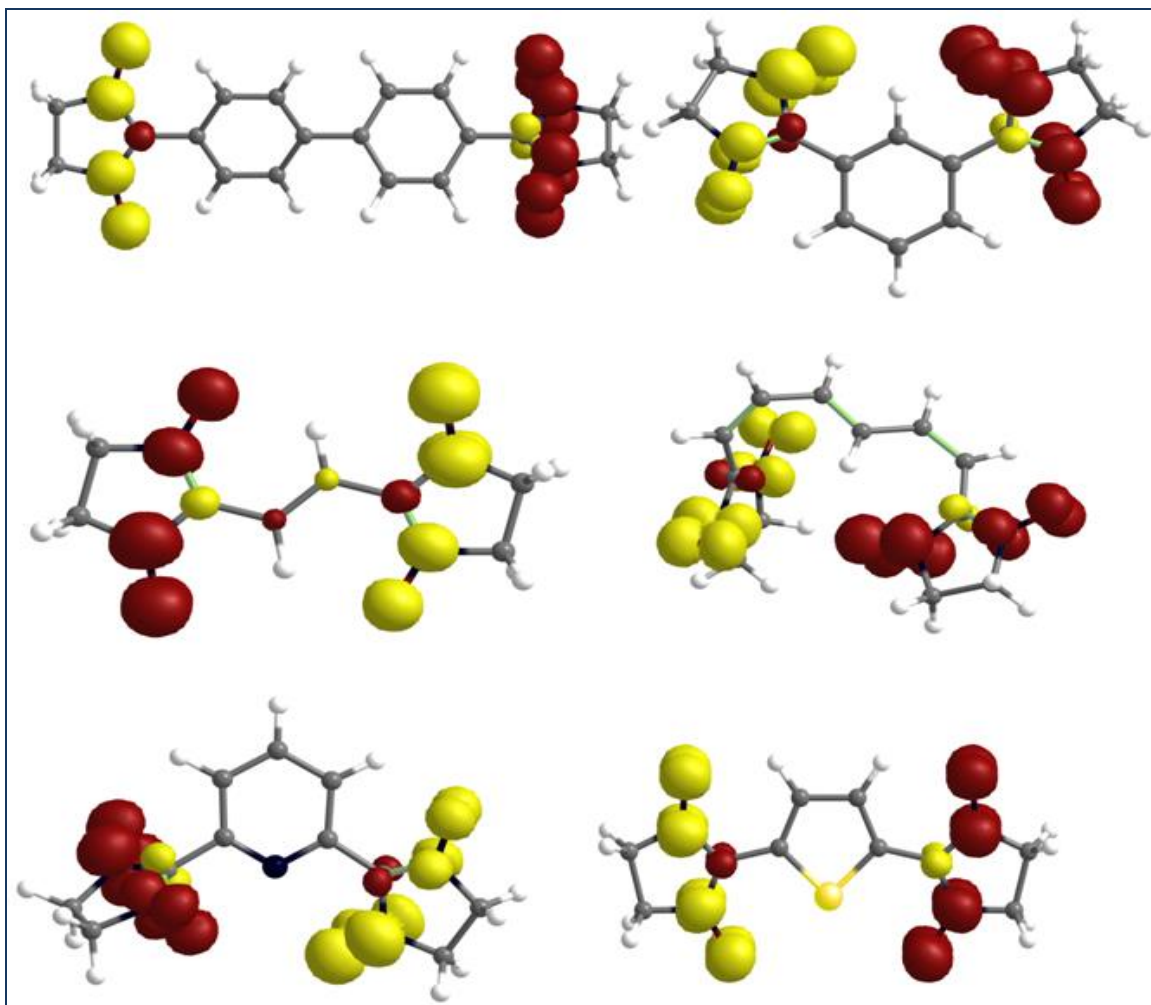
Figure 8. 5: Broken symmetry spin density plots for BNN based biradicals (Red=α , Yellow = β spin). All plots are drawn with the contour value=0.002).

8.4 Conclusions

A detailed assessment of a variety of density functionals in combination with basis sets has been made to predict the magnetic exchange couplings for nitronyl nitroxides (NNOs). All calculations done on nitronyl nitroxdes shows that the magnetic exchange coupling between two NNO units depends strongly on the dihedral angle. It was found that large dihedral angles lead to lower J values, and this is because that leads decreasing overlapping between magnetic orbitals.. Each of the methods used, predicted antiferromagnetic couplings in BNN radicals. Calculation on Nitronyl Nitroxide analogues BLYP, M06-L and PBE qualitative approximation of J and without any correction scheme these methods predict only correct sign of magnetic exchange couplings. An Applied correction schemes on NNO and its analogues with BLYP, M06-L and PBE does not lead any clear correction trends.

The linear regression correction scheme improves the calculated J value when the regression parameters are already obtained from a similar chemical system. For the experimentally known dihedral angle, the hybrid functional with 16% HF exchange produced the best results (BLYP-16%) and beyond this HF exchange contribution did not prove to be helpful. In conclusion, if calculations are done x-ray structures then BLYP , PBE M06-L in combination with 6-311+(G, d,p) can predict J within acceptable accuracy on other hand for the model molecules, no DFT functional in combination with broken symmetry is able to provide acceptable accuracy J values for NNOs and its analogues.

9. Overview and Summary

This thesis primarily covers a systematic assessment of quantum chemical methods to predict accurate ^{19}F NMR shifts for fluoroarenes and magnetic exchange coupling constant (J) in organic spin dimers which are basic building blocks for rational designing of organic magnetic materials.

One of the most important goals in chemistry is to design and synthesize molecules with optimum properties. This thesis is divided into two parts: the first part comprises of a systematic effort to find an inexpensive quantum chemical method to predict accurate ^{19}F NMR chemical shifts (within an accuracy of 2 ppm) for perfluoroaromatics. Essentially, these strenuous efforts have been devoted to find best DFT functional and basis set combination to predict accurate ^{19}F shifts. In addition,the influence of geometrical parameters, solvents, chemical environment was also analyzed. Various correction approaches were tested to correct the calculated shifts. The influence of various functionals and basis sets was also analyzed on the correction efficiency of an individual scheme. All the NMR calculation methods already being used and correction approaches were verified to predict shifts of three different fluorine-substituted molecular sets. These structure sets include fluorobenzenes, substituted benzenes and fluorine substituted aromatic fused rings (e.g. fluorine substituted anthracene).

In the second part of this thesis, we investigated the accurate prediction of magnetic exchange couplings (J) for organic spin dimers using quantum chemical methods. We analyzed the performance of various DFT methods and various post-HF methods, such as the CASSCF, CASPT2, MSTDISD, DDCI1, DDCI2, DDCI3, and FCI to predict magnetic exchange couplings (J).

Overview of the Chapters:

  Chapter 1, presents a brief theoretical introduction to the Schrödinger equation and its application in quantum mechanical calculations, the Hartree-Fock approximation, basis sets, electron correlation energy, and density functional theory (using pure and hybrid functionals).

In chapters 2 and 3, an introduction is given for quantum chemical approaches used to calculate NMR parameters and magnetic exchange coupling constants. We discuss an effective spin Hamiltonian, the Breit-Pauli Hamiltonian (BPH), chemical shielding tensor and total energy relationship, measuring of the NMR spectra, and different techniques to deal with gauge origin problem. In addition, the theoretical

background of magnetic exchange coupling constant calculation for spin dimers, the Heisenberg-Dirac-van-Vleck Hamiltonian (HDVV) and the Noodelman's broken-symmetry approach for calculating J values are briefly discussed.

Chapter 4, presents a benchmark study of various DFT functionals and basis sets to calculate accurate C-F bond lengths and ^{19}F chemical shifts. High-resolution NMR spectral data of complex molecules are often difficult to interpret. Great scientific efforts have been devoted to search for a computational approach to interpret experimental NMR data. Quantum chemical methods such as the CCSD(T) method offer high accuracy in calculation of NMR parameters but being computationally too demanding they cannot be applied to large chemical systems. On the other hand, density functional theory (DFT) is achieving a steady progress among diversity of computational techniques. An accuracy within 2 ppm deviation from the experimental values in ^{19}F chemical shifts can be achieved if the NMR calculation is performed using accurate equilibrium geometries, GIAO is used to tackle gauge origin problem and electron correlation is properly treated by employing a high level of theory (e.g. CCSD (T)/cc-pVQZ). We found that the calculation of ^{19}F shielding tensors with the density-functional theory does not provide any noticeable improvement over the HF method. Post-HF theory demands too much computational resources that makes them impossible to use for large systems [35] .

We found that a quantitative prediction of NMR shifts can be made as the errors introduced by theoretical methods are cancelled out while calculating shifts. Various benchmark studies in this thesis show that ^{19}F chemical shifts calculated for perfluoraromatics with the M06-L, BHandH, BHandHLYP in combination with the 6-311+G (2d,p) basis set are within 4 ppm deviation from the experiments. Furthermore, we noted that NMR calculations on accurate

C-F (e.g. PBE/6-311G (d, p)) bond lengths does not show any improvement if the NMR calculation and optimization are performed at the same level of theory. A significant improvement can be achieved on calculated ^{19}F NMR shifts, if some correction schemes are used.

In chapter 4 we discuss various correction schemes applied to correct the calculated ^{19}F chemical shifts. A multi-standard approach (MSTD) was used to minimize the error that may occur due to the difference in the nature of the reference compound and test molecules [122]. We propose another approach to correct shielding constants which is the reference corrected approach. This approach makes a correction similar to the MSTD. We also tested a Linear Regression Correction

Approach and we noted that this is the best approach amongst all. This is found to be less dependent on the theoretical method. We use conformation averaging corrections to correct the calculated shifts[126].

In chapter 5 we test the applicability of all the methods and correction schemes to correct the calculated shifts. We use NMR shifts calculation in identifying regioselectivity in aromatic nucleophilic substitution reactions. A comparison of NMR shifts based on identification of preferred sites for nucleophilic attack and Meisenheimer complex stability criteria was made [150, 151]. Nucleophilic substitution reaction on perfluoroanathrance offers a path to design substituted polyfluorinated annulated arenes, which are promising molecules for OFET devices [141].

The second part of this thesis emphasizes on predicting accurate magnetic exchange coupling constant (J/cm^{-1}) in spin dimer. We have analyzed the performance of various post-HF and DFT functionals in combination with various types of basis sets to predict J accurately.

The development of a novel magnetic material relies on solid-state synthesis protocols requiring harsh conditions. However, recently, an alternative approach is receiving increasing attention, which is the rational design of magnetic materials based on the self-assembly of tailor-made molecular precursors. As a part of a trans regional collaborative research project such a 'molecules-to-materials' strategy is envisaged aiming at a detailed control of material properties at a molecular level. To achieve this, a toolbox of molecular building blocks (i.e., spin-carriers and bridging elements) with smoothly varying properties (spin, magnetic moments, redox potentials, exchange coupling) is to be developed. Along these lines, the group of Wagner has successfully developed a coordination polymer based on CuII ions as spin carriers and 1,4-hydroquinone as linkers, which behaves as a spin S=1/2 dimer system with additional weak three-dimensional magnetic couplings [170].

New design targets include materials based on CuII ions or nitronyl nitroxide (NNs) as spin carriers, and rigid conjugated π-systems as bridges which are able to transmit spin-spin couplings. For a de-novo design of such building blocks and a detailed understanding of the resulting spin-spin interactions, accurate predictions by quantum chemical calculations and close interactions with the preparative groups are crucial ingredients for the research concept. Hence, from a quantum chemical perspective, the identification of methods which are able to quantitatively describe exchange interactions in coupled spin dimers is of paramount importance. To assess

the accuracy that can be expected from current DFT and post-HF methods for the description of the magnetic coupling constant J, extensive calibration calculations were performed for a H-He-H model system, which is small enough to allow for an application of the full-CI method at the (extrapolated) complete basis set limit. Further studies include the magnetic coupling in several NNs, which were characterized experimentally. Against this background, different broken-symmetry DFT approaches and various post-HF methods have been evaluated carefully.

10. Überblick und Zusammenfassung

Die vorliegende Arbeit beschäftigt sich mit der systematischen Evaluierung quantenchemischer Methoden zur Vorhersage von chemischen Verschiebungen und J Kopplungskonstanten bei der ^{19}F NMR-Spektroskopie für die Verbindungsklasse der Fuorarene und fluorhaltigen organischen Spin-Dimeren. Letztere werden als Bausteine für magnetische organische Verbindungen eingesetzt. Eines der wichtigsten Ziele in der Chemie ist die Synthese von Molekülen mit optimierten Eigenschaften.

Diese Arbeit ist in zwei Teile gegliedert:

Der erste Teil berichtet von der Suche nach einer effizienten quantenchemischen Methode, die genaue chemischen Verschiebungen für ^{19}F NMR-Spektren vorhersagen kann. Ziel ist hier für Perfluorverbindungen eine Genauigkeit von 2 ppm zu erreichen. Hierfür wurden vor allem DFT-Methoden getestet. Dabei wurde auch der Einfluss von Molekülgeometrie, Lösungsmittelmodellen und chemischer Umgebung untersucht. Verschiedene Korrekturmethoden wurden auf ihre Fähigkeit die Präzision der berechneten chemischen Verschiebungen zu erhöhen getestet. Die Referenzverbindungen für die Evaluation wurden in drei Datensäte unterteilt und enthalten Fluorbenzole und fluorhaltige Mono- und Polyaromaten.

Im zweiten Teil der Arbeit geht es um die Vorhersage von Kopplungskonstanten. Auch diese Untersuchung umfasst überwiegend DFT-Methoden. Darüber hinaus wurden auch einige Post-Hartree-Fock-Methoden (CASSCF, CASPT2, MSTDISD, DDCI1, DDCI2, DDCI3 und FCI) evaluiert.

Überblick über die Kapitel

Kapitel 1

Das erste Kapitel gibt einen Überblick zu den theoretischen Grundlagen der Arbeit. Dazu zählen die Schrödingergleichung, die Hartree-Fock-Methode, Basissätze, Elektronenkorrelation und die Dichtefunktionaltheorie.

Kapitel 2 und 3

Kapitel zwei beschreibt die Grundlagen der quantenchemischen Berechnung von NMR-Parametern wie chemische Verschiebung und Kopplungskonstanten. Dies

Umfasst den effektiven Spin-Hamilton-Operator, den Breit-Pauli-Hamilton-Operator und den NMR-Abschirmtensor. Die Messung von NMR-Spektren wird kurz beschrieben. Es werden verschiedene Ansätze zur Behandlung des Gauge Origin Problems besprochen. Zuletzt enthält das Kapitel eine Einführung zur quantenchemischen Berechnung von NMR Kopplungskonstanten, speziell den Heisenberg-Dirac-van-Vleck-Hamiton-Operator und Noodelmans broken-symetry Ansatz.

Kapitel 4

Kapitel drei beschreibt die systematische Evaluierung von DFT Methoden zur Vorhersage von C-F Bindungslängen und ^{19}F chemischen Verschiebungen. Die akkurate Vorhersage der NMR-Spektren hilft bei der für komplexe Moleküle oft schwierigen Signalzuordnung.

Viel Forschungsarbeit ist bereits in die Vorhersage von NMR-Spektren geflossen. Quantenchemische Methoden wie CCSD(T) erlauben zwar die genaue Vorhersage von NMR-Parametern, benötigen aber zu viel Rechenzeit um für komplexe Moleküle angewendet zu werden. Mit geeigneten Methoden kann für die hier getesteten Datenreihen eine Vorhersagegenauigkeit von 2 ppm im Vergleich zu experimentellen ^{19}F chemischen Verschiebungen erreicht werden, wenn gute Molekülgeometrien vorliegen, der GIAO Ansatz verwendet wird um das Gauge Origin Problem zu behandeln und die Elektronenkorrelation mit Post-Hartree-Fock-Methoden wie CCSD(T)/cc-pVQZ berücksichtigt wird.

Es stellte sich heraus, dass die Berechnung von ^{19}F NMR Abschirmtensoren mit DFT-Methoden keinen signifikanten Vorteil gegenüber HF-Methoden bietet. Post-Hartree-Fock-Methoden sind wegen der benötigten Rechenzeit nicht für größere Moleküle geeignet[35].

Die quantitative Vorhersage von NMR chemischen Verschiebungen ist möglich, da die durch die theoretischen Methoden eingeführten Fehler sich gegenseitig aufheben. Die verschiedenen Testreihen in dieser Arbeit zeigen, dass ^{19}F NMR chemische Verschiebungen für Perfluoraromaten mit den Funktionalen M06-L, BHandH, BHandHLYP in Kombination mit dem Basisisatz 6-311+G (2d,p) mit einer Genauigkeit von 4 ppm im Vergleich zum Experiment vorhergesagt werden können. Weiterhin hat sich gezeigt, dass genaue Geometrien (z. B. berechnet mit PBE/6-

311G(d,p)) keinen Vorteil gegenüber der Geometrieoptimierung mit der selben Methode die auch zur Berechnung der NMR-Parameter verwendet wird hat. Empirische Schemata zur Korrektur der berechneten chemischen Verschiebungen können eine signifikante Verbesserung bewirken.

Kapitel 5

Kapitel vier geht auf verschiedene empirische Korrekturmechanismen zur Verbesserung der berechneten chemischen Verschiebungen ein. Dazu zählt u. a. ein Multi-Standard Ansatz (MSTD), der systematische Fehler innerhalb verschiedener Verbindungsklassen ausgleichen soll [122]. Die lineare Skalierung mit durch zuvor durch lineare Regression ermittelten Parametern lieferte die besten Ergebnisse. Zuletzt wurde die Mittelung der chemischen Verschiebung über mehrere Konformationen untersucht [126].

Kapitel 6

In Kapitel fünf erfolgt die Anwendung der Korrekturschemata aus Kapitel vier für die Vorhersage der ^{19}F chemischen Verschiebung zur Identifikation der Regioselektivität von nucleophilen Angriffen. Die so erhaltenen Ergebnisse wurden mit denen aus der Abschätzung der Stabilität der entsprechenden Meisenheimer Komplexe verglichen [150, 153]. Als Studienobjekt diente hier Perfluoranthracen, welches ein Ausgangstoff zur Synthese von polyfluorierten annellierten Arenen, welche in OFETs Anwendung finden, sind [141, 208].

Zweiter Teil

Der zweite Teil der Arbeit konzentriert sich auf die Vorhersage von Kopplungskonstanten in Spin Dimeren. Dazu wurden diverse Post-Hartree-Fock und DFT-Methoden evaluiert.

Die Entwicklung neuartiger magnetischer Materialien basiert auf der Festphasensynthese unter drastischen Bedingungen. Ein alternativer Ansatz mit für den Einsatzzweck optimierten selbstorganisierenden Ausgangsmolekülen wird zunehmend verfolgt. Als Teil eines überregionalen Forschungsprojektes wird die Strategie Materialeigenschaften auf Molekülebene zu kontrollieren verfolgt. Dazu wird ein Satz molekularer Module (Spin-Träger, Brückenelemente, etc.) die eine

Bandbreite von Eigenschaften (Spin, magnetische Momente, Redoxpotenziale, Kopplungskonstanten) in kleinen Schritten abdecken können entworfen.

In diesen Zusammenhang hat die Arbeitsgruppe um Prof. Wagner Koordinationspolymere mit Cu(II) Ionen als Spinträgern und 1,4-Hydrochinonen als Brückenelemente entwickelt. Diese Systeme sind Spin S=1/2 Dimere mit zusätzlichen schwachen magnetischen Kopplungen [170]. Zu den neuen Zielmolekülen zählen auf Cu(II) Ionen oder Nitronylnitroxid (NN) als Spinträger basierende Verbindungen, die über starre π-Systeme verknüpft sind, welche auch Spin-Spin Wechselwirkungen übertragen können. Gute Vorhersagemethoden sind elementar für das Design solcher molekularen Bausteine.

Im ersten Schritt wurde das Modellsystem H-He-H evaluiert. Dieses ist klein genug um Full-CI Methoden mit Basissatzextrapolation anzuwenden. Im weiteren Verlauf dienten bekannte Nitronylnitroxid-Verbindungen mit experimentell bestimmten Kopplungskonstanten als Referenz für den systematischen Test verschiedener DFT- und Post-Hartree-Fock-Methoden.

Acknowledgement

It is a pleasure to thank those who made this thesis possible, who so generously helped me at various stages of my life.

First of all, I would like to thank my boss, supervisor, "meinem Doktorvater" **Prof. Dr. Max Holthausen** for accepting me as his PhD student. With Prof. Holthausen support and guidance, I've been able to gather rich experience on DFT calculations, besides that, I greatly appreciate his encouragement to go beyond the DFT calculation and digging out the problems and be open to learn, that I really enjoyed a lot and what eventually broadened the scope of my thesis.

I thank you **Prof. Dr. Mathias Wagner** for suggested me to join Prof. Holthausen group. I thank you him for his great support and encouragement and helping me during SB annual meetings.

I am grateful to our Nanobic project collaborator **Prof. Andreas Terfort** for his precious suggestions and discussions and accepting my request to review thesis as second reviewer, thank you so much.

I am highly indebted to **Prof. Dr. Jennifer Dressmann**, who has been a truly dedicated supporter for me. I thank you so much for your kind support.

I am deeply thankful to **Prof. Dr. N Saythamurthy**, director of IISER Mohali, wholeheartedly, not only for his tremendous academic support but also moral support and standing by me in my every tough time. I just request once to give his comment on my thesis and he checked my complete thesis thoroughly and gave precious suggestions. Sir I'm heartily thankful for your kind support.

I am deeply thankful to **Prof. Dr. S. Sarkar** wholeheartedly, not only for his tremendous academic support but also moral support and standing by me in my every tough time.

 I am thankful to Prof**. Dr. P. K. Bhardwaj** from Indian Institute of Technology allowing me to work in his lab at Kanpur and for giving me recommendation letters and positive suggestions all the time.

During my PhD, one person to whom I am deeply indebted is **Dr. Guido Wagner**. I am extremely grateful to him for supporting me in thesis writing and in results

Bibliography

[1].   Carey, F. A. *Organic Chemistry*, Vol. 5, McGraw-Hill, Boston.(2003)

[2].   Claridge, T. D. W. *High-Resolution NMR Techniques in Organic Chemistry*, Vol. 27.(2008)

[3].   Mohan, M., Jha, A. K. S., and Singh, N., *Physica Scripta*(2006), *73*, 601

[4].   Dejaegere, A. P., and Case, D. A., *J. Phys. Chem. A*(1998), *102*, 5280

[5].   Xu, X.-P., and Auae Yeung, S. C. F., *J. Phys. Chem. B*(2000), *104*, 5641

[6].   Claridge, T. D. *High-Resolution NMR Techniques in Organic Chemistry*, Vol. 1, Pergamon.(2000)

[7].   Frisch, M. J., Trucks, G. W., Schlegel, H. B., Scuseria, G. E., Robb, M. A., Cheeseman, J. R., Zakrzewski, V. G., Montgomery, J. A., Stratmann, R. E., Burant, J. C., Dapprich, S., Millam, J. M., Daniels, A. D., Kudin, K. N., Strain, M. C., Farkas, O., Tomasi, J., Barone, V., Cossi, M., Cammi, R., Mennucci, B., Pomelli, C., Adamo, C., Clifford, S., Ochterski, J., Petersson, G. A., Ayala, P. Y., Cui, Q., Morokuma, K., Malick, D. K., Rabuck, A. D., Raghavachari, K., Foresman, J. B., Cioslowski, J., Ortiz, J. V., Stefanov, B. B., Liu, G., Liashenko, A., Piskorz, P., Komaromi, I., Gomperts, R., Martin, R. L., Fox, D. J., Keith, T., Al-Laham, M. A., Peng, C. Y., Nanayakkara, A., Gonzalez, C., Challacombe, M., Gill, P. M. W., Johnson, B., Chen, W., Wong, M. W., Andres, J. L., Gonzalez, C., Head-Gordon, M., Replogle, E. S., and Pople, J. A. *Gaussian 98*.(1998)

[8].   Pedone, A., Pavone, M., Menziani, M. C., and Barone, V., *J. Comput. Chem.*(2008), *4*, 2130

[9].   Zhao, Y., and Truhlar, D. G., *J. Phys. Chem. A*(2008), *112*, 6794

[10].   Bagno, A., Rastrelli, F., and Saielli, G., *Chem. Eur. J*(2006), *12*, 5514

[11].   Baldridge, K. K., and Siegel, J. S., *J. Phys. Chem. A*(1999), *103*, 4038

[12].   Bifulco, G., Dambruoso, P., Gomez-Paloma, L., and Riccio, R., *Chem. Rev.*(2007), *107*, 3744

[13].   Taehtinen, P., Bagno, A., Klika, K. D., and Pihlaja, K., *J. Amer. Chem. Soc.*(2003), *125*, 4609

[14].   Aiello, A., Fattorusso, E., Luciano, P., Mangoni, A., and Menna, M., *European Journal of Organic Chemistry*(2005), *2005*, 5024

[15].   Forsyth, D. A., and Sebag, A. B., *J. Am. Chem Soc.*(1997), *119*, 9483

[16].   Brunet, V., and O'Hagan, D., *Angew. Chem., Int. Ed.*(2008), *47*, 1179

[17].   Kirsch, P. *Modern fluoroorganic chemistry*, Wiley-VCH, Weinheim.(2004)

[18].   R.Dolbier, W. *Guide to Fluorine NMR for Organic Chemists*, Jr. John Wiley & Sons Inc, Hoboken, NJ. 2009.(2009)

[19].   Mitronova, G. Y., Belov, V. N., Bossi, M. L., Wurm, C. A., Meyer, L., Medda, R., Moneron, G., Bretschneider, S., Eggeling, C., Jakobs, S., and Hell, S. W., *Chemistry*(2010), *16*, 4477

[20].   Purser, S., Moore, P. R., Swallow, S., and Gouverneur, V., *Chem. Soc. Rev.*(2008), *37*, 320

[21].   Haas, A., and Reinke, H., *Angew. Chem. Int. Ed*(1967), *6*, 705

[22].   Dalvit, C., Ardini, E., Fogliatto, G. P., Mongelli, N., and Veronesi, M., *Drug Discovery Today*(2004), *9*, 595

[23].   Dalvit, C., Ardini, E., Flocco, M., Fogliatto, G. P., Mongelli, N., and Veronesi, M., *J. Am. Chem.Soc.*(2003), *125*, 14620

[24].   Williams, D. E., Peters, M. B., Wang, B., and Merz, K. M., *J. Phys. Chem. A*(2008), *112*, 8829

[25].   Burroughes, J. H., Bradley, D. D. C., Brown, A. R., Marks, R. N., Mackay, K., Friend, R. H., Burns, P. L., and Holmes, A. B., *Nature*(1990), *347*, 539

[26]. Yu, G., Gao, J., Hummelen, J. C., Wudl, F., and Heeger, A. J., *Science*(1995), *270*, 1789

[27]. Sun, H., and DiMagno, S. G., *Angew. Chem. Int. Ed*(2006), *45*, 2720

[28]. Reichenbacher, K., Suss, H. I., and Hulliger, J., *Chem Soc Rev*(2005), *34*, 22

[29]. Kulkarni, A. P., Tonzola, C. J., Babel, A., and Jenekhe, S. A., *Chem. Mater.*(2004), *16*, 4556

[30]. Ochsenfeld, C., Kussmann, J., and Koziol, F., *Angew. Chem. Int. Ed*(2004), *43*, 4485

[31]. Konstantinov, I. A., and Broadbelt, L. J., *J. Phys. Chem. A*,

[32]. Zhao, Y., and Truhlar, D. G., *The Journal of Chemical Physics*(2009), *130*, 074103

[33]. Nicolaou, K. C., and Snyder, S. A., *Angew. Chem. Int. Ed*(2005), *44*, 1012

[34]. Helgaker, T., Jaszuaski, M., and Ruud, K., *Chem. Rev.*(1998), *99*, 293

[35]. Harding, M. E., Lenhart, M., Auer, A. A., and Gauss, J., *J Chem Phys*(2008), *128*, 244111

[36]. Miller, J. S., *Materials Today*(2014), *17*, 224

[37]. Adamo, C., Barone, V., Bencini, A., Totti, F., and Ciofini, I., *Inorg Chem.*(1999), *38*, 1996

[38]. Nishino, M., Yamanaka, S., Yoshioka, Y., and Yamaguchi, K., *Journal of Physical Chemistry A*(1997), *101*, 705

[39]. Ali, M. E., and Datta, S. N., *J. Phys. Chem. A*(2006), *110*, 2776

[40]. Soda, T., Kitagawa, Y., Onishi, T., Takano, Y., Shigeta, Y., Nagao, H., Yoshioka, Y., and Yamaguchi, K., *Chem. Phys. Lett.*(2000), *319*, 223

[41]. Miura, Y., Kato, I., and Teki, Y., *Dalton Trans.*(2006), 961

[42]. Koch, W., and Holthausen, M. C. The Kohn-Sham Approach, In *A Chemist's Guide to Density Functional Theory*, pp 41, Wiley-VCH Verlag GmbH.(2001)

[43]. Jensen, F. (2007) Introduction to Computational Chemistry, Wiley & Sons Ltd., Chichester.

[44]. Cramer, C. J. *Essentials of Computational Chemistry: Theories and Models*, John Wiley & Sons.(2004)

[45]. Levine, I. N. *Quantum Chemistry*, Vol. 5th Pearson Education, Inc.(2003)

[46]. Schrödinger, E., *Annalen der Physik*(1926), *384*, 361

[47]. Hammes-Schiffer, S., and Andersen, H. C., *J. Chem Phys.*(1994), *101*, 375

[48]. Bachrach, S. M., *Annual Reports Section "B" (Organic Chemistry)*(2008), *104*, 394

[49]. Bachrach, S. M. *Computational Organic Chemistry*, John Wiley & Sons.(2007)

[50]. Calaminici, P., Jug, K., and Köster, A. M., *J. Chem. Phys.*(1998), *109*, 7756

[51]. Becke, A. D., *Phys. Rev. A*(1988), *38*, 3098

[52]. Perdew, J. P., *Phys. Rev. B*(1986), *33*, 8822

[53]. Perdew, J. P., and Wang, Y., *Phys. Rev. B*(1992), *45*, 13244

[54]. Perdew, J. P., Burke, K., and Ernzerhof, M., *Phys. Rev. Lett.*(1996), *77*, 3865

[55]. Lee, C., Yang, W., and Parr, R. G., *Phys. Rev. B*(1988), *37*, 785

[56]. Hamprecht, F., *J. Chem. Phys.*(1998), *109*, 6264

[57]. Becke, A. D., *J. Chem. Phys.*(1997), *107*, 8554

[58]. Becke, A. D., *J. Chem. Phys.*(1993), *98*, 5648

[59]. Schindler, M., *J Chem Phys*(1982), *76*, 1919

[60]. Kaupp, M., Bühl, M., and Malkin, V. G. Introduction: The Quantum Chemical Calculation of NMR and EPR Parameters, In *Calculation of NMR and EPR Parameters*, pp 1, Wiley-VCH Verlag GmbH & Co. KGaA.(2004)

[61]. Gauss, J., *J. Chem. Phys.*(1993), *99*, 3629

[62]. Smith, S. A., Palke, W. E., and Gerig, J. T., *Concepts in Magnetic Resonance*(1992), *4*, 107

[63]. Fukui, H., *Prog Nucl Magn Reson Spectrosc*(1997), *31*, 317

[64]. Keith, T. A., and Bader, R. F. W., *Chem. Phy. Lett.*(1993), *210*, 223

[65]. Keith, T. A., and Bader, R. F. W., *Chem. Phy. Lett.*(1992), *194*, 1

[66]. Schindler, M., and Kutzelnigg, W., *J. Am. Chem Soc.*(1983), *105*, 1360

[67]. Ditchfield, R., *Molecular Physics*(1974), *27*, 789

[68]. Andersson, K., Malmqvist, P. Ã., Roos, B. O., Sadlej, A. J., and Wolinski, K., *J. Chem. Phys.*(1990), *94*, 5483

[69]. Heisenberg, W., *Z. Phys.*(1928), *49*, 619

[70]. Frank, N., *J. Phys. Chem. Solids*(2004), *65*, 781

[71]. Kahn, O. *Molecular Magnetism* New York, VCH Publishers, Inc.). .(1993)

[72]. Bencini, A., Totti, F., Daul, C. A., Doclo, K., Fantucci, P., and Barone, V., *Inorg Chem.*(1997), *36*, 5022

[73]. Noodleman, L., *J. Chem. Phys.*(1981), *74*, 5737

[74]. Noodleman, L., and Davidson, E. R., *Chem. Phy.*(1986), *109*, 131

[75]. Hay, P. J., Thibeault, J. C., and Hoffmann, R., *J. Am. Chem. Soc.*(1975), *97*, 4884

[76]. Noodleman, L., *J. Chem Phys.*(1981), *74*, 5737

[77]. Ghosh, P., Bill, E., Weyhermuller, T., Neese, F., and Wieghardt, K., *Journal of the American Chemical Society*(2003), *125*, 1293

[78]. Noh, E. A. A., and Zhang, n., *J. Chem. Phys.*(2006), *330*, 82

[79]. Wiitala, K. W., Hoye, T. R., and Cramer, C. J., *Journal of Chemical Theory and Computation*(2006), *2*, 1085

[80]. Wolinski, K., Hinton, J. F., and Pulay, P., *J. Am. Chem Soc.*(1990), *112*, 8251

[81]. Hoe, W.-M., Cohen, A. J., and Handy, N. C., *Chem. Phys. Lett.*(2001), *341*, 319

[82]. Adamo, C., and Barone, V., *Chem. Phys. Lett.*(1998), *298*, 113

[83]. Koch, W., and Holthausen, M. C. Magnetic Properties, In *A Chemist's Guide to Density Functional Theory*, pp 197, Wiley-VCH Verlag GmbH.(2001)

[84]. Cheeseman, J. R., Trucks, G. W., Keith, T. A., and Frisch, M. J., *J. Chem Phys.*(1996), *104*, 5497

[85]. Cai, S.-H., Chen, Z., Xu, X., and Wan, H.-L., *Chem. Phys. Lett.*(1999), *302*, 73

[86]. Sanders, L. K., and Oldfield, E., *J. Phys. Chem. A*(2001), *105*, 8098

[87]. Frisch, M. J. T., G. W.; Schlegel, H. B.; Scuseria, G. E.; Robb, M. A.; Cheeseman, J. R.; Montgomery, J. A., Jr.; Vreven, T.; Kudin, K. N.; Burant, J. C.; Millam, J. M.; Iyengar, S. S.; Tomasi, J.; Barone, V.; Mennucci, B.; Cossi, M.; Scalmani, G.; Rega, N.; Petersson, G. A.; Nakatsuji, H.; Hada, M.; Ehara, M.; Toyota, K.; Fukuda, R.; Hasegawa, J.; Ishida, M.; Nakajima, T.; Honda, Y.; Kitao, O.; Nakai, H.; Klene, M.; Li, X.; Knox, J. E.; Hratchian, H. P.; Cross, J. B.; Adamo, C.; Jaramillo, J.; Gomperts, R.; Stratmann, R. E.; Yazyev, O.; Austin, A. J.; Cammi, R.; Pomelli, C.; Ochterski, J. W.; Ayala, P. Y.; Morokuma, K.; Voth, G. A.; Salvador, P.; Dannenberg, J. J.; Zakrzewski, V. G.; Dapprich, S.; Daniels, A. D.; Strain, M. C.; Farkas, O.; Malick, D. K.; Rabuck, A. D.; Raghavachari, K.; Foresman, J. B.; Ortiz, J. V.; Cui, Q.; Baboul, A. G.; Clifford, S.; Cioslowski, J.; Stefanov, B. B.; Liu, G.; Liashenko, A.; Piskorz, P.; Komaromi, I.; Martin, R. L.; Fox, D. J.; Keith, T.; Al-Laham, M. A.; Peng, C. Y.; Nanayakkara, A.; Challacombe, M.; Gill, P. M. W.; Johnson, B.; Chen, W.; Wong, M. W.; Gonzalez, C..; Pople, J.A. (2009) Gaussian09, A.02, Gaussian, Inc.: Wallingford, CT, 2009.

[88]. Zhang, Y., Xu, X., and Yan, Y., *Journal of Computational Chemistry*(2008), *29*, 1798

[89]. Zhao, Y., and Truhlar, D. G., *Journal of Chemical Theory and Computation*(2005), *1*, 415

[90]. Zhao, Y., and Truhlar, D. G., *The Journal of Chemical Physics*(2006), *125*, 194101

[91]. Vosko, S. H., Wilk, L., and Nusair, M., *Can. J. Phys.*(1980), *58*, 1200

[92]. Becke, A. D., *Phys. Rev. A*(1988), *38*, 3098

[93]. Busacca, C. A., Campbell, S., Gonnella, N. C., and Senanayake, C. H., *Mag.Res.Chem.*(2009), *48*, 74

[94]. Staroverov, V., *J. Chem. Phys.*(2003), *119*, 12129

[95]. Tao, J., Perdew, J. P., Staroverov, V. N., and Scuseria, G. E., *Phys. Rev. Lett.*(2003), *91*, 146401

[96]. Grimme, S., *J. Comput. Chem.*(2006), *27*, 1787

[97]. Buehl, M., Van Eikema Hommes, N. J. R., Schleyer, P. v. R., Fleischer, U., and Kutzelnigg, W., *J. Am. Chem Soc.*(1991), *113*, 2459

[98]. Kupka, T., Ruscic, B., and Botto, R. E., *J. Phys. Chem. A*(2002), *106*, 10396

[99]. Kupka, T., Stachaw, M., Nieradka, M., Kaminsky, J., and Pluta, T., *Journal of Chemical Theory and Computation*(2010), *6*, 1580

[100]. Binkley, J. S., Pople, J. A., and Hehre, W. J., *J. Am. Chem Soc.*(1980), *102*, 939

[101]. Francl, M. M., *J. Chem. Phys.*(1982), *77*, 3654

[102]. Vosko, S. H., Wilk, L., and Nusair, M., *Can. J. Phys.*(1980), *58*, 1200

[103]. Thom H. Dunning, J., *J. Chem. Phys.*(1989), *90*, 1007

[104]. Wilson, A. K., Woon, D. E., Peterson, K. A., and Dunning, T. H., *J. Chem. Phys.*(1999), *110*, 7667

[105]. J. A. Montgomery, J., Frisch, M. J., Ochterski, J. W., and Petersson, G. A., *The Journal of Chemical Physics*(1999), *110*, 2822

[106]. J. A. Montgomery, J., Frisch, M. J., Ochterski, J. W., and Petersson, G. A., *J. Chem Phys.*(2000), *112*, 6532

[107]. Kirchner, M. T., Blaser, D., Boese, R., Thakur, T. S., and Desiraju, G. R., *Acta Crystallogr., Sect. E: Struct. Rep. Online*(2009), *65*, o2668

[108]. Thalladi, V. R., Weiss, H.-C., Boese, R., Nangia, A., and Desiraju, G. R., *J. Am. Chem Soc.*(1998), *120*, 8702

[109]. Shorafa, H., Mollenhauer, D., Paulus, B., and Seppelt, K., *Angew. Chem. Int. Ed*(2009), *48*, 5845

[110]. Laali, K. K., Okazaki, T., and Bunge, S. D., *The Journal of Organic Chemistry*(2007), *72*, 6758

[111]. Stuart, A. M., Coe, P. L., and Moody, D. J., *Journal of Fluorine Chemistry*(1998), *88*, 179

[112]. Fujita, M., Egawa, H., Miyamoto, T., Nakano, J., and Matsumoto, J., *European Journal of Medicinal Chemistry*(1996), *31*, 981

[113]. Andraos, J., *J. Chem. Edu.*(1996), *73*, 150

[114]. Cybulski, S. M., Bledson, T. M., and Toczylowski, R. R., *J. Chem. Phys.*(2002), *116*, 11039

[115]. He, X., Fusti-Molnar, L., Cui, G., and Merz, K. M., *J. Phys. Chem. B.*(2009), *113*, 5290

[116]. Koch, H., Jo/rgensen, P., and Helgaker, T., *J Chem Phys*(1996), *104*, 9528

[117]. Fifolt, M. J., Sojka, S. A., Wolfe, R. A., Hojnicki, D. S., Bieron, J. F., and Dinan, F. J., *The Journal of Organic Chemistry*(1989), *54*, 3019

[118]. Facelli, J. C., Grant, D. M., Bouman, T. D., and Hansen, A. E., *J. Comput. Chem.*(1990), *11*, 32

[119]. Zhao, Y., Pu, J., Lynch, B. J., and Truhlar, D. G., *Phys. Chem. Chem. Phys.*(2004), *6*, 673

[120]. Woon, D. E., and Dunning, J. T. H., *J. Chem. Phys.*(1993), *98*, 1358

[121]. Lodewyk, M. W., Siebert, M. R., and Tantillo, D. J., *Chem. Rev.112*, 1839

[122]. Sarotti, A. M., and Pellegrinet, S. C., *J. Org. Chem*(2009), *74*, 7254

[123]. Smith, S. G., and Goodman, J. M., *J. Org. Chem.*(2009), *74*, 4597

[124]. Jain, R., Bally, T., and Rablen, P. R., *J. Org. Chem.*(2009), *74*, 4017

[125]. Colherinhas, G., Fonseca, T. L., and Castro, M. A., *Chem. Phy. Lett.503*, 191

[126]. Barone, G., Duca, D., Silvestri, A., Gomez-Paloma, L., Riccio, R., and Bifulco, G., *Chem. Eur. J*(2002), *8*, 3240

[127]. Sarotti, A. M., and Pellegrinet, S. C., *J Org Chem*(2012), *77*, 6059

[128]. Schuler, R. H., Albarran, G., Zajicek, J., George, M. V., Fessenden, R. W., and Carmichael, I., *J. Phys. Chem. A*(2002), *106*, 12178

[129]. Timmons, C., and Wipf, P., *J. Org. Chem.*(2008), *73*, 9168

[130]. Raber, H., and Mehring, M., *Chem. Phy.*(1977), *26*, 123

[131]. Matthews, R. S., *J. Fluorine Chem.*(1998), *91*, 203

[132]. Donghi, D., Maggioni, D., Beringhelli, T., and D'Alfonso, G., *Eur J. Inorg. Chem.*(2008), *2008*, 3606

[133]. Sebag, A. B., Forsyth, D. A., and Plante, M. A., *J. Org. Chem.*(2001), *66*, 7967

[134]. Costa, F. L. P., de Albuquerque, A. C. F., dos Santos, F. M., and de Amorim, M. B., *J. Phy. Org. Chem.23*, 972

[135]. Eikema Hommes, N., and Clark, T., *J. Mol. Model.*(2005), *11*, 175

[136]. Giesen, D. J., and Zumbulyadis, N., *Phys. Chem. Chem. Phys.*(2002), *4*, 5498

[137]. Costa, F. L. P., de Albuquerque, A. C. F., dos Santos, F. M., and de Amorim, M. B., *J Phy Org Chem*(2010), *23*, 972

[138]. Rablen, P. R., Pearlman, S. A., and Finkbiner, J., *J. Phys. Chem. A*(1999), *103*, 7357

[139]. Valero, R., Gomes, J. R. B., Truhlar, D. G., and Illas, F., *The Journal of Chemical Physics132*, 104701

[140]. Suzuki, H., and Kimura, Y., *J Fluorine Chem.*(1991), *52*, 341

[141]. Chesneau, F., Hamoudi, H., Schüpbach, B., Terfort, A., and Zharnikov, M., *J. Phys. Chem. C.*(2012), *115*, 4773

[142]. Sakamoto, Y., Suzuki, T., Kobayashi, M., Gao, Y., Inoue, Y., and Tokito, S., *Molecular Crystals and Liquid Crystals*(2006), *444*, 225

[143]. Burdon, J., and Rimmington, T. W., *J. Fluorine Chem.*(1985), *27*, 257

[144]. Tannaci, J. F., Noji, M., McBee, J., and Tilley, T. D., *J. Org. Chem.*(2007), *72*, 5567

[145]. Burdon, J., Childs, A. C., Parsons, I. W., and Tatlow, J. C., *J. Chem. Soc. Chem. Commun.*(1982), 534

[146]. Liljenberg, M., Brinck, T., Herschend, B., Rein, T., Rockwell, G., and Svensson, M., *Tetrahedron Lett.52*, 3150

[147]. MacNicol, D. D., McGregor, W. M., Mallinson, P. R., and Robertson, C. D., *J. chem. soc. perkin trans. 1*(1991), 3380

[148]. Alkorta, I., Rozas, I., and Elguero, J., *J. Am. Chem Soc.*(2002), *124*, 8593

[149]. Anthes, A. (2009) Untersuchungen zur nucleophilen Substitution am Perfluoranthracen, In *Institut für Anorganische und Analytische Chemie* Goethe-Universität Frankfurt/Main.

[150]. Baker, J., and Muir, M., *Can. J. Chem.*(2010), *88*, 588

[151]. Baker, J., and Muir, M., *Can. J. Chem.88*, 588

[152]. Burdon, J., *Tetrahedron*(1965), *21*, 3373

[153]. Muir, M., and Baker, J., *J. Fluorine Chem.*(2005), *126*, 727

[154]. Budarin, V. L., Clark, J. H., Hale, S. E., Tavener, S. J., Mueller, K. T., and Washton, N. M., *Langmuir*(2007), *23*, 5412

[155]. Glukhovtsev, M. N., Bach, R. D., and Laiter, S., *J. Org. Chem.*(1997), *62*, 4036

[156]. Vaganova, T. A., Kusov, S. Z., Rodionov, V. I., Shundrina, I. K., Sal'nikov, G. E., Mamatyuk, V. I., and Malykhin, E. V., *J. Fluorine Chem.*(2008), *129*, 253

[157]. Anthes, A. *Untersuchungen zur nucleophilen Substitution am Perfluoranthracen*, Vol. Bachelor, Goethe-Universität Frankfurt/Main.(2009)

[158]. Allen, J. G., Burdon, J., and Tatlow, J. C., *Journal of the Chemical Society* (1965), 6329

[159]. Lodewyk, M. W., Siebert, M. R., and Tantillo, D. J., *Chem Rev*(2012), *112*, 1839

[160]. Gerald M, B., *J. Fluorine Chem.*(1989), *43*, 393

[161]. Brooke, G. M., *J. Fluorine Chem.*(1997), *86*, 1

[162]. Chambers, R. D., Seabury, M. J., Williams, D. L. H., and Hughes, N., *J. chem. soc. perkin trans. I*(1988), 251

[163]. Vaganova, T. A., Kusov, S. Z., Rodionov, V. I., Shundrina, I. K., Sal'nikov, G. E., Mamatyuk, V. I., and Malykhin, E. V., *J Fluorine Chem.*(2008), *129*, 253

[164]. Jensen, F., *J. Chem. Theory. Comput.*(2006), *2*, 1360

[165]. Vostrikova, K. E., *Coord. Chem. Rev.*(2008), *252*, 1409

[166]. Ruiz, E., Cirera, J., and Alvarez, S., *Coord. Chem. Rev.*(2005), *249*, 2649

[167]. Kira E, V., *Coord. Chem. Rev.*(2008), *252*, 1409

[168]. Ruiz, E., Llunell, M., and Alemany, P., *J. Solid State Chem.*(2003), *176*, 400

[169]. Salem, L., and Rowland, C., *Angew. Chem., Int. Ed. Engl.*(1972), *11*, 92

[170]. Kretz, T., Bats, J. W., Losi, S., Wolf, B., Lerner, H.-W., Lang, M., Zanello, P., and Wagner, M., *Dalton Trans.*(2006), 4914

[171]. Garca, V. M., Reguero, M., and Caballol, R., *Theor. Chem. Acc.*(1997), *98*, 50

[172]. Pardo, E., Carrasco, R., Ruiz-Garca, R., Julve, M., Lloret, F., Muoz, M. C., Journaux, Y., Ruiz, E., and Cano, J., *J. Am. Chem Soc.*(2007), *130*, 576

[173]. Feller, D., and Davidson, E. R. Basis Sets for Ab Initio Molecular Orbital Calculations and Intermolecular Interactions, In *Reviews in Computational Chemistry*, pp 1, John Wiley & Sons, Inc.(2007)

[174]. Vancoillie, S., Ruliì☐sÌŒek, L. r., Neese, F., and Pierloot, K., *The Journal of Physical Chemistry A*(2009), *113*, 6149

[175]. Hart, J. R., Rappe, A. K., Gorun, S. M., and Upton, T. H., *J. Phy. Chem*(1992), *96*, 6264

[176]. Werner, H.-J. K., P. J.; Lindh, R.; Manby, F. R.; Schütz, M.; Celani, P.; Korona, T.; Rauhut, G.; Amos, R. D.; Bernhardsson, A.; Berning, A.; Cooper, D. L.; Deegan, M. J. O.; Dobbyn, A. J.; Eckert, F.; Hampel, C.; Hetzer, G.; Lloyd, A. W.; McNicholas, S. J.; Meyer, W.; Mura, M. E.; Nicklass, A.; Palmieri, P.; Pitzer, R.; Schumann, U.; Stoll, H.; Stone, A. J.; Tarroni, R.; Thorsteinsson, T. (2009) MOLPRO, Version 2009; 2009.1 ed. , 2009. ed.

[177]. Becke, A. D., *The Journal of Chemical Physics*(1993), *98*, 5648

[178]. Lara-Castells, M. P. d., Krems, R. V., Buchachenko, A. A., Delgado-Barrio, G., and Villarreal, P., *J. Chem Phys.*(2001), *115*, 10438

[179]. Petersson, G. A., and Frisch, M. J., *J. Phys. Chem. A*(1999), *104*, 2183

[180]. Feller, D., *J. Chem. Phys.*(1992), *96*, 6104

[181]. Jensen, F. (2007) Introduction to Computational Chemistry, Wiley & Sons Ltd., Chichester.

[182]. Heisenberg, W., *Z. Phys.*(1926), *38*, 411

[183]. Castell, O., Caballoll, R., Garca, V. M., and Handrick, K., *Inorg. Chem.*(1996), *35*, 1609

[184]. Castell, O., and Caballol, R., *Inorg. Chem.*(1999), *38*, 668

[185]. Hart, J. R., Rappe, A. K., Gorun, S. M., and Upton, T. H., *J. Phys. Chem.*(1992), *96*, 6255

[186]. Anderson, P. W., *Phys. Rev.*(1959), *2*, 115

[187]. Anderson, J. A., Crager, J., Federoff, L., and Tschumper, G. S., *J. Chem. Phys.*(2004), *121*, 11023

[188]. Anderson, P. W., *Phys. Rev.*(1950), *79*, 350

[189]. Barone, V., Cacelli, I., Ferretti, A., and Prampolini, G., *J. Chem. Phys.*(2009), *131*, 224103

[190]. Ciofini, I., Illas, F., and Adamo, C., *The Journal of Chemical Physics*(2004), *120*, 3811

[191]. Valero, R., Costa, R., Moreira, I. d. P. R., Truhlar, D. G., and Illas, F., *J. Chem. Phys.*(2008), *128*, 114103

[192]. Ruiz, E., Alemany, P., Alvarez, S., and Cano, J., *J. Am. Chem. Soc.*(1997), *119*, 1297

[193]. Perez-Jimenez, A. J., Perez-Jorda, J. M., Moreira, I. d. P. R., and Illas, F., *J. Comput. Chem.*(2007), *28*, 2559

[194]. Rajadurai, C., Ostrovsky, S., Falk, K., Enkelmann, V., Haase, W., and Baumgarten, M., *Inorg. Chim. Acta*(2004), *357*, 581

[195]. Miller, J. S., *Inorg Chem.*(2000), *39*, 4392

[196]. Pratt, F. L., *Physica B*(2000), *289-290*, 710

[197]. Zein, S., Kalhor, M. P., Chibotaru, L. F., and Chermette, H., *J. Chem. Phys.*(2009), *131*, 224316

[198]. Barone, V., Bencini, A., and di Matteo, A., *J. Am. Chem.Soc.*(1997), *119*, 10831

[199]. Train, C., Norel, L., and Baumgarten, M., *Coord. Chem. Rev.*(2009), *253*, 2342

[200]. Mostovich, E. A., Borozdina, Y., Enkelmann, V., Remović-Langer, K., Wolf, B., Lang, M., and Baumgarten, M., *Crystal Growth & Design*(2011), *12*, 54

[201]. Adamo, C., di Matteo, A., Rey, P., and Barone, V., *J. Phys. Chem. A*(1999), *103*, 3481

[202]. Neese, F., Orca. (2009) In *revision 2.7.0 ;*, Universitaet Bonn.

[203]. Karton, A., Tarnopolsky, A., Lameire, J.-F., Schatz, G. C., and Martin, J. M. L., *J. Phys. Chem. A*(2008), *112*, 12868

[204]. Kozuch, S., Gruzman, D., and Martin, J. M. L., *J. Phys. Chem. C.114*, 20801

[205]. Alies, F., Luneau, D., Laugier, J., and Rey, P., *J. Phys. Chem.*(1993), *97*, 2922

[206]. Schwabe, T., and Grimme, S., *J. Phys. Chem. Lett.1*, 1201

[207]. Zein, S., Borshch, S. A., Fleurat-Lessard, P., Casida, M. E., and Chermette, H., *J. Chem Phys.*(2007), *126*, 014105

[208]. Chesneau, F., Hamoudi, H., Schüpbach, B. r., Terfort, A., and Zharnikov, M., *J Phy Chem C*(2011), *115*, 4773

Curriculum Vitae

Personal Data

Ram Niwas
Date of Birth: 14. August 1978

Nationality	Nationality: Indian
Place of Birth	Place of Birth: Muzaffarnagar (India)
Marital Status	Marital Status: Married to Anamika Singh, One daughter : Anushka Singh and One Son: Aadvik Singh
Nationality	Indian

School

07/1985-06/1992	Primary education, Dulla Kheri, Muzaffarnagar
07/1992-06/1994	High School S.S Inter college Titron, Sharnpure
07/1994-06/1997	Intermediate D.A.V Inter college Unn, Muzaffarnagar

University Education and Working Experience

07/1997-06/2000	BSc, in Chemistry, D.A.V College Muzaffarnagar (C.C.S Uni. Meerut)
07/2000-06/2002	MSc in Chemistry, Indian Institute of Technology Roorkee, India
10/2003-07/2006	Junior Research fellow (Indian Institute of Technology Kanpur) India
08/2006-04/2007	Graduate Teaching Assistant (Marquette University), USA
05/2007-12/2007	Junior Research fellow (Indian Institute of Technology Kanpur) India
01/2008-04/2012	PhD student with Prof. Max Holthausen, Goethe-University, Frankfurt, Germany.
09/2012-07/2013	Manager Trainee (part time) , Fresenius-Kabi Bad Homburg, Germany
08/2013-Current	Manager, Kao Germany

Academic Teachers

Prof.Dr. Max Holthausen, Prof. Dr. S. Sarkar, Prof. Dr. N. Sathyamurthy. Prof. Dr. P.K. Bhardwaj

Prof. Dr. G.Bhattacharjee,   Prof. Dr. A.K. Jain, Prof. Dr. M.R. Maurya, Prof. Dr. Mala Nath, Prof. Dr. Ravi

Bhushan, Prof. Dr. U.P Singh, Prof. Dr. S.M. Sondhi, Prof. Dr. K.C. Gupta, Prof. Dr. P.P Thankachan, Prof.

Dr. William A. Donaldson, Prof. Dr. James R. Kincaid,   Prof. Dr. Mark G. Steinmetz, Prof. Dr. Dmitri

Babikov, Dr. Mradula Mittal, Smt. Kalpna, Dr. R.P. Singh, Dr. Shashi Sharma